ABSTRACT

NITHYANANDAM, PRANESHNANDAN. A Study of Electrochemically Controlled Interfacial Tension of Eutectic Gallium Indium. (Under the direction of Dr. Michael D. Dickey).

This master's thesis focuses on the role of electrochemical oxidation of eutectic gallium indium (eGaIn) – a liquid metal – to lower the interfacial tension in aqueous solutions of sodium hydroxide. Electrochemical oxidation has been shown previously to lower the effective interfacial tension of liquid metal, but the mechanism is poorly understood. In this thesis, we use voltammetric techniques and electrochemical impedance spectroscopy (EIS) to provide some new insights into what occurs at the interface between the liquid metal and the aqueous electrolyte as a function of potential.

Chapter 1 briefly introduces gallium-based liquid metal and gives some background and motivation for this work. **Chapter 2** provides a background on the experimental techniques and the tools used to acquire and analyze the data. **Chapter 3** briefly introduces the existing electrochemical reactions for gallium electrodes and proposes an oxidation mechanism for eutectic gallium indium sodium hydroxide. The oxidation mechanism of eGaIn has been divided into five regimes namely, 'cathodic protection', 'oxidizing', 'passivation', 'passivation breakdown', and 'partial re-passivation'. We present the chemical and electrochemical reactions that may occur in these regimes with sufficient evidence. **Chapter 4** provides the electrochemical impedance analysis of eGaIn electrodes in 1M NaOH. Impedance spectra at potentials near the transition of oxidation regimes have been recorded for both forward potential sweep (FS) and backward potential sweep (BS) to better understand the oxidation mechanism and its physical implications. The EIS analysis showed five unique impedance trends that include capacitive behavior, non-ideal mass transport behavior, inductive behavior, and the appearance of a second capacitive loop. We

discuss these impedance trends in detail based on the oxidation mechanism presented in chapter 3. We also characterized the surface oxide film and estimated its thickness indirectly using EIS. Finally, **Chapter 5** demonstrates the unique interfacial tension behavior of eGaIn during electro-oxidation. The interfacial tension suddenly dropped in the passivation regime and continued to decrease linearly in the passivation breakdown regime during the FS, contrary to the parabolic decrease observed in other liquid metals like mercury. Additionally, the interfacial tension increased linearly in the BS showing hysteresis behavior. Based on the electrochemical oxidation mechanism and the impedance trends, we discuss the reason behind this in detail.

The research reported in this thesis serves as an update to the previously reported work on interfacial tension modulation phenomena in gallium-based liquid metal.

A Study of Electrochemically Controlled Interfacial Tension of Eutectic Gallium Indium.

by
Praneshnandan Nithyanandam

A thesis submitted to the Graduate Faculty of
North Carolina State University
in partial fulfillment of the
requirements for the degree of
Master of Science

Chemical Engineering

Raleigh, North Carolina
2022

APPROVED BY:

_____	_____
Dr. Peter S. Fedkiw	Dr. Karen E. Daniels

_____
Dr. Michael D. Dickey
Committee Chair

DEDICATION

To my beloved parents and brother.

Thank you for your unconditional support, sacrifice, and encouragement with my studies and work.

BIOGRAPHY

Praneshnandan Nithyanandam was born to Physician parents Dr. Nithyanandam Allimuthu and Dr. Ashalatha Bhoopalan in Vellore, India, on April 27, 1997. He has one younger brother Swaroop Nithyanandam.

In 1998, he moved to Chennai and did his schooling at SBOA School and Junior College and D.A.V Senior Secondary School. To fulfill his dream of becoming an engineer, he cracked the competitive exam JEE. He joined an Undergraduate course in Chemical Engineering in July 2014 at the National Institute of Technology, Tiruchirappalli (Trichy). Apart from his academics, He also served as Vice-Treasurer and Treasurer of the Chemical Engineering Association (ChEA) and played an integral role in organizing cultural and technological events at NIT Trichy; and graduated in July 2018 with a Bachelor of Technology in Chemical Engineering.

His undergraduate internship training at IIT Madras under the guidance of Prof. Dr. A. Mani inclined him to pursue higher education. He moved to the United States in the fall of 2019 for his Master's at the chemical and biomolecular engineering department at North Carolina State University, Raleigh. In Jan 2020 he joined the Dickey group to study *liquid metals* under the supervision of Dr. Michael D. Dickey.

In 2021, he was awarded the DAAD Rise Pro fellowship to pursue research at Leibnitz-Institut für innovative Mikroelektronik (IHP) in Frankfurt (Oder), Germany. He spent the fall of 2021 at IHP working on the 'Electrical characterization of SiGe heterostructure to realize functional qubits'. He returned to NC State in Jan 2022 to complete his thesis work to understand the interfacial tension behavior of liquid metal during electro-oxidation, under the supervision of Dr. Michael Dickey.

ACKNOWLEDGMENTS

First and foremost, I wish to express my gratitude to my committee members: Dr. Michael Dickey, Dr. Karen Daniels, and Dr. Peter Fedkiw. They have been both great teachers and mentors and have had a profoundly positive impact on my graduate school experience.

I would like to thank my advisor, Dr. Michael Dickey, for his guidance, invaluable advice, continued support and most of all, the opportunity to work for his group. I would also like to thank Dr. Shar Nadimi and Dr. Abolfazl Kiani for teaching me the fundamentals of electrochemistry thereby laying the foundation for my research.

I am grateful to Sandra Bailey, Dr. Saad Khan, and Seth Parrish, for supporting me and allowing me to pursue my internship at IHP -Institut für innovative Mikroelektronik at Frankfurt (Oder), Germany offered by the DAAD fellowship despite rigid COVID restrictions.

I would also like to thank my dear friends: Arvind, Vikram, Jebilson, and others, for their unwavering support and belief in me. A special thanks to my childhood friend and mentor, Karthik Suresh, for helping me navigate my way through graduate school. I was lucky enough to make a few good friends along the way: Surendar, Ninada, Srikanth, Nita and Swathi. Together they made my graduate school experience wholesome and exciting. I would also like to extend my sincere thanks to Raji Shanmugam and her family for their hospitality.

I am also thankful to my peers in Dr. Dickey's group: Adam Bachmann, Joe, Jiayi Yang, Jinwoo Ma, Milad Shamsi, Minyung Song, Dr. Omar, Sooik Im, Shreyas, Veena Vallem, Dr. Vi Khanh Truong, and Keith Hillarie from Dr. Daniel's group. They have all shaped me to become a better researcher and individual over the time I've spent with them.

Finally, I wish to thank my family for their blessing and undying support. All my accomplishments are a direct result of their hard work and dedication. Thank you for everything.

TABLE OF CONTENTS

LIST OF TABLES

LIST OF FIGURES

Chapter 1 : Why are liquid metals interesting?

Abstract:

This chapter provides a brief introduction of gallium-based liquid metal and its properties. One of its unique properties is surface tension, liquid metals have a large surface tension compared to any other liquids (eGaIn in vacuum ~634 mN/m compared to water 72 mN/m). Prior work demonstrated that the interfacial tension of eGaIn can be lowered to near-zero values by applying an oxidative potential, and the resulting oxide formation is suspected to be the cause for it. However, the details behind this mechanism is not clearly understood. In this master's thesis we discuss the role of electrochemical oxidation of eutectic gallium indium — a liquid metal – in aqueous sodium hydroxide solutions. We use electrochemical techniques in this thesis to get fresh insights into what happens at the liquid metal-aqueous electrolyte interface as a function of potential. This chapter provides some context and rationale for the project.

Introduction:

Liquid metals are defined here as metals that exist as liquids at or near room temperature. Mercury (Hg), francium (Fr), cesium (Cs), rubidium (Rb), and gallium (Ga) are among the few metals that have such properties; cesium and francium are radioactive, whereas rubidium is explosive. Therefore, only mercury and gallium are fit for practical applications[1]. Mercury is one of the most widely recognized liquid metals found in dental amalgams, thermometers, barometers, and fluorescent lamps[2]. Other applications include using calomel (Hg_2Cl_2) in medicine, pyrotechnics, electrodes for electrochemistry, and catalysts[3]. However, the use of mercury has been on the decline due to its toxic nature[3]. For this reason, silver-silver chloride (Ag/AgCl) reference electrode has replaced the hazardous standard calomel reference electrode. In contrast, gallium is considered to have low-toxicity[4], as Ga^{3+} has similar properties to Fe^{3+} and Al^{3+}, so

blood can absorb Ga^{3+} to form a transferrin-gallium complex much like Fe^{3+}. However, increasing concentrations of Gallium ions tend to become toxic []. It also does not evaporate since it has ultra-low vapor pressure (effectively zero at room temperature and only 1 kPa at 1037˚K[5]), making it a suitable replacement for mercury[6]. This thesis uses gallium and gallium alloys.

Gallium was discovered and extracted from zinc blend ores in Paris by Paul-Émile Lecoq de Boisbaudrab in 1875[7]. Unlike mercury, pure gallium is solid at room temperature and has a low melting point of 29.75˚C (slightly higher than room temperature)[16–19,8,9]. Gallium can easily form alloys with most metals and is commonly used to prepare eutectic alloys (i.e., the melting point of the resultant alloy is smaller than the source metals). Some of the most popular eutectic alloys include Galinstan (68.5 wt.% Ga, 21.5 wt.% In, 10.0 wt.% Sn) with a melting point of 10.7˚C and eutectic gallium-indium (eGaIn) (75.5 wt.% Ga, 24.5 wt.% In) with a melting point of 15.5˚C[10]. Gallium-based liquid metals have low viscosity, high electrical and thermal conductivity that make them suitable for both stretchable electronics[4] and other applications such as antimicrobial coatings[11], microfluidics[12], batteries[13], and wearable devices[4,14].

The surface of the gallium-based liquid metal reacts rapidly with air to form a ~3 nm native oxide skin and is made up primarily of amorphous or poorly crystallized gallium oxide (Ga_2O_3)[4,15], although in pH neutral solutions the oxide becomes GaOOH[16,17]. The tendency for gallium to form oxides is greater than the other elements in these eutectics (i.e., Zn, Sn, In), even under low oxygen concentrations. Hence all gallium-based liquid metals show similar interfacial surface behaviors in oxidative environments[15]. Furthermore, the oxide skin can adhere to any surface it comes in contact with and maintain shapes that would not be possible due to surface tension[4,18]. The presence of oxide skin is a critical feature that allows the possibility of soft and stretchable electronics and printing 3D structures[19].

Although the oxide skin does not significantly impact the electrical transport across the interface, the presence of oxide can interfere with sensitive electrical measurements[4]. This oxide skin can be removed using an aqueous acid (e.g., HCL) or base (e.g., NaOH). NaOH (aq) is the most frequently used electrolyte in most literature as it is safe and less volatile than commonly used acids (HCl)[4].

Motivation:

In the absence of an oxide skin, gallium-based liquid metals have a high surface tension (~624 mN/m in ambient conditions for a pendant droplet of eGaIn[20,21]); for reference, water's surface tension is 72 mN/m[15,22]. Because of the strength of metal-metal bonding, the surface tension of liquid metals is higher than that of other non-metallic liquids[5]. It should be made clear that the term "surface tension" corresponds to the force measured in vacuum, whereas the term "interfacial tension" corresponds to the interfacial forces in liquid medium. We use the term 'effective interfacial tension' to include the contribution of oxidation. The interfacial forces become dominant and significant at smaller length scales because Laplace pressure is proportional to γR^{-1}, generating large forces when the material has a small radius of curvature (R)[15]. Thus, controlling the interfacial tension is an effective way to generate forces that can move and manipulate the shape and position of liquid metals. The ability to do so enables shape reconfiguration of the liquid metal for electromechanical soft actuators[23], functional microfluidics[24–27], LM valves, pumps[28], liquid metal wires[29] and thermal switches[3017,26]. Hence the ability to control and manipulate surface tension of liquid metal is sought after for applications in soft, stretchable, and shape-reconfigurable devices, especially in sub-millimeter scale.

The surface tension of liquids can be controlled using a wide variety of methods, including temperature[18,2631], light[32], surface chemistry[33], and electrostatics[34], but these methods have limited

utility for modulating liquids with high surface tension. Among these methods, 1) changing the surface chemistry (surfactants) and 2) electrostatics are most effective especially for liquid metals[15,18]. Surface active agents or surfactants are compounds used to lower the surface tension of two liquids, they are usually amphiphilic organic compounds, meaning they have both a hydrophobic group (tail) and a hydrophilic group (head) that helps in decreasing the surface tension [35,36]. This decrease in surface tension is inversely proportional to surfactant concentration until the critical micelle concentration (CMC), beyond CMC no significant change in surface tension occurs. Fluoro-surfactants are the most effective surfactants available for lowering the surface tension of water; for example, perfluorooctanoic acid (PFOA) can lower the surface tension of water from 72 mN/m to 15.2 mN/m[37], while sodium dodecyl sulfate (SDS) can also reduce the tension of water to ~27 mN/m[38]. SDS are preferred over fluro-surfactants for most applications due to their biocompatibility. Surfactants can only induce modest tension changes in liquid metals; for example, alkythiol was found to reduce the surface tension of mercury by ~438.6 mN/m[39] to ~378.6 mN/m[40], and SDS was found to reduce the surface tension of Galinstan from 420 mN/m to 385 mN/m[41]. The major disadvantage of using surfactants is that this process is irreversible[41]. **Figure 1.1a**. shows the interfacial tension of eGaIn (in vacuum) in comparison with water, water + SDS, Silicon Oil[15].

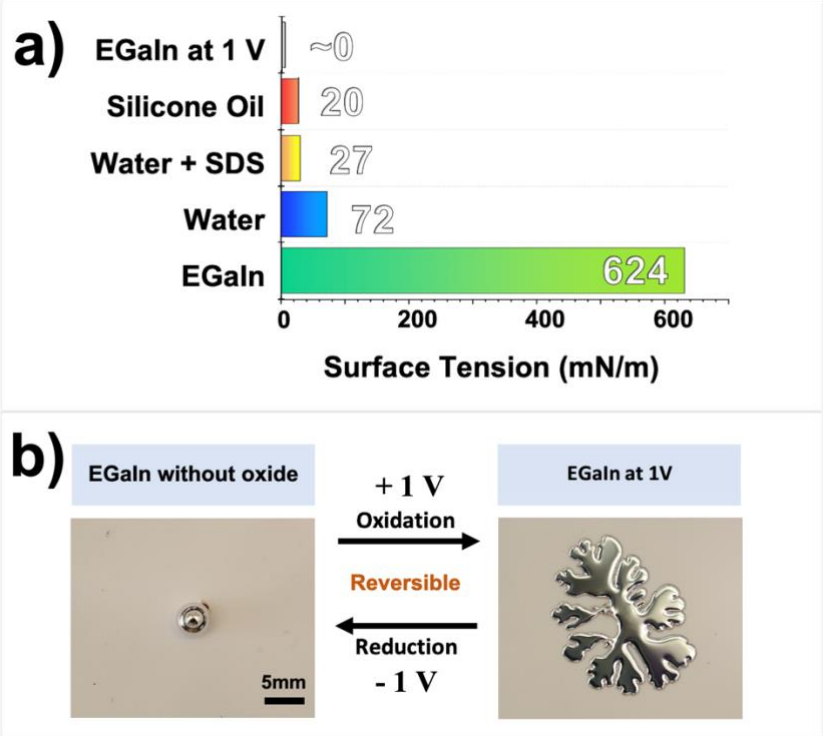

Figure 1.1 a) Shows the surface tension of oxide free eGaIn in vacuum[21] in comparison with water [37,42], Silicon Oil[42], water + SDS[38] and eGaIn in 1M NaOH when ~1 V is applied[15,18], and b) Demonstrates the reversible interfacial tension nature of eGaIn, when an oxidizing potential of 1 V is applied, the eGaIn droplet forms irregular fractal patterns during oxidation and reverts back to its original spherical morphology once a reducing potential of -1V is applied to, adapted from[15].

An alternative method to control surface tension of liquid metal is to apply an electric potential. Applying an oxidative potential to an eGaIn electrode in 1M NaOH causes an enormous drop in interfacial tension from ~500 mN/m at 0.0 V to near-zero values at ~ 1.0 V (here, the reported voltages are applied relative to open circuit potential). **Figure 1.1** shows the effectiveness of using electroactive methods to lower interfacial tension of eGaIn[15]. This method is attractive because of its ability to tune the interfacial tension on command reversibly. This phenomenon is often associated with electrocapillarity[43,44]. Electrocapillarity is a thermodynamic phenomenon that is observed at charged interfaces, and it is especially attributed to changes in interfacial energy (stress or tension) as a function of electrode potential or composition of electrolyte[45]. From its initial observation in mercury, electrocapillarity has been extended to other solid electrodes to study the equilibrium properties of electrode/electrolyte interfaces[46]. The interpretation of

electrocapillary observed in liquid metals in contact with an electrolyte is based on the concept of ideal polarizability[45,46]. For a ideally polarized electrode the relationship between interfacial tension, surface charge density and applied potential can be described by Lippman equation derived from Gibbs relations, shown by **equation 1.1** , where γ_{pzc} is the interfacial tension at the point of zero charge, *C* is the capacitance per unit area of double layer, and V is the applied voltage[15,45–47] .

$$\gamma(V) = \gamma_{pzc} - \frac{1}{2} C\left(V - V_{pzc}\right)^2 \tag{1.1}$$

In electrolytes, liquid metals develop a net surface charge across the interfacial boundary due to ion transfer, creating an electrical double layer (EDL)[15,48]. Typical capacitance values for EDL in literature are in the range of ~ 20 to 30 µF/cm^2 [49,50]. Applying a potential *'V'*, changes the amount of charge stored in the EDL (and therefore capacitive energy) at the interface, which dictates how much the tension drops, according to **equation 1.1**. It has been shown that at sufficiently large potentials the charges across the interface can start combining via Faradaic reactions. For example, if the electrolyte is aqueous, these reactions can generate oxygen or hydrogen bubbles via oxidation or reduction of water, respectively[17]. So, **equation 1.1** is only valid in a limited potential window where only capacitive behavior exists and fails when electrochemical reactions occur. This is limitation is particularly important for Ga-based liquid metals due to their reactivity toward oxygen and water[15].

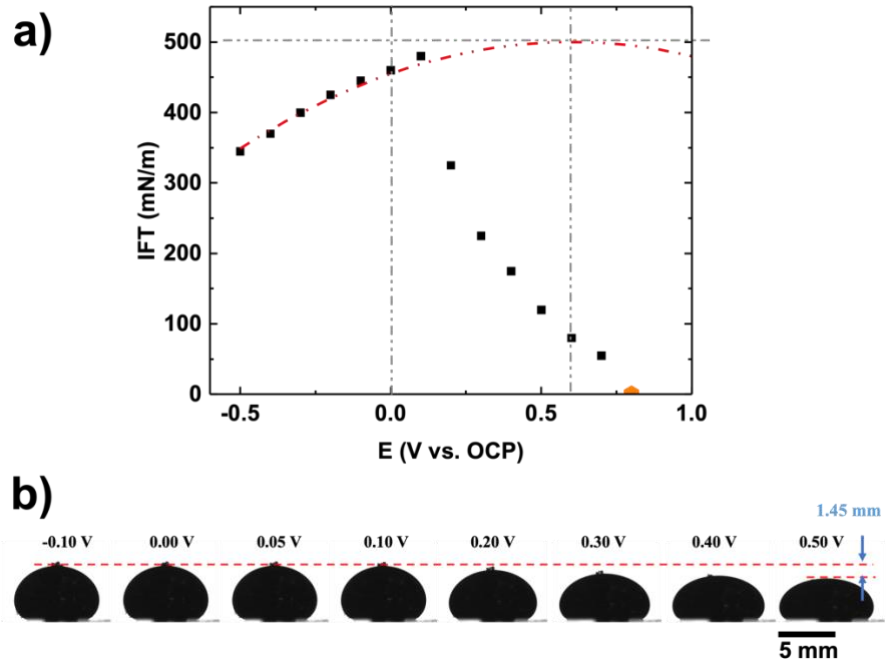

Figure 1.2: a) Shows effective interfacial tension (black squares) of eGaIn in 1M NaOH as function of applied potential (data retrieved from [15]. The red dotted line represents the hypothetical interfacial tension if eGaIn followed the electrocapillary equation (**equation 1.1**). The orange circle is the estimated effective interfacial tension based on the capillary height of the droplet[15,47]. and b) Shows the gradual decrease in the interfacial tension of 0.1ml eGaIn sessile electrode in 1M NaOH for a potential range from -0.1 V to 0.5 V (side view).

Figure 1.2a shows the electrocapillarity trends of eGaIn in 1M NaOH calculated using **equation 1.1** (for a typical EDL capacitance ~ 25 µF/cm^2)[50]. The measured effective interfacial tension of EGaIn in 1M NaOH was found to follow electrocapillarity trends for potential (cathodic potentials) up to 0.05 V, after which the interfacial tension drops significantly and deviates[15,18]. This is because the electrocapillarity equation which derived by integrating the Lippmann equation; does not account for Faradaic reactions that produce oxide[15] and gallium based liquid metals form an oxide layer at potentials greater than 0.05 V[15,17,18].

Despite the growing interest in this anomalous interfacial behavior, the mechanism by which electric potential lowers interfacial tension is poorly understood. Our group's first report speculated that the surface oxide formed during oxidation acts as a surfactant and significantly

lowers interfacial tension[18]. Nevertheless, this report did not explain the continued drop of interfacial tension after oxide formation nor provide an explanation for its mechanism. The presence of surface oxides complicates the interfacial behavior of liquid metals. To capture this complexity, the term 'effective interfacial tension' is used hereafter to account for all of the effects (e.g. stress in the electrodeposited oxide species, electrocapillary effects, and the tension of the liquids that interface with the oxide)[15].

Normally, understanding interfacial phenomenon requires elucidating what species at the interface. However, in the case of electrochemical oxidation of Ga, this is difficult to do for several reasons. First, although anodizing EGaIn makes the oxide thicker (a technique used commercially on metals such as Al to improve corrosion and wear resistance[51,52], using 1M NaOH dissolves the oxide as gallates. As a result, both electrochemical oxidation and dissolution happen simultaneously; in such a case, assessing the steady state thickness of the oxide is challenging. Furthermore, when the potential is returned to zero, any species on the surface dissolve, making chemical identification of species on the surface difficult. In case of other electrolytes such as 1M HCl and organic solvents the oxide skin formed during the anodizing process does not disappear, the presence of a thick oxide shell affects the electrical property and restricts its use for applications such as microfluidic channels. Our group's recent work suggests that the liquid metal interface has viscoelastic properties under oxidative potentials[15]. This property of the oxide allows the liquid metal to maintain its shape at reasonable electrode potentials as the interfacial tension decreases. However, at high oxidative potentials as the oxide thickness increases there is considerable Marangoni stress on the interface of liquid metal causing the interface to flow, forming fingering instabilities[53]. Hence making it difficult to retrieve information about the oxide species from s dynamic interface[15,18,22].

Despite these challenges, cyclic voltammetry studies of gallium in alkaline solution with a limited potential window of 0.0 V to 0.5 V show a oxidation peak at 0.05 V (for a scan rate of 3 mV/s) that correspond to oxide formation [15,17]. The surface tension drop was also observed in the same potential window, suggesting a direct correlation between oxide formation and interfacial tension change[54]. Ongoing work in our group seeks to use electrochemistry techniques to indirectly provide information about what is chemically on the surface versus potential.

Although it is challenging to know what species are on the surface, it is possible to measure the interfacial tension of EGaIn as a function of potential by evaluating the shape of sessile droplets. The shape of a droplet is initially spherical (at 0 V, γ~500 mN/m) and flattens as a function of potential from 0 V to 0.7 V, shown in **Figure 1.2**. It flattens due to the effects of gravity as the tension lowers. At potentials near 0.8 V, the morphology of the droplet becomes irregular (fingering instabilities), creating fractals shapes, shown in **Figure 1.1b**[18,22]. Such high surface area protruding shapes would only be possible if interfacial tension was very low. That work speculated that the oxidation creates a compressive force at the interface that helps lower the effective tension.

Electrochemical impedance spectroscopy (EIS) is another technique that can indirectly give information about what is at the surface. The focus of this thesis is on using EIS to give new insights into electrochemical oxidation of EGaIn in aqueous electrolytes. Prior work shows that the electrochemical oxidation behavior of eGaIn was classified into 1) oxidation 2) passivation and 3) transpassive regions[15]. The impedance analysis of eGaIn in the oxidation and the transpassive regime show behavior that suggest the presence of pit formation on the oxide surface while the surface of eGaIn is completely covered by oxide in the passivation regime [54]. Although these reported results are consistent with the prior cyclic voltammetry observations, they do not accurately describe the electrochemical oxidation behavior and its accompanying physical changes

to the eGaIn electrode. The role of the oxidation and the accompanying interfacial tension change will be discussed in detail in **chapter 4** and **chapter 5**.

With this thesis, we use voltammetric techniques and EIS to provide new insights into the interfacial behavior of EGaIn during electrochemical oxidation. **Chapter 2** discusses the experimental techniques that we use to collect and analyze the data. In **Chapter 3**, we provide a brief introduction of the existing mechanism for oxide formation and discuss the current speculated oxidation mechanism in detail; **Chapter 4** explores the electrochemical techniques used to indirectly characterize the surface oxide, such as electrochemical impedance spectroscopy (EIS), dissolution and dissociation. Finally, **Chapter 5** summarizes the thesis and provides suggestions for next steps to build on this work.

References

(1) Kalantar-Zadeh, K.; Rahim, Md. A.; Tang, J. Low Melting Temperature Liquid Metals and Their Impacts on Physical Chemistry. Acc. Mater. Res. 2021, 2 (8), 577–580. https://doi.org/10.1021/accountsmr.1c00143.

(2) Kozin, L. F.; Hansen, S. 13.2 Demercurization of a Chlor-Alkali Plant. In Mercury Handbook - Chemistry, Applications and Environmental Impact; Royal Society of Chemistry.

(3) Kozin, L. F.; Hansen, S. 12.1 History and Uses of Mercury. In Mercury Handbook - Chemistry, Applications and Environmental Impact; Royal Society of Chemistry.

(4) Dickey, M. D. Stretchable and Soft Electronics Using Liquid Metals. Adv. Mater. 2017, 29 (27), 1606425. https://doi.org/10.1002/adma.201606425.

(5) Chemical Rubber Company; NCSU Retired Faculty and Staff Library Endowment. CRC Handbook of Chemistry and Physics.; Cleveland, Ohio: [Chemical Rubber Company Press].: Cleveland, Ohio, 2022.

(6) Chiechi, R. C.; Weiss, E. A.; Dickey, M. D.; Whitesides, G. M. Eutectic Gallium-Indium (EGaIn): A Moldable Liquid Metal for Electrical Characterization of Self-Assembled Monolayers. Angewandte Chemie, International Edition 2008, 47 (1), 142–144.

(7) Britannica, The Editors of Encyclopaedia. “Gallium”. Encyclopedia Britannica, 23 May. 2021, Https://Www.Britannica.Com/Science/Gallium. Accessed 25 January 2022.

(8) Kalantar-Zadeh, K.; Tang, J.; Daeneke, T.; O’Mullane, A. P.; Stewart, L. A.; Liu, J.; Majidi, C.; Ruoff, R. S.; Weiss, P. S.; Dickey, M. D. Emergence of Liquid Metals in Nanotechnology. ACS Nano 2019, 13 (7), 7388–7395. https://doi.org/10.1021/acsnano.9b04843.

(9) Daeneke, T.; Khoshmanesh, K.; Mahmood, N.; de Castro, I. A.; Esrafilzadeh, D.; Barrow, S. J.; Dickey, M. D.; Kalantar-zadeh, K. Liquid Metals: Fundamentals and Applications in Chemistry. Chem. Soc. Rev. 2018, 47 (11), 4073–4111. https://doi.org/10.1039/C7CS00043J.

(10) Liu, J.; Yi, L. Liquid Metal Biomaterials: Principles and Applications; Springer Series in Biomaterials Science and Engineering; Springer Singapore: Singapore, 2018; Vol. 10. https://doi.org/10.1007/978-981-10-5607-9.

(11) Kwon, K. Y.; Cheeseman, S.; Frias-De-Diego, A.; Hong, H.; Yang, J.; Jung, W.; Yin, H.; Murdoch, B. J.; Scholle, F.; Crook, N.; Crisci, E.; Dickey, M. D.; Truong, V. K.; Kim, T. A Liquid Metal Mediated Metallic Coating for Antimicrobial and Antiviral Fabrics. Adv. Mater. 2021, 33 (45), 2104298. https://doi.org/10.1002/adma.202104298.

(12) So, J.-H.; Dickey, M. D. Inherently Aligned Microfluidic Electrodes Composed of Liquid Metal. Lab Chip 2011, 11 (5), 905. https://doi.org/10.1039/c0lc00501k.

(13) Kim, H.; Boysen, D. A.; Newhouse, J. M.; Spatocco, B. L.; Chung, B.; Burke, P. J.; Bradwell, D. J.; Jiang, K.; Tomaszowska, A. A.; Wang, K.; Wei, W.; Ortiz, L. A.; Barriga, S. A.; Poizeau, S. M.; Sadoway, D. R. Liquid Metal Batteries: Past, Present, and Future. Chem. Rev. 2013, 113 (3), 2075–2099. https://doi.org/10.1021/cr300205k.

(14) Anderson, A.; Menguc, Y.; Wood, R. J.; Newman, D. Development of the Polipo Pressure Sensing System for Dynamic Space-Suited Motion. IEEE Sensors J. 2015, 15 (11), 6229–6237. https://doi.org/10.1109/JSEN.2015.2449304.

(15) Song, M.; Daniels, K. E.; Kiani, A.; Rashid-Nadimi, S.; Dickey, M. D. Interfacial Tension Modulation of Liquid Metal via Electrochemical Oxidation. Advanced Intelligent Systems 2021, 3 (8), 2100024. https://doi.org/10.1002/aisy.202100024.

(16) Khan, M. R.; Trlica, C.; So, J.-H.; Valeri, M.; Dickey, M. D. Influence of Water on the Interfacial Behavior of Gallium Liquid Metal Alloys. ACS Appl. Mater. Interfaces 2014, 6 (24), 22467–22473. https://doi.org/10.1021/am506496u.

(17) Chung, Y.; Lee, C.-W. Electrochemistry of Gallium. Journal of Electrochemical Science and Technology 2013, 4 (1), 1–18. https://doi.org/10.5229/JECST.2013.4.1.1.

(18) Khan, M. R.; Eaker, C. B.; Bowden, E. F.; Dickey, M. D. Giant and Switchable Surface Activity of Liquid Metal via Surface Oxidation. Proc Natl Acad Sci USA 2014, 111 (39), 14047–14051. https://doi.org/10.1073/pnas.1412227111.

(19) Neumann, T. V.; Dickey, M. D. Liquid Metal Direct Write and 3D Printing: A Review. Advanced Materials Technologies n/a (n/a), 2000070. https://doi.org/10.1002/admt.202000070.

(20) Dickey, M. D.; Chiechi, R. C.; Larsen, R. J.; Weiss, E. A.; Weitz, D. A.; Whitesides, G. M. Eutectic Gallium-Indium (EGaIn): A Liquid Metal Alloy for the Formation of Stable Structures in Microchannels at Room Temperature. Adv. Funct. Mater. 2008, 18 (7), 1097–1104. https://doi.org/10.1002/adfm.200701216.

(21) Zrnic, D.; Swatik, D. S. Resistivity and Surface Tension of the Eutectic Alloy of Gallium and Indium. Journal of the Less-Common Metals 1969, 18 (1), 67–68.

(22) Eaker, C. B.; Hight, D. C.; O'Regan, J. D.; Dickey, M. D.; Daniels, K. E. Oxidation-Mediated Fingering in Liquid Metals. Phys. Rev. Lett. 2017, 119 (17), 174502. https://doi.org/10.1103/PhysRevLett.119.174502.

(23) Liao, J.; Majidi, C. Soft Actuators by Electrochemical Oxidation of Liquid Metal Surfaces. Soft Matter 2021, 17 (7), 1921–1928. https://doi.org/10.1039/D0SM01851A.

(24) Khan, M. R.; Trlica, C.; Dickey, M. D. Recapillarity: Electrochemically Controlled Capillary Withdrawal of a Liquid Metal Alloy from Microchannels. Adv. Funct. Mater. 2015, 25 (5), 671–678. https://doi.org/10.1002/adfm.201403042.

(25) Kornyshev, A. A.; Kucernak, A. R.; Marinescu, M.; Monroe, C. W.; Sleightholme, A. E. S.; Urbakh, M. Ultra-Low-Voltage Electrowetting. J. Phys. Chem. C 2010, 114 (35), 14885–14890. https://doi.org/10.1021/jp101051e.

(26) Khoshmanesh, K.; Tang, S.-Y.; Zhu, J. Y.; Schaefer, S.; Mitchell, A.; Kalantar-zadeh, K.; Dickey, M. D. Liquid Metal Enabled Microfluidics. Lab Chip 2017, 17 (6), 974–993. https://doi.org/10.1039/C7LC00046D.

(27) M. Le Berre, Y. C. Electrocapillary Force Actuation of Microfluidic Elements. Microelectronic Engineering 2005, 78–79, 93–99. https://doi.org/10.1016/j.mee.2004.12.014.

(28) Tang, S.-Y.; Khoshmanesh, K.; Sivan, V.; Petersen, P.; O'Mullane, A. P.; Abbott, D.; Mitchell, A.; Kalantar-zadeh, K. Liquid Metal Enabled Pump. PNAS 2014, 111 (9), 3304–3309. https://doi.org/10.1073/pnas.1319878111.

(29) Zhu, S.; So, J.-H.; Mays, R.; Desai, S.; Barnes, W. R.; Pourdeyhimi, B.; Dickey, M. D. Ultrastretchable Fibers with Metallic Conductivity Using a Liquid Metal Alloy Core. Adv. Funct. Mater. 2013, 23 (18), 2308–2314. https://doi.org/10.1002/adfm.201202405.

(30) Yang, T.; Foulkes, T.; Kwon, B.; Kang, J. G.; Braun, P. V.; King, W. P.; Miljkovic, N. An Integrated Liquid Metal Thermal Switch for Active Thermal Management of Electronics. IEEE Transactions on Components, Packaging and Manufacturing Technology 2019, 9 (12), 2341–2351. https://doi.org/10.1109/TCPMT.2019.2930089.

(31) Daniel, S.; Chaudhury, M. K.; Chen, J. C. Fast Drop Movements Resulting from the Phase Change on a Gradient Surface. Science 2001, 291 (5504), 633–636. https://doi.org/10.1126/science.291.5504.633.

(32) Ichimura, K.; Oh, S.-K.; Nakagawa, M. Light-Driven Motion of Liquids on a Photoresponsive Surface. Science 2000, 288 (5471), 1624–1626. https://doi.org/10.1126/science.288.5471.1624.

(33) Gallardo, B. S.; Gupta, V. K.; Eagerton, F. D.; Jong, L. I.; Craig, V. S.; Shah, R. R.; Abbott, N. L. Electrochemical Principles for Active Control of Liquids on Submillimeter Scales. Science 1999, 283 (5398), 57–60. https://doi.org/10.1126/science.283.5398.57.

(34) Lahann, J.; Mitragotri, S.; Tran, T.-N.; Kaido, H.; Sundaram, J.; Choi, I. S.; Hoffer, S.; Somorjai, G. A.; Langer, R. A Reversibly Switching Surface. Science 2003, 299 (5605), 371–374. https://doi.org/10.1126/science.1078933.

(35) Furse, D. S. "Bubbles, Bubbles, Everywhere, But Not a Drop to Drink." The Lipid chronicles.

(36) Rosen, M. J.; Kunjappu, J. T. Surfactants and Interfacial Phenomena; Wiley, 2012.

(37) Kovalchuk, N. M.; Trybala, A.; Starov, V.; Matar, O.; Ivanova, N. Fluoro- vs Hydrocarbon Surfactants: Why Do They Differ in Wetting Performance? Advances in Colloid and Interface Science 2014, 210, 65–71. https://doi.org/10.1016/j.cis.2014.04.003.

(38) Holmberg, K., 1946-. Novel Surfactants: Preparation, Applications, and Biodegradability; New York ; Basel : M. Dekker, [2003]: New York, 2003.

(39) Kernaghan, M. Surface Tension of Mercury. Phys. Rev. 1931, 37 (8), 990–997. https://doi.org/10.1103/PhysRev.37.990.

(40) Iakovlev, A.; Bedrov, D.; Müller, M. Molecular Dynamics Simulation of Alkylthiol Self-Assembled Monolayers on Liquid Mercury. Langmuir 2017, 33 (3), 744–754. https://doi.org/10.1021/acs.langmuir.6b03774.

(41) Handschuh-Wang, S.; Rauf, M.; Gan, T.; Shang, W.; Zhou, X. On the Interaction of Surfactants with Gallium-Based Liquid Metals. ChemistrySelect 2021, 6 (39), 10625–10636. https://doi.org/10.1002/slct.202103343.

(42) Barca, F.; Caporossi, T.; Rizzo, S. Silicone Oil: Different Physical Proprieties and Clinical Applications. BioMed Research International 2014, 2014, 502143. https://doi.org/10.1155/2014/502143.

(43) Gough, R. C.; Morishita, A. M.; Dang, J. H.; Moorefield, M. R.; Shiroma, W. A.; Ohta, A. T. Rapid Electrocapillary Deformation of Liquid Metal with Reversible Shape Retention. Micro and Nano Syst Lett 2015, 3 (1), 4. https://doi.org/10.1186/s40486-015-0017-z.

(44) Shantharama; Kalpathy, S. K. Electrocapillary Effect in Liquid Films with an Electrically Charged Interface. Materials Today: Proceedings 2021, 44, 3006–3011. https://doi.org/10.1016/j.matpr.2021.02.406.

(45) Láng, G. G. Basic Thermodynamics of Electrified Interfaces. In Encyclopedia of Interfacial Chemistry; Wandelt, K., Ed.; Elsevier: Oxford, 2018; pp 1–14. https://doi.org/10.1016/B978-0-12-409547-2.13608-X.

(46) Haiss, W. Surface Stress of Clean and Adsorbate-Covered Solids. Rep. Prog. Phys. 2001, 64 (5), 591–648. https://doi.org/10.1088/0034-4885/64/5/201.

(47) Khan, M. R.; Eaker, C. B.; Bowden, E. F.; Dickey, M. D. Giant and Switchable Surface Activity of Liquid Metal via Surface Oxidation. Proc Natl Acad Sci USA 2014, 111 (39), 14047–14051. https://doi.org/10.1073/pnas.1412227111.

(48) Eaker, C. B.; Dickey, M. D. Liquid Metals as Ultra-Stretchable, Soft, and Shape Reconfigurable Conductors; 2015; Vol. 9467, pp 946708-946708–946710. https://doi.org/10.1117/12.2175988.

(49) Garche, J.; Karden, E.; Moseley, P. T.; Rand, D. Lead-Acid Batteries for Future Automobiles; 2017; p 674.

(50) Ricci, E.; Sangiorgi, R.; Passerone, A. Density and Surface Tension of Dioctylphthalate, Silicone Oil and Their Solutions. Surface and Coatings Technology 1986, 28 (2), 215–223. https://doi.org/10.1016/0257-8972(86)90060-5.

(51) Zhang, X. G. Passivation and Surface Film Formation. In Corrosion and Electrochemistry of Zinc; Zhang, X. G., Ed.; Springer US: Boston, MA, 1996; pp 65–91. https://doi.org/10.1007/978-1-4757-9877-7_3.

(52) Arnott, D. R.; Baxter, W. J.; Rouze, S. R. Oxide Film Rupture, Reanodization, and Stress Corrosion Cracking in Aluminum. Journal of The Electrochemical Society 1982, 129 (12), 2660–2665. https://doi.org/10.1149/1.2123642.

(53) Hillaire, K. D.; Dickey, M. D.; Daniels, K. E. Marangoni Fingering Instabilities in Oxidizing Liquid Metals. arXiv:2011.10016 [cond-mat, physics:physics] 2020.

(54) Song, M. Interfacial Tension Modulation of Liquid Metal via Electrochemical Oxidation and Its Application. Doctor of Philosophy, North Carolina State University, Raleigh, 2020.

Chapter 2 : Experimental Techniques

Abstract:

In this chapter we discuss the experimental techniques and the tools used to acquire and analyze the data.

Materials and Methods:

Electrodes and electrochemical cell

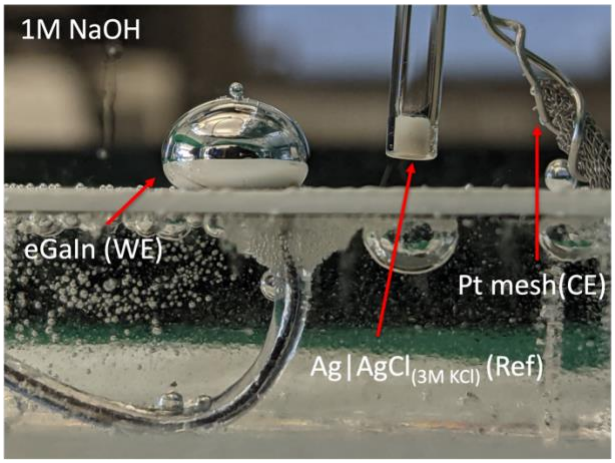

Figure 2.1: A three electrode Electrochemical cell. Where, eGaIn is the working electrode (WE), platinum mesh is the counter electrode (CE) and Ag/AgCl $_{3M\ KCl}$ is the reference electrode (Ref) in 1M NaOH electrolyte solution.

The working electrode was a 0.1 ml eutectic gallium indium alloy (eGaIn) droplet, with a composition of 75% Ga and 25% In. The electrochemical cell consisted primarily of a three-electrode system. A platinum mesh electrode and a silver/silver chloride reference electrode Ag |AgCl | 3M KCl are used as the counter and reference electrode. The electrochemical cell holds the eGaIn droplet on an acrylic platform. A copper wire is completely wetted with eGaIn to avoid any exposed copper and attached to the platform; this wire supplies voltage to the liquid metal electrode and prevents the droplet from moving laterally, as shown in **Figure 2.1.** The copper contacts were inspected for corrosion and cleaned by sanding the corroded part before performing the experiment. 1M sodium hydroxide was used as the electrolyte and was prepared freshly before use.

Electrochemical Measurements

All the experiments were conducted using a Biologic electrochemical test station (VMP3 Potentiostat- galvanostat). We used a three-electrode electrochemical cell shown in **Figure 2.1**, for Cyclic voltammetry (CV), chronoamperometry (CA), linear sweep voltammetry (LSV), and electrochemical impedance spectroscopy (EIS) experiments. The surface area of the electrode was ~120 mm^2 for a spherical 0.1 ml eGaIn droplet at open circuit potential. In all coming discussions, *'E'* represents electrical potential. The electrochemical cell was covered by a Faraday cage to prevent noise and external disturbances during the experiment. All experiments were performed at room temperature of 25±1 ˚C.

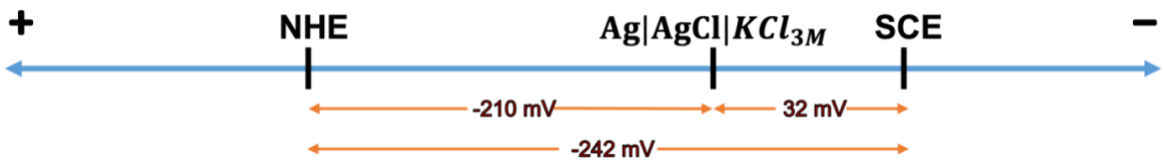

Figure 2.2: Conversion factors to convert electrode potential to Ag| $AgCl_{(3M\ KCl)}$, adapted from [1]

The open-circuit potential of eGaIn in 1M NaOH is approximate -1.5 ± 0.01 V vs. Ag | AgCl || 3M KCl reference electrode. **Figure 2.2** shows the conversion factors and how to convert applied potential between different reference electrodes. For example, a -1.0 V vs. Ag | AgCl | KCl 3M is equivalent to -0.79 V vs. NHE (Normal hydrogen electrode) and -1.032 V vs. SCE (Saturated Calomel electrode)[2,3]. For clarity for the sake of non-electrochemists, all subsequently reported potentials are shifted relative to open circuit potential (OCP) by adding to the observed value (i.e., $E_{(Ag|AgCl||3M\ KCl)} = -1.5\ V$ is equivalent to $E_{OC} = 0\ V$). All measurements were performed in 1M NaOH electrolyte (unless otherwise stated).

Impedance experimental parameters

The impedance measurements were performed in the frequency range of 100 MHz to 100mHz with 12 sampling frequencies per decade at various potentials. The working electrode was stabilized for 5 sec before the impedance run to allow the electrode to attain a steady state to achieve a reproducible initial state. the experimental impedance data were analyzed using EC-Lab software[4]. The impedance spectra were plotted in complex plane diagrams (Nyquist plots), and the equivalent circuit models were fit using the simplex minimization function.

Interfacial tension measurement

During eGaIn electro-oxidation, we measured the electrical current (I) and interfacial tension (IFT, γ) simultaneously. To quantify IFT, we used a microscope camera to record images taken from the side with a goniometer (FTA32 software, First Ten Angstroms Company, USA) and interfacial tension (γ) measurements are made using a custom-written MATLAB code, explained in the later sections. Theory:

Interfacial tension measurement using sessile droplet:

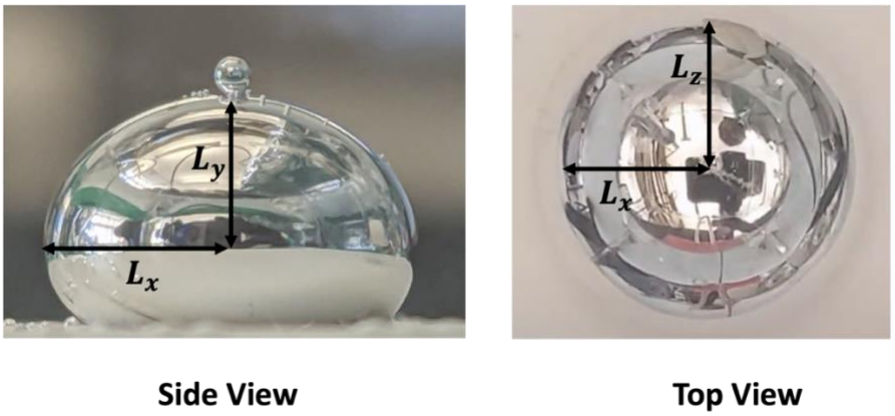

Figure 2.3: Profile of a sessile droplet computed by integrating the Laplace equation using standard numerical methods, taken from [5].

Studying the shape of sessile as a function of electrical potential provides insights into the physical impact of electrochemical oxidation on the effective interfacial tension of the liquid metal. A sessile droplet refers to the droplet configuration when resting on a surface, as shown schematically in **Figure 2.3**. To accurately measure the interfacial tension of droplets, the diameter of the droplet must be large enough for the gravitational forces to act on it, as surface tension forces balance the gravitational forces when the droplet is in equilibrium, and the size of the this droplet is called 'capillary length,' given by $\lambda_c = \left(\gamma/\rho g\right)^{1/2}$[6], where λ_c is the capillary length, γ is the surface tension, g is the acceleration due to gravity, and ρ is the density of the eGaIn (if a droplet is immersed in a second immiscible fluid, then the ρ is the difference in the density of fluids). eGaIn has an effective interfacial tension of ~500 mN/m in the 1M NaOH[2,7], As the presence of oxide creates two interfaces, namely the liquid metal/oxide and the oxide/electrolyte. Hence, we use the ρ as the difference in the density of fluids to calculate the capillary length (λ_c) and for of eGaIn in 1M NaOH it is found to be 3 mm. For droplets with a radius smaller than 3 mm, the shape of the droplet does not distort as the effect of gravity becomes negligible.

The surface tension of a sessile droplet is calculated using the formula developed in [5] using Morse-Witten theory. This method uses only two length measurements, L_x (the maximum equatorial droplet radius) and L_y (the distance from the midpoint of the equator to the apex of the droplet), assuming the droplet is symmetric in *x* and *y* length scales, as shown in **Figure 2.3.** The formula is given by:

$$\gamma_{MW} = \frac{\Delta\rho g \ln 2}{24} \frac{\left(L_x + L_y\right)^3}{\left|L_x - L_y\right|} \left[1 \mp 3c + 3c^2 \mp c^3\right] \tag{2.1}$$

With $c = \left(\frac{1-\ln 2}{\ln 2}\right)\frac{|L_x - L_y|}{(L_x + L_y)}$ ($\mp$: $-$ for sessile droplet, $+$ for pendant droplet). This expression holds until the sessile droplet maintains its shape and is accurate in the limit $\gamma^{-1} \to 0$. Furthermore, the Morse-Witten results were found to be asymptotically exact in the limit of small deformations.

DC electrochemical techniques:

Linear sweep voltammetry (LSV)

LSV is a technique to study the behavior of an electrochemical system by recording the Faradaic current during a potential sweep from an initial potential (E_i) to a final potential (E_f) at a particular scan rate [3]. This technique can be used to obtain preliminary information regarding the electrochemical reactions and the electron-transfer steps. An advanced version of this technique is cyclic voltammetry.

Cyclic voltammetry (CV)

CV is a powerful and popular technique used commonly used to investigate the reduction and oxidation process of molecular species [8]. Like LSV, this method involves sweeping potential from an initial potential (E_i) to a final potential (E_f) at a particular scan rate, however instead of terminating the potential, we sweep it back to E_i while recording the faradic current [3,8]. Additionally, it can be used to study electron transfer-initiated chemical reactions [3,8]. The current response increases or decreases depending on the reactions that happen near the electrode surface; at potentials where oxidation or reduction occur, peaks are observed. This method can be used to probe the nature of the electrochemical reactions system by studying the shapes and position of the oxidation and reduction peaks[3,9,10]. Depending on the position of the peaks, the electrochemical system could be either chemically reversible or irreversible or electrochemically reversible or

irreversible. The position and the magnitude of the peaks also change with scan rate. Due to this reason, it is said that CV is like a fingerprint of an electrochemical system. The Randels-Sevcik equation determines the shape of the LSV and CV plots for planar electrodes [3],

$$i_p = 0.446nFAC_\infty \left(\frac{nF\nu D_o}{RT}\right)^{1/2} \quad (2.2)$$

where i_p Is the current, ν is scan rate, C_∞ is the bulk concentration of the analyte, A is area of electrode, F is the faradic constant (96485C/mol), R is the gas constat, T is the temperature, n is the number of electrons transferred, and D_o is the diffusion coefficient of the oxidized analyte. For spherical electrodes (e.g., Hanging droplet mercury drop) a correction is required, and the peak current is given by equation 2.3, where r_o is the radius of electrode[3].

$$i_p = i_p(plate) + 0.725 \times 10^5 \left(\frac{nAC_\infty D_o}{r_o}\right) \quad (2.3)$$

Chronoamperometry (CA)

CA is a steady-state potential step technique where the potential of the working electrode is changed instantaneously while recording the current response with respect to time[3]. This technique is useful for studying electrochemical systems at long- and short-time scales. The time scale is a significant parameter to understand electrochemical systems. At long-time scales, diffusion becomes the rate-determining step, whereas, at short-time scales, reaction kinetics dominates. The electrode and electrolyte interface charging can also be inferred from the short-time scale studies [3]. Furthermore, this technique can be used to determine the adsorption isotherms and obtain information about the kinetics of the electrochemical system. The current response is given by the Cottrell equation for spherical electrodes[3,11].

$$i = nFAC_\infty \left(\left(\frac{D_o}{\pi t}\right)^{1/2} + \frac{D_o}{r_o}\right) \quad (2.4)$$

AC techniques:

Impedance spectroscopy is an AC technique that uses traverse function to describe the input and output relationship of time-variant system. The input and output signals of transverse function are generally expressed as a sum of sines and cosines[12,13]. Methods that use sinusoidal signals to analyze the current response were first employed to study fast electron transfer kinetics[9]. So, AC techniques have gained a tremendous importance in corrosion studies, where a complete analysis of the kinetics near the surface and in bulk is studied[3,9,12].

Electrochemical impedance theory is a well-developed branch electrochemical technique that describes the current response (I) of a circuit when an AC voltage source (V) is applied to probe the electrochemical system[9,12,13]. In DC theory (a special case where the frequency is 0 Hz), The resistance to the flow of electrons in an electrical system is defined by Ohm's law: $R = E/I$, where E is the applied dc source potential, I is the measured current and $R\,(ohm)$ is the resistance[3,9,12,13]. However, in AC theory where both E & I are a function of frequency, the equation analogous to Ohm's law is $E(\omega) = ZI(\omega)$, where Z is defined as impedance that describes the resistance to the flow of electrons as function of frequency. Unlike In dc circuits, resistors (R), capacitors(C) and inductors (L) resist the flow of electrons[12,13]. So, an electrochemical cell can be described using impedance by an AC voltage source, where the impedance is expressed as a circuit with a combination of resistors, capacitors, and inductors[3,13].

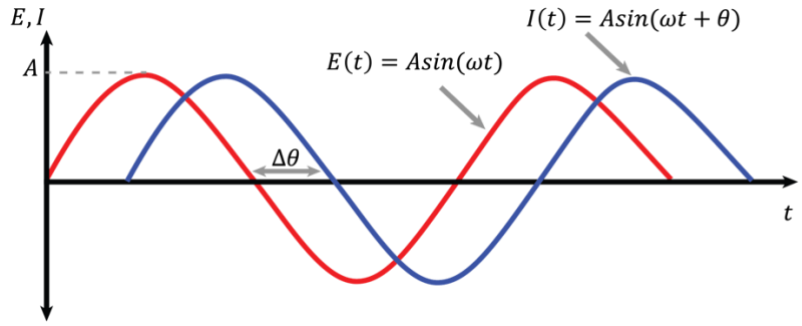

Figure 2.4. Waveforms for an ac potential and its resulting current across an arbitrary circuit., where $E(t)$ and $I(t)$ are ac potential and resulting current waveforms, A is the amplitude, and ø is the phase difference between the two waveforms, respectively[13].

Figure 2.4 shows the plot of a typical input and output signals across an arbitrary circuit (electrochemical cell), where A is the amplitude, ω is the frequency in radians ($\omega = 2\pi f$), t is the time period, and ø is the phase angle. Based on the recorded current response the impedance (Z) values of the electrical system for a range of frequencies are calculated. Impedance values are generally expressed in terms of complex numbers: $Z = Re(Z) + j\,Im(Z)$, where $j = \sqrt{-1}$ (to avoid confusion with current notation) and the phase angle is given by $tan\,\theta = Im(Z)/Re(Z)$. [12,13] The rear part of impedance $Re(Z)$ describes the resistive behaviors whereas the imaginary part $Im(Z)$ describes the capacitive and inductive behaviors associated with the system. These impedance behaviors can be represented with appropriate circuit elements in an equivalent circuit, and the circuits are designed to describe the electrochemical and physical behaviors associated with it, for example electrode/electrolyte reactions at the interface[3,12,13]. In the following sections we will discuss the common circuit elements used in electrochemical impedance spectroscopy (EIS) and some frequently seen equivalent circuits.

Circuit elements:

Table 2.1 Represents the circuit elements used to model the electrochemical circuit [12–14]

Circuit elements	Notation	Equation	Physical representation
	Resistance (R)	$Z_R = R + 0\,j,$	Solution resistance, circuit resistance etc.
	Capacitance (C)	$Z_C = 0 + 1/j\omega C, \omega = 2\pi f$ $\alpha = 1$	Represents an ideal capacitive element, e.g., electrical double layer.
	Inductance (L)	$Z_L = 0 + j\omega \mathrm{L},\ \omega = 2\pi f$	An element that lowers current flow but allows charge transfer.
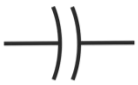	Constant phase element (Q)	$Z_Q = 0 + {}^{1}/_{\mathrm{Q}(j\omega)^{\alpha}},$ $\omega = 2\pi f$ and α = the ideality factor	Represents circuit elements with non-ideal behavior.
	Warburg impedance (W)	$Z_W = 0 + {}^{1}/_{\mathrm{Q}(j\omega)^{0.5}}, \omega = 2\pi f$	Resistance toward mass transfer
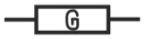	Gerischer phase element (G)	$Z_G = 0 + {}^{1}/_{\mathrm{Q}(\mathrm{K}+j\omega)^{0.5}}, \omega = 2\pi f$ K= equilibrium constant	Electrochemical reaction coupled with diffusion or (irreversible chemical reaction).

The impedance expressions for various circuit elements are shown in **Table 2.1**. Passive circuit elements do not generate any current or potential and are used to construct electrical circuits. A combination of resistors (R), capacitors(C) And inductors (L) can be used to make equivalent circuits representing the current responses. Resistors have no imaginary component, and the phase shift between the current and voltage is zero. So, current and impedance are independent of the frequency for a resistive element[12,13].

Conversely, the capacitor's impedance depends on both the frequency and capacitance. The current is always out of phase by π/2 for an ideal capacitor. As $C \propto 1/\omega$, meaning at high frequencies, the capacitor acts as a short circuit ($Z \to 0$), and at low frequencies, it is in an open circuit (i.e., $Z \to \infty$). Like a capacitor, the current flowing through the inductor is out of phase with

the voltage but by -π/2. Unlike capacitance, inductance (L) is proportional to frequency, so the impedance increases with frequency[9,12,13].

However, the impedance behavior of an electrochemical system cannot be completely captured only by using ideal resistors (R), capacitors(C) And inductors (L). To represent electrochemical specific behaviors, circuit elements like constant phase element (CPE), Warburg impedance (W), and Gerischer phase element (G) were created; these elements as they change with frequency and are most suited to represent non-ideal behavior of a system[9,12–14]. A constant phase element (CPE) is used to describe any non-ideal behavior of a capacitive or inductive element and can also improve the circuit model's fit. Warburg impedance (W)[12] and Gerischer phase element (G)[5] are special forms of *CPE* that represent the resistance offered by diffusion/ mass transfer and an electrochemical reaction coupled with diffusion, respectively. The relationship of impedance of circuit elements with frequency response is shown in **Table 2.1**

Equivalent circuits and representation

An electrochemical cell is essentially an impedance to a small sinusoidal signal; the impedance offered by the solution, electrode, chemical reactions, and mass transfer can be expressed as an equivalent circuit using a combination of circuit elements mentioned in Table 1. Macdonald says that equivalent circuits are more merely analogs, rather than models that describe an electrochemical system[16]. The impedance responses of the system and equivalent circuit represented by plotting the real ($Re(Z(\omega))$) and imaginary ($Im(Z(\omega))$) components of impedance from high to low frequency (i.e., from right to left respectively). This plot of $Re(Z)\ vs. Im(Z)$ is called a Nyquist plot and is a popular format for evaluating the electrochemical impedance behavior[12,13]. Alternative representations to study impedance include 'Nyquist admittance', 'Bode plot', and 'Bode admittance' [13]. **Figure 2.5.** shows some of the frequently used equivalent circuits

and its corresponding impedance behaviors (Nyquist plot) in the literature. The equivalent circuits are built based on the impedance response. Also, an equation for impedance of the equivalent circuit can be derived mathematically using impedance circuit elements.

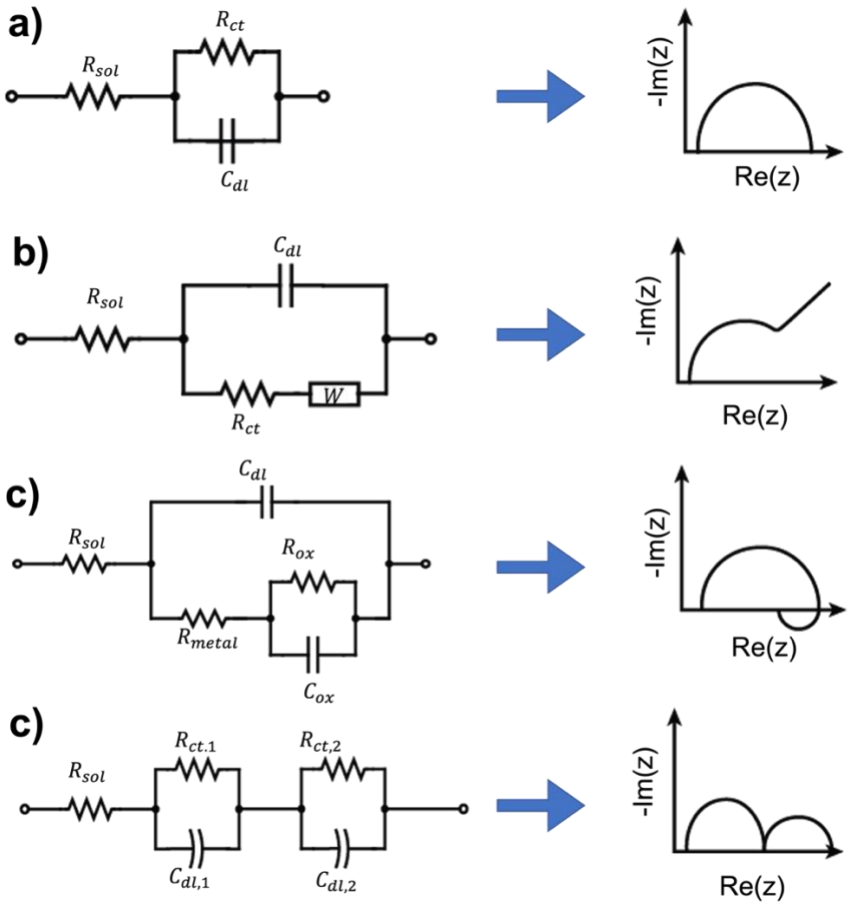

Figure 2.5 shows the most common equivalent circuits used for the EIS. a) Randels circuit[13], b) a Mixed kinetic and diffusion control circuit [12], c) Ladder circuit [9] and d) Voigt circuit[12] with their corresponding impedance behaviors represented by Nyquist diagrams.

Figure 2.5a Shows the Randels equivalent circuit and its respective Nyquist plot. This circuit often describes the electrode/electrolyte interface[9,12,13]. The current flowing at an electrified interface due to an electrochemical reaction always contain both faradic and non-faradic components[15]. The faradic component is due the charge transferred via a reaction by overcoming a potential barrier (R_{ct}) along with the solution resistance is given by a resistor (R_{sol}), while the

non-faradic component arises from charging the electrical double layer C_{dl}. The circuit elements in Randel's circuit can easily be equated to familiar physical phenomena such as adsorption or film formation and a semicircle trend in the Nyquist plot indicates a capacitive loop that represents the impedance behavior of a typical Randels circuit[13,15]. **Figure 2.5b.** shows an equivalent circuit for Mixed kinetic and diffusion control behavior; this circuit describes the electrode/electrolyte interface that has a mass transport element associated with the reactions at the interface[12]. So, an additional element called Warberg element is added the Randell's circuit to represent the mass transport (diffusion) phenomena. The impedance response in the Nyquist plot shows a straight line with a $45^{\cdot}$ slope in the low frequency region. The straight line is present in the low-frequency region, indicates a mixed phenomenon due to reaction kinetics and diffusion[9,12,13].

Ladder equivalent circuit shown by **Figure 2.5c.** often describes a corrosion of the electrode surface (pitting behavior)[9,12]. The Nyquist plot for this circuit has negative capacitance loop (also called inductive loop) in the low frequency region and this impedance behavior is typically observed in systems where the surface of the electrode experiences a change on its surface or near the electrode/oxide interface. **Figure 2.5d.** describes a Voigt circuit, this circuit is used to model the existence of a second (or incomplete) film formations or adsorbed interface[12], each existing film present on the surface is represented by a RC circuit in series with the solution resistance. The Nyquist plot shows the impedance behavior of this system as dual capacitance loops (i.e., A second capacitance loop in the low frequency region).

Diagnostic criteria and the determination of the equivalent circuit

Based on the trends in the Nyquist plot, a suitable equivalent circuit model that can model the impedance data can be built. It is possible to have more than one explanation (i.e., one electrical circuit) for a particular observation, as the transfer function approach is universal and can be

applied to various mechanical, electrical, and optical systems[12,13]. A good equivalent circuit should equate its circuit elements to the physical or chemical aspects of the electrochemical system. Finally, the measured impedance data needs to be validated before analysis.

Kramers-Kronig (K-K) analysis, relations are used to evaluate the quality of impedance data. K-K relations works on the principle that there is dependence between magnitude and phase [4,12,13]. For impedance data to satisfy K-K relations the data must be linear, causal, and stable; but K-K transform requires integration of frequency from 0 to infinity. Hence, evaluation of K-K relations using integration is not practical (as the spectral range need to evaluate this data is not generally measured). K-K analysis in practice is done by fitting a series of Voigt circuit proposed by [17] to the spectral data (**Figure 2.6**). The Voigt circuit is made up of a resistance in series with 'm' Voigt elements, and Voigt elements is a resistor in parallel with a capacitor. The parameter m depends on the number of data points in the complex plane. The measured impedance data points are fit for modeling if they are compliant with the K-K analysis[4].

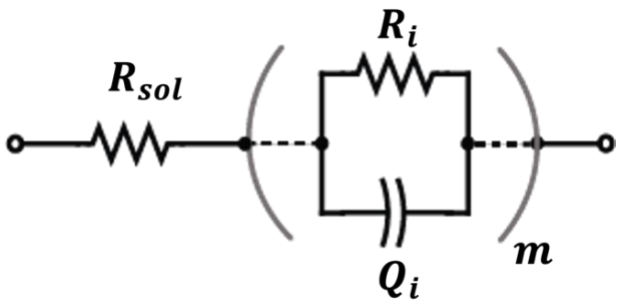

Figure 2.6 Shows the Voigt equivalent circuit used for Kramers-Kronig (K-K) analysis. Where *m* Voigt elements are present and $2 < n < m$ [4,13,17].

Impedance data modeling, All the impedance spectra analysis are performed using EC-lab software has a tool called Z- fit. For a given equivalent circuit, all the circuit element parameters are assigned initial random values using a randomizer, and the error (χ^2) between the experimental and the estimated impedance is minimized. The best set of parameter values are the

values that yield low χ^2 (error) and are consistent with its physical attributes. χ^2 gives the estimated difference between the real data and simulated data, assuming the standard deviation σ is constant for each frequency value. the expression for χ^2 is given by:[4]

$$\chi^2 = \sum_{i=1}^{n} \frac{|Z_{meas}(i) - Z_{simul}(f_i, p)|^2}{\sigma_i^2} \tag{2.5}$$

Where, $Z_{meas}(i)$ is the measured impedance at the frequency f_i, $Z_{simul}(f_i, p)$ is the estimated impedance for the circuit model, f_i is the i^{th} frequency, p is the circuit element used in the model (such as R_{ct},R_{sol}, C_{dl} …) and σ_i is the standard deviation.

The tool contains three minimization methods for minimizing χ^2, as follows: (1). *Randomization* (the software picks random values for parameters and minimize χ^2), this method is mostly used to find the initial values for further minimization (2). *Simplex* method, this method is mostly used to minimize linear functions, and (3). *Levenberg-Marquardt* method, used for non-linear minimization, and often used for linear squares problems [4].

We use the randomization function in the Z- fit tool that assigns random values to the circuit parameters to yield low χ^2 (error), and subsequently use *Levenberg-Marquardt* minimization method to find the model that fits best our equivalent circuit[4]. A parameter called dev is calculated using *Levenberg-Marquardt* minimization algorithm provides an estimate of the relevancy of the circuit parameters used in an equivalent circuit, a high dev value means the variation of the parameter value is high and the absence of the parameter will not affect the fit of the circuit model. it also means that the said parameter is not critical to the minimization process and can be omitted form the equivalent circuit model[4].

References

(1) Song, M. Interfacial Tension Modulation of Liquid Metal via Electrochemical Oxidation and Its Application. Doctor of Philosophy, North Carolina State University, Raleigh, 2020.

(2) Song, M.; Daniels, K. E.; Kiani, A.; Rashid-Nadimi, S.; Dickey, M. D. Interfacial Tension Modulation of Liquid Metal via Electrochemical Oxidation. *Advanced Intelligent Systems* **2021**, *3* (8), 2100024. https://doi.org/10.1002/aisy.202100024.

(3) Allen J. Bard and Larry R. Faulkner, Electrochemical Methods: Fundamentals and Applications, New York: Wiley, 2001, 2nd Ed. *Russian Journal of Electrochemistry* **2002**, *38* (12), 1364–1365. https://doi.org/10.1023/A:1021637209564.

(4) BioLogic (2017). Potentiostat: BT-Lab & EC-Lab software Analysis and Data Process manual, France. MA: Author.

(5) Hutzler, S.; Ryan-Purcell, J. C. F.; Dunne, F. F.; Weaire, D. A Simple Formula for the Estimation of Surface Tension from Two Length Measurements for a Sessile or Pendant Drop. *Philosophical Magazine Letters* **2018**, *98* (1), 9–16. https://doi.org/10.1080/09500839.2018.1434320.

(6) Okumura, K. Continuum Mechanics and Its Practical Applications at the Level of Scaling Laws. In *Encyclopedia of Biomedical Engineering*; Narayan, R., Ed.; Elsevier: Oxford, 2019; pp 111–118. https://doi.org/10.1016/B978-0-12-801238-3.99927-6.

(7) Khan, M. R.; Eaker, C. B.; Bowden, E. F.; Dickey, M. D. Giant and Switchable Surface Activity of Liquid Metal via Surface Oxidation. *Proc Natl Acad Sci USA* **2014**, *111* (39), 14047–14051. https://doi.org/10.1073/pnas.1412227111.

(8) Kingston, C.; Palkowitz, M. D.; Takahira, Y.; Vantourout, J. C.; Peters, B. K.; Kawamata, Y.; Baran, P. S. A Survival Guide for the "Electro-Curious." *Acc. Chem. Res.* **2020**, *53* (1), 72–83. https://doi.org/10.1021/acs.accounts.9b00539.

(9) Pletcher, D.; Greff, R.; Peat, R.; Peter, L. M.; Robinson, J. *Instrumental Methods in Electrochemistry*; Chemical Science; Elsevier Science, 2001.

(10) Kingston, C.; Palkowitz, M. D.; Takahira, Y.; Vantourout, J. C.; Peters, B. K.; Kawamata, Y.; Baran, P. S. A Survival Guide for the "Electro-Curious." *Acc. Chem. Res.* **2019**. https://doi.org/10.1021/acs.accounts.9b00539.

(11) Bansal, N. P.; Plambeck, J. A. An Aid to the Interpretation of Electrochemical Data Measured with Spherical and Cylindrical Electrodes: Corrections to the Cottrell Equation. *Can. J. Chem.* **1978**, *56* (2), 155–156. https://doi.org/10.1139/v78-024.

(12) Orazem, M. E.; Tribollet, B. *Electrochemical Impedance Spectroscopy*; The ECS Series of Texts and Monographs; Wiley, 2017.

(13) Basics-of-EIS, Application Note Rev. 1.0 9/3/2010 @ Copyright 1990-2009 Gamry Instruments, Inc.

(14) Boukamp, B.; Bouwmeester, H. Interpretation of the Gerischer Impedance in Solid State Ionics. *Solid State Ionics* **2003**, *157*, 29–33. https://doi.org/10.1016/S0167-2738(02)00185-6.

(15) Chang, B.-Y.; Park, S.-M. Electrochemical Impedance Spectroscopy. *Annual Rev. Anal. Chem.* **2010**, *3* (1), 207–229. https://doi.org/10.1146/annurev.anchem.012809.102211.

(16) Macdonald, D. D. Reflections on the History of Electrochemical Impedance Spectroscopy. *Electrochimica Acta* **2006**, *51* (8), 1376–1388. https://doi.org/10.1016/j.electacta.2005.02.107.

(17) Boukamp, B. A. A Linear Kronig-Kramers Transform Test for Immittance Data Validation. *Journal of The Electrochemical Society* **1995**, *142* (6), 1885–1894. https://doi.org/10.1149/1.2044210.

Chapter 3 : Role of Electrochemistry on the Interfacial Phenomena of Eutectic Gallium Indium

Abstract:

The electrochemical oxidation of gallium-based liquid metals decreases its interfacial tension dramatically[1,2]. This chapter discusses the electrochemistry of liquid metals (eutectic gallium indium) in sodium hydroxide solution to elucidate the species formed on the surface as a function of potential and how these surface species affect interfacial tension. This chapter provides insights into the surface oxide species such as GaOOH and $Ga(OH)_4^-$, that can be controlled electrochemically to manipulate the interfacial tension.

Introduction:

The electrochemistry of Ga and its alloys is important for a variety of reasons. Liquid metals have been utilized as electrodes in batteries and capacitors for quite some time now[3,4] , as a replacement for mercury in an electrochemical technique known as polarography, however Ga is normally avoided due to its reactivity[5]. Finally, electrochemical processes can deposit or remove species from a liquid metal's surface. Furthermore, electrochemical oxidation of liquid gallium significantly lowers its interfacial tension[1,6].. This final phenomenon prompted the research reported here, as it is critical to quantify what is known about the liquid metals contact.

The electrochemistry of Ga and its alloys is important for a variety of reasons. Liquid metals have been utilized as electrodes in batteries and capacitors for quite some time now[3,4] , as a replacement for mercury in an electrochemical technique known as polarography, however Ga is normally avoided due to its reactivity[5]. Finally, electrochemical processes can deposit or remove species from a liquid metal's surface. Furthermore, electrochemical oxidation of liquid gallium significantly lowers its interfacial tension[1,6]. This final phenomenon prompted the research reported here, as it is critical to quantify what is known about the liquid metals contact.

In the absence of oxide skin, liquid metals have high surface tension, ~ 624 mN/m[7,8] in vacuum and ~500 mN/m in NaOH[1]. Electrochemistry offers a compelling way to remove and deposit oxide layers, thereby modulating the interfacial tension[9–11]. Sufficiently reductive potentials can keep the liquid metal oxide-free by reducing the oxide layer to metallic gallium, putting the bare metal in a state of high tension[12]. However, applying oxidizing potentials have been found to drive surface oxidation thereby lowering the interfacial tension as a function of potential[2]. Remarkably, the tension decreases from ~500 mN/m (bare metal) to near zero at ≈ 0.8 V (vs. OCP). This low tension causes spherical droplets to undergo instabilities to form highly fingered fractals [13], streams of liquid metal to form stable cylinders[6], and other unusual morphologies. These enormous tension changes have been used to manipulate liquid[14] in applications such as soft actuators [15].

The specific reason for this decrease in interfacial tension remains a topic of ongoing investigation. We previously showed that the electrocapillarity equation (**equation 1.1**) is insufficient to explain the enormous drop in effective interfacial tension of an eGaIn in alkaline solution[2]. However, it has been speculated that the presence of surface oxides contributes significantly to this decrease in effective interfacial tension[1]. Furthermore, there are multiple reaction mechanism that claim the existence of different oxide species on the surface of a gallium electrode[16–19]. As a step toward better understanding this phenomenon, we study the electrochemistry of eGaIn during electro-oxidation to understand what species form on the surface as a function of potential in this chapter.

Electrochemistry of Gallium:

In air, the interface of Ga-based liquid metals rapidly forms a thin oxide skin consisting of amorphous or poorly crystallized Ga_2O_3[7], although in an aqueous environment (neutral solution),

the surface oxide becomes GaOOH [20,21]. In alkaline solutions, the native oxide film dissolves into soluble gallates. The most stable oxidative state of gallium is 3+, corresponding to the gallates in basic solution and the solvated Ga^{3+} in acidic solution. In aqueous solutions, gallium species such as Ga^{3+}, $Ga(OH)^{2+}$, GaO^{+}, GaO_2^{-}, $H_2GaO_3^{-}$, $Ga(OH)_4^{-}$, $HGaO_3^{2-}$, and GaO_3^{3-} may exist; the composition and concentration of these oxides depend on the pH of the solution[22] . The Pourbaix diagram suggests the possible equilibrium states of gallium species for the Ga^{3+} in aqueous state (**Figure 3.1**).

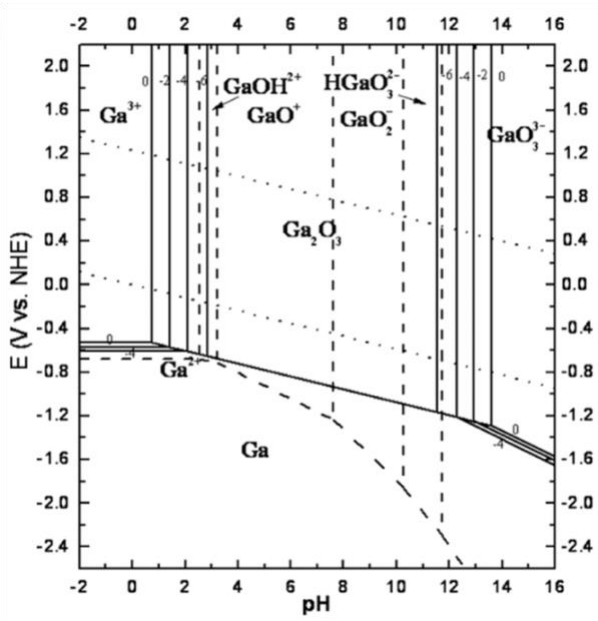

Figure 3.1. Potential vs. pH equilibrium diagram (Pourbaix diagram) at 25˚C for gallium in aqueous solutions.[23]

The following reactions have been suggested for gallium oxidation in an alkaline solution based on the Pourbaix diagram[23]. Gallium metal in aqueous solutions forms $Ga(OH)_3$, and the resulting $Ga(OH)_3$ can lose water to form hydrated gallium-oxyhydroxide (GaOOH) or dry gallium oxides (Ga_2O_3); These gallium oxides dissolve in basic solutions by forming water-soluble gallates[23–25].

$$Ga + 3OH^- \rightleftharpoons Ga(OH)_3 + 3e^- \quad (1)$$

$$Ga + 3OH^- \rightleftharpoons GaOOH + H_2O + 3e^- \quad (2)$$

$$2Ga + 6OH^- \rightleftharpoons Ga_2O_3 + 3H_2O + 3e^- \quad (3)$$

$$Ga_2O_3 + 3H_2O + 2OH^- \rightleftharpoons 2Ga(OH)_4^- \quad (4)$$

There have been several previous investigations on the electrochemistry of pure gallium in both solid and liquid form[26]. All previous studies agree with the presence of a passivation film during the electro-oxidation in alkaline solution; however, the composition of this film is still under debate. One study [17] reported that in basic solutions, the anodic films consist of gallium-oxyhydroxide ($GaOOH$), while another[27] proposes gallium oxide (Ga_2O_3) or gallium hydroxide ($Ga(OH)_3$ at the surface of gallium.

Later studies [16,18] of the anodic oxidation of gallium presume that a passive Ga_2O_3 layer forms in a small potential window, and at higher potentials, the reaction product (GaO_3^{3-}) formed might be dissolved in the solution. Cyclic voltammetric studies of gallium films [19] in alkaline solution within a limited potential window show three oxidation peaks in forward scan and one reduction peak during the backward scan, leading the authors to attribute the first oxidation peak to the formation of a monolayer of gallium oxide and present an electrochemical mechanism based on the formation of gallium sub-oxide (Ga_2O) and a disproportionation reaction. These contradictory proposals for reactions and mechanisms highlight that the electrochemical behavior of Ga-based liquid metal remains poorly understood. Here, we seek to revisit the electrochemistry of liquid Ga within the context of the recent discovery of the role of electrochemical oxidation on effective interfacial tension in 1M NaOH.

Results and Discussion:

Figure 3.2a shows the LSV of a 0.1 ml eGaIn electrode in 1 M NaOH. We observe three oxidation peaks in the LSV plot and are labeled as P_1, P_2, P_3, respectively. Based on these oxidation peaks in **Figure 3.2a**, the electro-oxidation mechanism of eGaIn can be divided into five distinct regimes, namely '*cathodic protection*', '*oxidizing*', '*passivation*', '*passivation breakdown*', and 'partial re-passivation', separated by color (gray, blue, orange, green, purple, respectively).

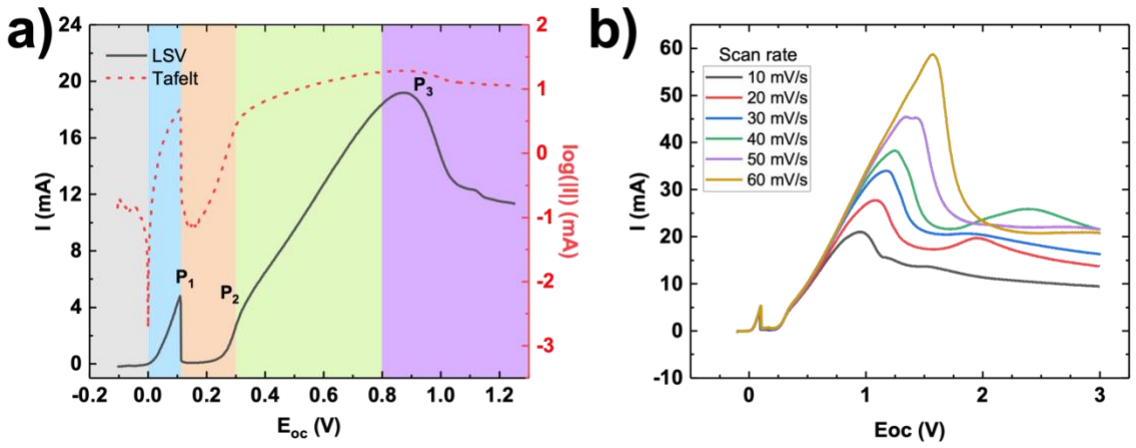

Figure 3.2. Linear sweep voltammograms of liquid metal (eGaIn) in 1M NaOH measured using a potentiostat. a) A linear sweep voltammogram (solid black line) with corresponding logarithmic plots of current (dotted red) at 1 mV/s, where, the various oxidation regimes are labeled by color as cathodic protection (grey), oxidizing (blue), passivation (orange), passivation breakdown (green) and partial re-passivation (purple) regimes, respectively and b) Linear sweep voltammograms at different scan rates to show the shift of P3 peak.

At *E < 0 V (OCP)*, the liquid metal surface is free of any passivating oxide, as applying a reductive potential keeps the surface of the metal oxide-free. Thus, we call this regime *'cathodic protection'* or 'non-oxidizing regime'. When a potential larger than OCP is applied *(E > 0 V)*, a distinct oxidation peak (P_1) appears followed by a sudden drop in the current near 0.1 V. This sudden drop in current is attributed to the formation of a thin oxide film that blocks electrochemical reactions; hence we call this regime *'oxidation regime'*. Increasing the electrode potential causes the OH- ions in the bulk move to the surface of the electrode leading to forming either $Ga(OH)_3$

or Ga_2O_3 or GaOOH as the oxide film, since Ga^{3+} is the more stable oxidation state. The low potential scan rate provides a large time scale to form the most stable oxides. Although most gallium oxides are soluble in alkaline solution, the oxidative potential appears to help hold the oxide layer in place, perhaps the negatively charged gallate species near the oxide surface prevents OH^- groups from dissolving the oxide. The decrease in the current response marks the end of the oxidation regime as the oxide film is suspected to be completely formed.

In the potential range $0.1\ V < E < 0.3\ V$, the presence of low current suggests the absence of significant electrochemical reactions and the presence of a passive oxide layer. Hence, this regime is termed as 'passivation regime'. By applying a considerably large potential in this regime, the concentration of OH^-near the electrolyte/passive film interface increases; thus, compensating the positive charge of the liquid metal electrode. The presence of OH^- at the proximity to the electrode surface may further lead to the formation of gallates, so we reason that the composition of the surface oxide in this regime may change. The Tafel plot also shows an increase in logarithmic current at ~0.20 V suggesting that increasing the potential further leads to the breakdown or reconstruction of the surface oxide film (i.e., loss of passivation). Additionally, Additionally, A previous study about gallium speciation in aqueous solutions has reported an equilibrium constant of 0.692 for **reaction 5**[25.]

$$GaOOH_{surf} + H_2O + OH^- \rightleftharpoons 2Ga(OH)_4^- \qquad K_5 = \frac{[Ga(OH)_4^-]^2}{[GaOOH_{surf}][OH^-]} = 0.692 \qquad (5)$$

This expression implies that when the concentration of OH^- in the vicinity of the surface is 1.445 M (pH≈14.16), the surface concentrations of reactants ($GaOOH_{surf}$) and products ($Ga(OH)_4^-$) are equal. This value has also been experimentally derived and was found to be ~ 14.3. which is consistent with the literature (the details of this experiment will be discussed in the later

section). At pH below 14.16, GaOOH is precipitated on the electrode surface and is the dominant surface oxide species; when at pH above 14.16, GaOOH dissolves as soluble $Ga(OH)_4^-$.

Applying a larger potential presumably increases the accumulation of OH^- ions at the surface (surface pH increases). Consequently, we reason that **reaction 5** operates in reverse direction converting the solid GaOOH oxide on the surface to soluble $Ga(OH)_4^-$, causing the increase in current at E ≈ 0.20 V plot as seen in Tafel plot **Figure 3.2a,** and further leading to a second oxidation peak (P_2) at $E \approx 0.30\ V$. For this reason, we call this regime *'passivation breakdown'* (within the range $0.30\ V \leq E \leq 0.80\ V$). We speculate that, the high concentration of OH^- ions near the electrode surface forms $Ga(OH)_3$ and they in turn react with NaOH to form soluble gallates according to **reaction 6** [24].

$$Ga(OH)_3 + OH^- \rightleftharpoons Ga(OH)_4^- \qquad K_6 = \frac{[Ga(OH)_4^-]}{[Ga(OH)_3]_{surf}[OH^-]} = 1.408 \times 10^7 \qquad (6)$$

The current increases with increase in the applied potential for potentials greater than. 0.8 V. Additionally, the electrode surface remains shiny and fluid for E < 0.8 V, meaning the oxidation produces soluble gallates (the oxide does not form a thick shell in this regime). This observation further supports our hypothesis regarding the formation of soluble gallates.

As $E > 0.8\ V$ is applied, the current increases with increase in the applied potential and a third oxidation peak (P_3) is observed at E ≈ 0.90 V. In Addition to the increase in oxide thickness, its texture changes form shiny to matte and is recognizable to the naked eye. Hence, this regime is termed as *'partial re-passivation'*. The peak currents of P_1 and P_3 measured from in **Figure 3.2b** shows a linear relationship with the square root scan rate while shows a linear relationship with scan rate. This relationship (shown in **Figure 3.3**)provides evidence that the reaction mechanism in the *oxidation regime* (near peak P_1) is diffusion controlled whereas the mechanism in *passivation breakdown regime* (near peak P_3) is adsorption controlled [28]; as the gallate anions may

get electrostatically attracted and are most likely to get adsorbed to the surface of the eGaIn electrode. At high potentials (E > 0.90 V), the negatively charged anions repel the OH^- anions and prevent them from reaching the eGaIn surface and thereby reducing the surface pH, hence the decrease in current.

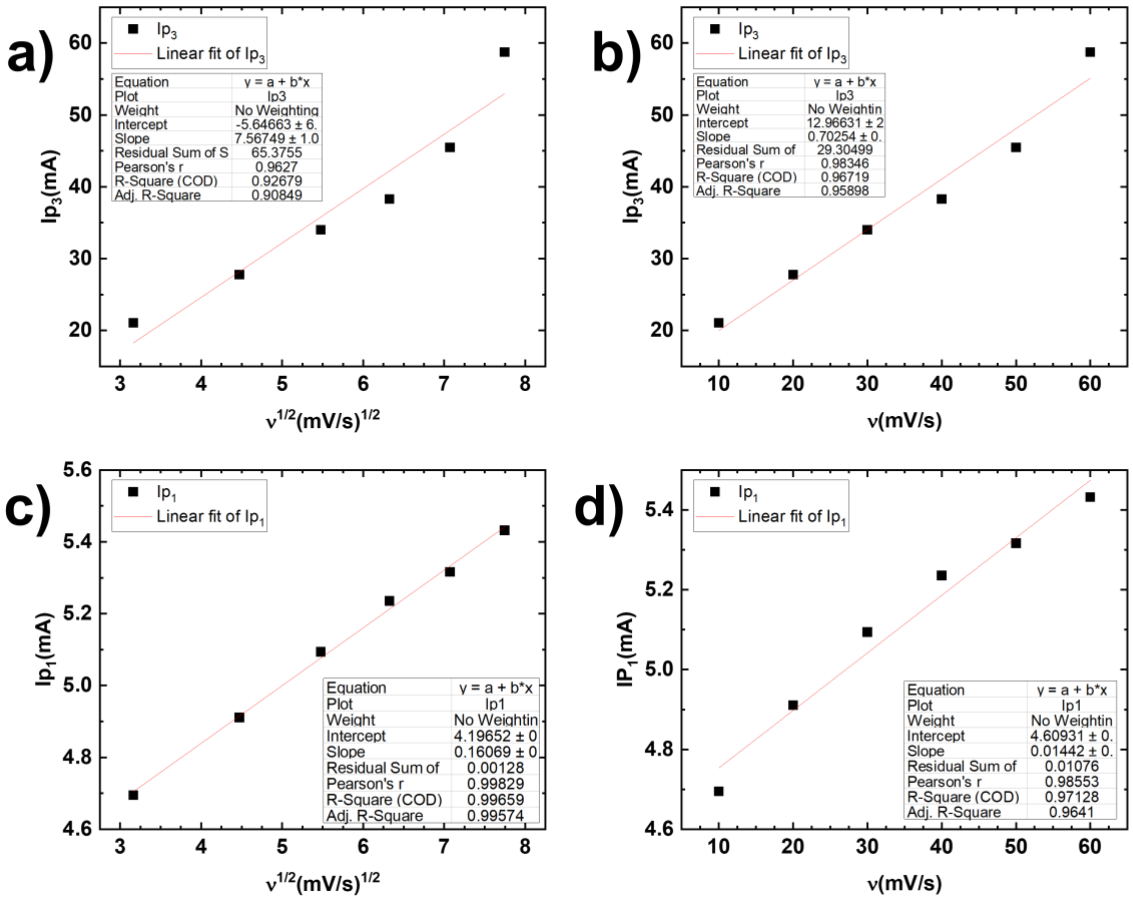

Figure 3.3 The plots of current (I_{P3}) at peak P_3 vs. (a) square root of potential scan rate and (b) potential scan rate, and current (I_{P1}) at peak P_1 vs. (c) square root of potential scan rate and (d) potential scan rate. The current fit shows a linear relationship with the scan rate for peak P_3, which suggests the electrochemical reaction is controlled by the adsorption at the interface of some species, while the current for peak P_1 shows a linear relationship with the square root of scan rate, that suggests a diffusion-controlled behavior.

An alternative mechanism that could deplete OH^- from the surface: At high electrical currents, the rate of consumption of OH^- anions in the electro-oxidation reaction is more than the rate of diffusion of fresh OH^- from solution. This lowers the surface pH at the eGaIn electrode

compared to the bulk of the electrolyte. If the surface pH decreases, the formation of GaOOH becomes more favorable. Additionally, the reaction pathway for **reactions 5** and **6** proceed in the reverse direction (i.e., formation of GaOOH and $Ga(OH)_3$ near the potential that corresponds to the peak formation). Since $K_5 \ll K_6$, at a lower surface pH the formation of GaOOH is more favorable than $Ga(OH)_3$. In other words, a fraction of adsorbed gallate anions converts to poorly soluble species such as GaOOH and $Ga(OH)_3$, and may be the reason for the matte appearance of the eGaIn electrode at potentials larger the 0.8 V. Peak P_3 shows a partial re-passivation behavior; the electric current decreases slightly but the species on the surface do not entirely block the oxidation reaction.

Although we speculate on the electrochemistry using LSV data, it cannot be used to identify the chemical composition of the species. However, we will present a mechanism for the oxidation of the eGaIn electrode based on cyclic voltammetric data discussed below.

The oxide film formation and breakdown mechanism:

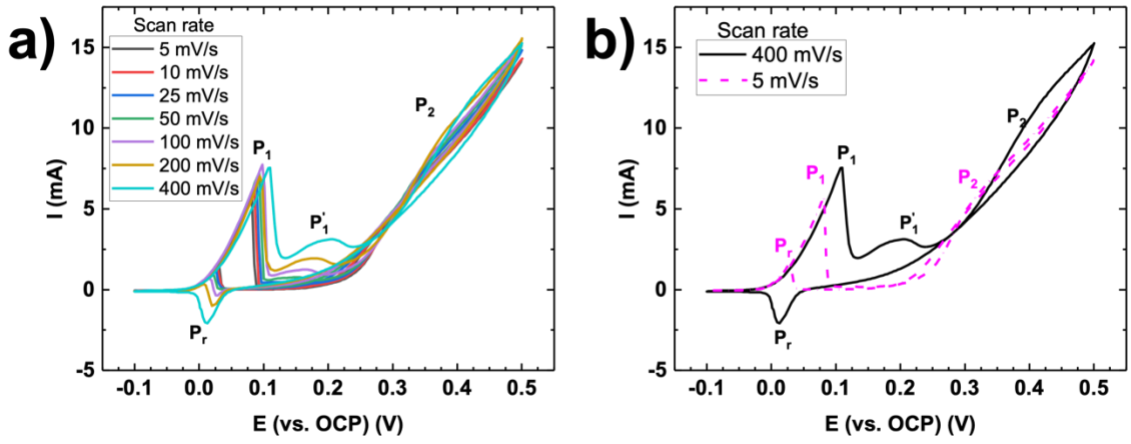

Figure 3.4 Shows Cyclic voltammogram of 0.1ml eGaIn electrode for a potential scan rate of a) 5-400 mV/s and b) 400 mV/s (black) and 5 mV/s (magenta) in 1M NaOH.

To understand the mechanism of the passive film formation and breakdown, we performed cyclic voltammetry at various scan rates in 1M NaOH, **Figure 3.4a**. Overall, the oxidation

behavior for all scan rates is similar. However, at the higher scan rates, the cyclic voltammogram broadens along the potential axis, and peak potentials shift to higher potentials which could be due to the ohmic drop (IR drop) between the electrodes. At higher scan rates, in addition to the P'_1 oxidation peak, which occurs near ~0.2 V in the forward sweep, a reduction peak (P_r) is observed in the backward potential scan. One reduction peak (P_r) for the three oxidation peaks (P_1, P_2 & P_3) suggests that the oxidation products formed are irreversible and cannot be reduced. This behavior depends on the potential scan rate. Electrochemical oxidation rate increases with an increased potential scan rate, while the chemical dissolution rate does not change. Thus, we reason that gallates dissolve in the NaOH before they can be reduced during the reverse scan. At fast scan rates, oxidation products accumulate at the electrode surface, and need a higher electrical potential to completely form an oxide film. Consequently, the peak potentials shift to higher potentials due to a declining effect of dissolution reaction at higher scan rates [28].

In **Figure 3.4b**, the cyclic voltammogram shows a noticeable difference between the high (400 mV/s) and low (5 mV/s) potential scan rates. At large scan rates, only one small reduction peak is evident during the backward potential scan; we attribute the peak (P_r) to the reduction of the remaining gallium oxide species on the surface. However, at low scan rates, there is no reduction peak (P_r). Instead, an oxidation peak appears in the backward scan near $E \approx 0.025$ V for a scan rate of 5 mV/s. This finding is surprising because cathodic scans typically yield cathodic (reductive or negative) current peaks. At high potential scan rates (short time scale), there is not enough time to completely dissolve and/or convert the deposited oxide layer to the hydroxide species. Consequently, there are oxide species present on the surface does not get reduced completely during the backward scan. In contrast, at low potential scan rates, the surface oxide is converted to a layer of soluble gallate anions that cannot be reduced during the backward scan. We

speculate that the surface concentration of adsorbed anions decreases during the cathodic scan, which allows the exposed metal surface to oxidize again at favorable potentials (0.075 V).

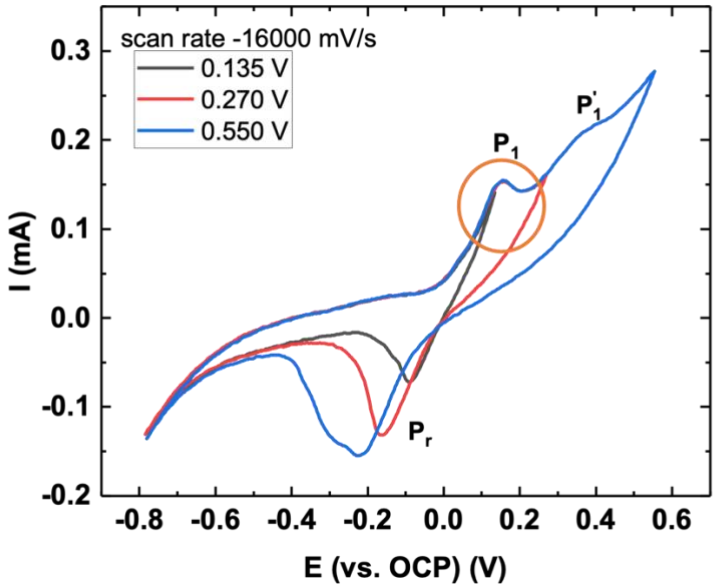

Figure 3.5 Shows a fast scan cyclic voltammograms of eGaIn recorded in three different potential windows; for a 25µl eGaIn electrode at the scan rate of 16000 mV/s in 1M NaOH. data contribution: Dr. Sahar Nadmi.

Figure 3.5. shows high speed cyclic voltammograms of eGaIn recorded in three different potential windows. Fast scan Cyclic voltammetry at different potential windows provide insights about the electron transfer mechanism, especially the difference between the electrochemical reactions and chemical reactions. Firstly, As the potential window for the scan becomes wider, we observe the current intensity of the reduction peak (P_r) to increases. This observation implies that oxidized species produced at both P_1 and P'_1 contribute to the formation of reduction peak at P_r. Second, we note that a small shoulder (within the orange circle in **Figure 3.5**) appears before the first oxidation peak (P_1). The shoulder and P_1 peak current ratios suggest that each of them involves one step for a net transfer of two electrons. The relationship of peak current with scan rate (Radles-Sevcik equation) is shown in **equation 2.3**. We reason that the shoulder and peak (P_1) are attributed to the $Ga \rightarrow Ga^{+}$ (Reaction 7) and $Ga^{+} \rightarrow Ga^{2+}$(Reaction 8) reactions steps

respectively. Peak P'_1 is the final electron transfer step $Ga^{2+} to\ Ga^{3+}$(Reactions 9 or 10 of Ga electro-oxidation).

Thus, it can be reasoned that the electro-oxidation of gallium consists of three electron transfer steps showing chemical reversibility only at very high scan rates of potential. GaOH (**Reactions 7**) is unstable and is only detected at higher scan rates (**Figure 3.5**). $Ga(OH)_2$ also is an unstable intermediate that reacts chemically to convert to a stable oxidation product either Ga_2O_3or GaOOH through a disproportionation reaction, as these are the most stable gallium solid phase in Ga-O-H system at saturated water vapor pressure below 573 K[29].

$$2Ga + OH^- \rightleftharpoons GaOH + e^- \quad (7)$$

$$GaOH + OH^- \rightleftharpoons Ga(OH)_2 + e^- \quad (8)$$

$$2Ga(OH)_2 + 2OH^- \rightleftharpoons Ga_2O_3 + 3H_2O + 2e^- \quad (9)$$

$$Ga(OH)_2 + OH^- \rightleftharpoons GaOOH + H_2O + e^- \quad (10)$$

Reaction 9 assumes that gallium hydroxide loses water molecules to form gallium oxide at the final step of oxidation. However, some studies have reported that gallium oxide hydroxide (GaOOH), is also a stable gallium oxidation product, especially in neutral and alkaline media [23–25,29].

Increasing the potential scan rate for eGaIn electrode (**Figure 3.4a**) increases the current of the second oxidation peak (P'_1). This peak can be attributed to the oxidation of $Ga(OH)_2$ to the more stable GaOOH. Because Ga^{2+} is an unstable state of Ga, it can only be observed at the highest scan rates (smaller time scales). However, at lower scan rates $Ga(OH)_2$ undergoes a chemical reaction (as opposed to the electrochemical reaction) to form GaOOH. A proposed reaction for P'_1 that is consistent with the data is the chemical disproportionation of $Ga(OH)_2$to produce both metallic gallium and GaOOH.

$$3Ga(OH)_2 \rightleftharpoons Ga(M) + 2GaOOH + H_2O \quad (13)$$

At very low scan rates, almost all $Ga(OH)_2$ formed in reaction step P_1 converts chemically to Ga and GaOOH. This observation is consistent with the absence of P'_1 peak at slow scan rates. This disproportionation mechanism is also consistent with prior reports . In most of the reported mechanisms for electro-oxidation of gallium, Ga^+ has been suggested as the disproportioned species. However, high-speed voltammetry data shows that Ga^{2+} is the main species contributing to the disproportionation reaction, which is sensible considering it is the least stable form of Ga. At high potential scan rates, chemical **reaction 13** cannot progress fast enough and thus converts $Ga(OH)_2$ to GaOOH electrochemically; consequently, the P'_1 peak grows. Since GaOOH can be reduced to metallic Ga electrochemically, its reduction peak appears during the cathodic sweep. It is difficult to confirm this claim chemically as the surface species dissolve immediately in the absence of potential. **Schematic 1** shows proposed electro-oxidation process and the attributed reactions with each regime.

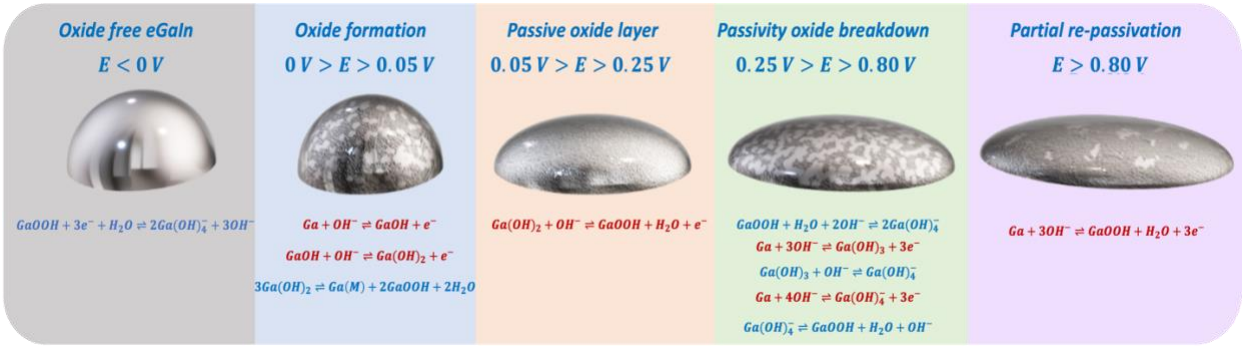

Schematic 1: Proposed mechanism for eGaIn passive film formation and breakdown. Here reactions and potentials have been reported based on the potential scan rate of 1 mV/s. Reactions in red occur electrochemically and reactions in blue occur chemically.

Effect of pH on oxidation mechanism:

The concentration of hydroxide anions plays a crucial role that affects the surface chemistry of the electrode. Thus, at high concentrations of NaOH we expect the film formation and breakdown to be favorable than at low concentrations. To test this hypothesis, we measured cyclic

voltammograms at different NaOH concentrations, **Figure 3.6**. Increasing the concentration of NaOH shows an increase in the oxidation current, as at high concentrations (or high pH) the NaOH dissolving oxide species on the surface thereby exposing the more reactive metal surface. Additionally, the oxidation peaks (P_1, P'_1, P_2) shift to the right for lower electrolyte concentrations. This suggests that the passive film formation is more favorable at higher concentrations. Furthermore, the passive film breakdown (P_2) occurs at smaller oxidative potentials as increasing the OH^- concentrations favor formation of soluble gallates. For concentrations smaller than 0.1 M, the cyclic voltammograms show a significant change in their shape, suggesting that the oxide mechanism changes as the bulk pH drops by an order of magnitude

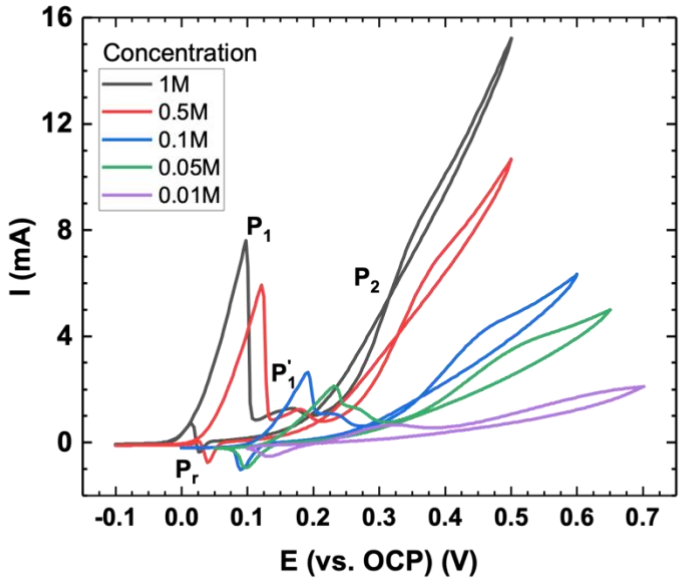

Figure 3.6. Shows the cyclic voltammogram of 0.1 ml eGaIn droplet with a potential scan rate of 100mV/s in various NaOH concentrations. Note: The potential scale is scaled with respective to open circuit potential of 1M NaOH (-1.5 V vs. Ag|AgCl|(3M KCl))

In contrast to the peaks P_1 and P_2, the peak P_3 shifts to the left as the OH^- concentration decreases, shown in the Error! Reference source not found.. At higher concentrations of NaOH, a larger potential is required to reach the diffusion limited state where the OH- ions near the electrode surface is depleted, also called as partial re-passivation.

Estimation of acidic dissolution constant (pK_a):

Applying an oxidative potential causes the OH- ions in the bulk to accumulate near the surface, hence the pH near the electrode surface is larger than the bulk. we additionally showed that the position of the oxidation peaks depends on the concentration of the electrolyte, thereby affecting the passive film formation and breakdown. We previously calculated the surface pH to be theoretically ~14.16, using **reaction 2.5**. Drawing parallels to self-assembled monolayers and the passive oxide layer of eGaIn electrode, we use two methods to determine the acid dissociation constant (pKa) of the oxide species on the surface, 1) electrochemical titration[30–32] and 2) faradic titration using impedance spectroscopy[31–33].

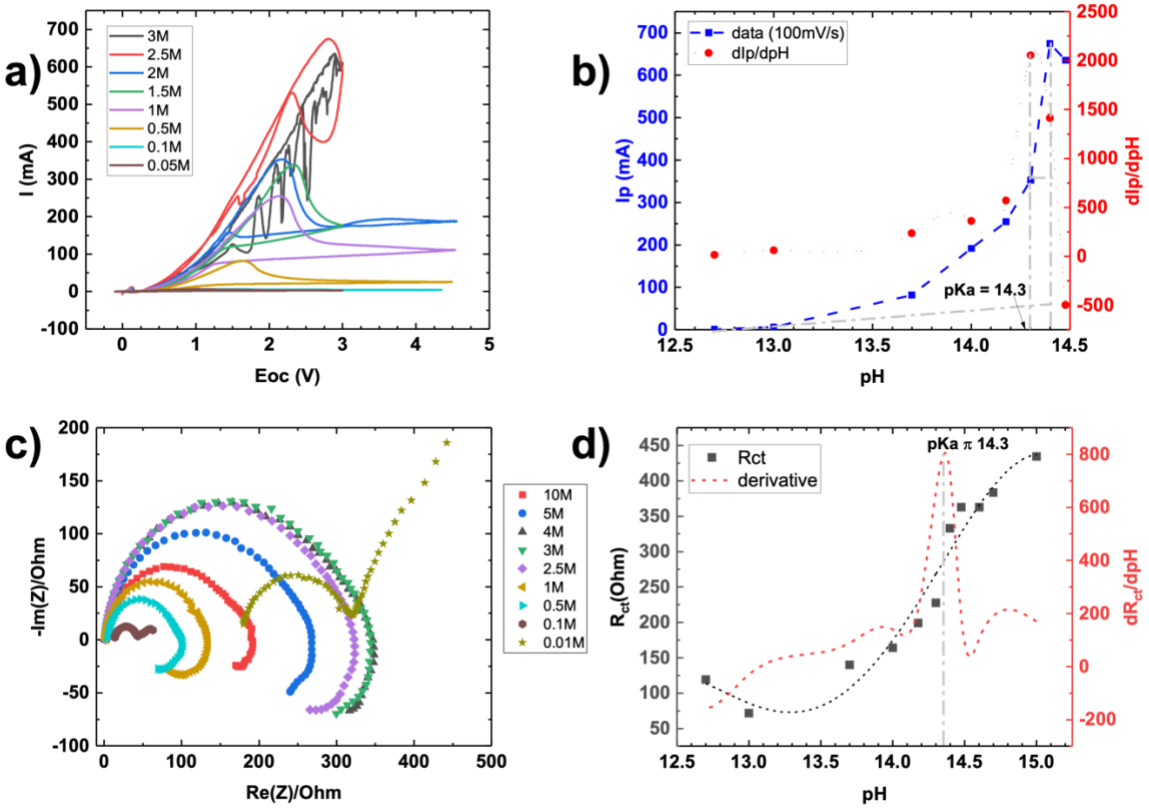

Figure 3.7. Determination of acid dissociation constant (pKa) of surface oxide species on a 0.1 ml eGaIn droplet electrode. a) Cyclic voltammetry of eGaIn electrode in different concentrations of NaOH using a potential scan rate of 100 mV/s, b) Peak current of the P3 peak (Ip3) plotted as a function of solution pH and its derivative as a function of solution pH, c) the Nyquist plots of oxide on eGaIn electrode in different concentrations of NaOH at the passivation breakdown potential 0.27 V and d) Faradic impedance titration plots (charge transfer resistance (R_{ct}) and its derivative as a function of solution pH for eGaIn electrode). The

red dotted lines show the derivative of R_{ct} and Ip vs. pH and the maxima show the pKa of the surface oxide species as ~14.3.

A cyclic voltammetry obtained from a 0.1ml eGaIn electrode at various concentrations of NaOH (converted to pH) to helps illustrate the role of OH- anion [30–32], shown in **Figure 3.7a**. The P_3 peak current and its derivative are plotted as a function of pH in **Figure 3.7b**. The peak current starts to increase at pH = 13 (0.1 M NaOH) and reaches a maximum of ~ 14.4 near (2.5 M NaOH). The current pH plot can be considered as titration plot, so the pKa of surface species (Ka is acid dissociation constant) is equal to pH ~ 14.3, the maxima of the peak current derivative plot.

Electrochemical Impedance spectroscopy (EIS) is a versatile tool that has been used to determine the interfacial acid-base properties. For example, it has been used to determine the pKa of surface modified electrodes such as benzoic acid modified gold.[33] We hypothesized that this property can also be translated to eGaIn electrodes with surface oxides. EIS of eGaIn electrode for an arbitrary potential of 0.27 V for various concentrations of NaOH is plotted in **Figure 3.7c** . The impedance values are fitted to standard Randel's equivalent circuit comprising of a series combination of oxide resistance R_{Ox} with capacitance (C_p) in parallel with charge transfer resistance R_{ct}, an inductor (L) and constant phase elements (CPE) of Q_{Ox} for the complete range of frequencies, **Figure 3.7c** . The R_{ct} values calculated from impedance analysis in different concentrations of NaOH are plotted against pH[31–33] in **Figure 3.7d.** The R_{ct} increases with increases in solution pH due to the accumulation of OH- ions at the electrode surface and passive oxide formation. The results of EIS measurements also show that the pKa of surface oxide species is ~14.3 and is consistent with our CV measurements. Interestingly, the pKa values obtained experimentally are close to the previously calculated **reaction 2.5** equilibrium pH = 14.16. This observation is consistent with our speculation of a pH dependent equilibrium between GaOOH and

$Ga(OH)_4^-$ at the eGaIn surface. At pH > pKa the formation of gallates is favorable and for pKa > pH the deposition of GaOOH occurs.

Effect of oxidation on effective interfacial tension:

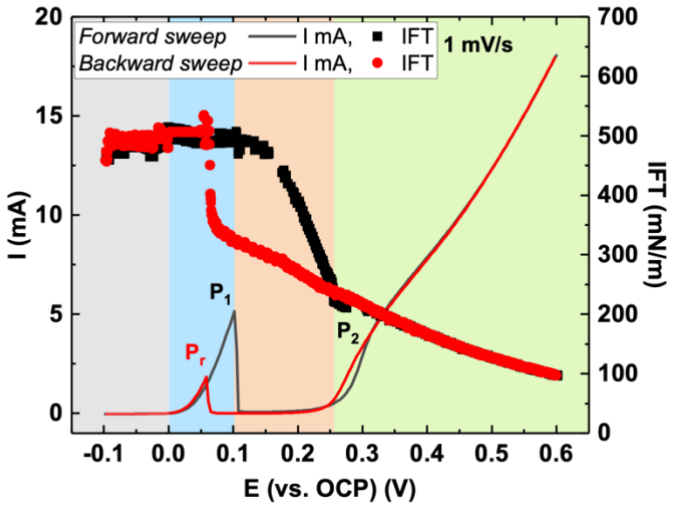

Figure 3.8. The effective interfacial tension of liquid metal (eGaIn) in 1M NaOH. A cyclic voltammogram co-plotted with effective interfacial tension of liquid metal vs. electrical potential. The volume of eGaIn droplet and the potential scan rate is 0.1 ml and 1 mV/s, respectively. Red and black colors are used to represent forward sweep (FS) and backward sweep (BS) respectively, lines correspond to cyclic voltammetry data and dots correspond to interfacial tension data (IFT, γ).

Figure 3.8 shows the effective interfacial tension (IFT, γ) of a 0.1ml eGaln droplet in 1M NaOH during electro-oxidation. The effective interfacial tension of the eGaIn droplet is ~ 500 mN/m in the absence of potential as NaOH dissolves the surface oxide. Previous work from our group speculated that the oxide acts as a surfactant (possibly in conjunction with electrocapillarity) to lower interfacial tension; contrary to our expectations, interfacial tension analysis shows no change in *IFT* in the *'oxidizing regime'* and starts to show signs of change only in the 'passivation regime' at $E \sim 0.15\,V$. When $E > 0.15$ V is applied, the effective interfacial tension suddenly drops from 500 mN/m to 200 mN/m in a narrow potential window between 0.150 V to 0.275 V in the *'passivation regime'*.

In this regime, we speculate that this change occurs due to the accumulation of OH^- ions (i.e., charges) near the electrolyte/oxide interface increases the surface pH; thus, leading to change in the composition of the already existing oxide film, resulting in the formation of either $GaOOH$ or $Ga(OH)_4^-$ as the new passive oxide film. Initially in the passivation regime, the passive oxide film (most likely $GaOOH$) does not change the effective interfacial tension. However, it decreases the electrochemical reactions that occur, thus leading to low current readings. This leads to increase in surface charges and consequently decrease in effective interfacial tension.

At $E > 0.275\ V$**,** the effective interfacial tension decreases linearly with applied potential in the *'passivation breakdown'* regime *(from 0.25 V to 0.5 V)*. A decrease in interfacial tension suggests a change in the surface of the electrode. We speculate that the linear drop in interfacial tension in this regime is most likely due to the adsorbed gallate anions near the electrode surface.

An interesting observation is that the interfacial behavior shows hysteresis during the backward sweep. During the backward sweep, the effective interfacial tension increases with applied potential linearly in all the oxidation regimes and returns to 500 mN/m in the oxidation regime (**Figure 3.8**). This hysteresis indicates that the interface is different in the passivation regime during the forward and reverse scans. Given the linear increase in tension during the reverse scan (through the passivation regime), we reason that the oxide species on the surface continues does not disappear until ~0.15 V during the reverse scan.

Table 3.1. Reactions consistent with the suggested mechanism of the passive film formation and breakdown at an eGaIn droplet for scan rate 1 mV/s.

Regime	Electrical Potential (V)	Reaction	Reaction Type	Location on Voltammogram	Notes	IFT (mN/m)
Cathodic protection: oxide-free surface.	E < 0.0 V	$GaOOH + 3e^- + H_2O \rightleftharpoons Ga + 3OH^-$	Electrochemical	Pr	No reduction peak in low potential scan rate	No significant change during both FS and BS
Oxidizing: $Ga(OH)_2$ forms and partially converts to GaOOH through disproportionation reaction**.**	$0.0\ V \leq E \leq 0.05\ V$	$Ga + OH^- \rightleftharpoons GaOH + e^-$	Electrochemical	P_1 (Shoulder)	Electron transfer step 1	**FS:** No significant change **BS:** returns to 500 mN/m
		$GaOH + OH^- \rightleftharpoons Ga(OH)_2 + e^-$	Electrochemical	P_1	Electron transfer step 2	
		$3Ga(OH)_2 \rightarrow Ga(M) + 2GaOOH + H_2O$	Chemical disproportionation		More critical in low potential scan rate	
Passivation: The rest of $Ga(OH)_2$ converts to GaOOH electrochemically. A very thin layer of GaOOH film forms.	0.05 V < E < 0.25 V	$Ga(OH)_2 + OH^- \rightleftharpoons GaOOH + H_2O + e^-$	Electrochemical	P'_1	Electron transfer step 3	**FS:** 1) No significant change until E = 0.15 V. 2) At 0.15 V < E < 0.25 V, IFT dramatically decreased from 500 mN/m to 350 mN/m **BS:** linearly increases
Passivation breakdown: GaOOH film dissolves due to increasing pH in the vicinity of the eGaIn electrode, and metallic gallium is oxidized to $\mathbf{Ga(OH)_4^-}$	$0.25\ V \leq E \leq 0.80\ V$	$GaOOH + H_2O + OH^- \rightleftharpoons Ga(OH)_4^-$	Chemical passive film dissolution	P_2	More critical in low potential scan rate	**FS:** IFT decreases from 300 mN/m to 200 mN/m, at $0.25\ V < E < 0.50\ V$ **BS:** linearly increases
		$Ga + 3OH^- \rightleftharpoons Ga(OH)_3 + 3e^-$	Electrochemical			
		$Ga(OH)_3 + OH^- \rightleftharpoons Ga(OH)_4^-$	Chemical			
		$Ga + 4OH^- \rightleftharpoons Ga(OH)_4^- + 3e^-$	Electrochemical	$P_2 < E < P_3$	Due to low pH near eGaIn electrode surface	
		$Ga(OH)_4^- \rightleftharpoons GaOOH + H_2O + OH^-$	Chemical	$E \approx P_3$		
Partial re-passivation: Solid GaOOH forms due to diffusion-limited depletion of OH^- anions at the surface of the eGaIn electrode	$E > 0.80\ V$	$Ga + 3OH^- \rightleftharpoons GaOOH + H_2O + 3e^-$	Electrochemical	E > P_3	A thick film that has matt texture forms.	not measured

Conclusion:

Based on the experimental results presented, we summarize reactions that likely happen during electro-oxidation of an EGaIn droplet in **Table 3.1.**

Starting from the open circuit voltage, during eGaIn electro-oxidation, a passive oxide film first forms via the oxidation of gallium ($Ga \rightarrow Ga^{2+}$) at P_1, by chemical reactions to form Ga_2O_3 or GaOOH (i.e., more stable oxidation states of Ga^{3+}) while also regenerating metal. The effect of the chemical reactions becomes more significant relative to electrochemical reactions when the time window of reaction is larger (i.e., low potential scan rate). The current drops precipitously because this passive oxide film blocks reactions by preventing the electrolyte from reaching the surface of eGaIn.

In the *passivation regime (0.10 V to 0.30 V),* positive charges on the metal and OH- anions from the electrolyte accumulate at the metal/film and film/electrolyte interfaces, respectively. With increased potential (0.30 V to 0.80 V), the passive film starts to breakdown corresponding with an increase in current (P_2) and the formation of $Ga(OH)_3$ and soluble gallate species. Thus, at E > 0.30 V, electro-oxidation of eGaIn forms soluble sodium gallate, the film breaks down, and the surface undergoes continuous oxidation / dissolution.

However, at high oxidation potential $E \geq 0.8$ V (around P_3 peak), adsorbed gallate anions convert to GaOOH and precipitate due to diffusion-limited depletion of OH^- anions at the surface of the eGaIn electrode. The GaOOH precipitate converts to gallate and dissolves immediately after stopping the applied potential or switching the potential to reverse direction. During the backward sweep, the gallate species do not get reduced because presumably they dissolve rather than remain on the surface. Thus, when the scan rate is low enough, no significant reduction peaks are observed in the cathodic scan; in fact, oxidation peaks are observed in some cases. Based on speciation

studies in the literature and our electrochemical data, the P_3 peak could be assigned to the electrochemical formation of gallate and subsequent precipitation of GaOOH, resulting in the matte appearance at $E \geq 0.8$ V.

Acknowledgements and contributions:

I wish to acknowledge *Dr. Sahar Rashid-Nadimi* (CSU, Bakersfield) who helped with the electrochemical measurements for high-speed cyclic voltammetry and formulating the oxidation reaction mechanism of eutectic gallium indium in 1M NaOH. Also, I wish to thank *Keith Hillaire* (Physics Dept, NCSU) provided the software to measure the interfacial tension as a function of applied potential.

References

(1) Song, M.; Daniels, K. E.; Kiani, A.; Rashid-Nadimi, S.; Dickey, M. D. Interfacial Tension Modulation of Liquid Metal via Electrochemical Oxidation. *Advanced Intelligent Systems* **2021**, 2100024. https://doi.org/10.1002/aisy.202100024.

(2) Khan, M. R.; Eaker, C. B.; Bowden, E. F.; Dickey, M. D. Giant and Switchable Surface Activity of Liquid Metal via Surface Oxidation. *Proc Natl Acad Sci USA* **2014**, *111* (39), 14047–14051. https://doi.org/10.1073/pnas.1412227111.

(3) Ding, Y.; Guo, X.; Qian, Y.; Xue, L.; Dolocan, A.; Yu, G. Room-Temperature All-Liquid-Metal Batteries Based on Fusible Alloys with Regulated Interfacial Chemistry and Wetting. *Advanced Materials n/a* (n/a), 2002577. https://doi.org/10.1002/adma.202002577.

(4) Guo, X.; Zhang, L.; Ding, Y.; Goodenough, J. B.; Yu, G. Room-Temperature Liquid Metal and Alloy Systems for Energy Storage Applications. *Energy Environ. Sci.* **2019**, *12* (9), 2605–2619. https://doi.org/10.1039/C9EE01707K.

(5) Giguère, P. A.; Lamontagne, D. Polarography with a Dropping Gallium Electrode. *Science* **1954**, *120* (3114), 390–391. https://doi.org/10.1126/science.120.3114.390.

(6) Song, M.; Kartawira, K.; Hillaire, K. D.; Li, C.; Eaker, C. B.; Kiani, A.; Daniels, K. E.; Dickey, M. D. Overcoming Rayleigh–Plateau Instabilities: Stabilizing and Destabilizing Liquid-Metal Streams via Electrochemical Oxidation. *Proc Natl Acad Sci USA* **2020**, *117* (32), 19026–19032. https://doi.org/10.1073/pnas.2006122117.

(7) Dickey, M. D.; Chiechi, R. C.; Larsen, R. J.; Weiss, E. A.; Weitz, D. A.; Whitesides, G. M. Eutectic Gallium-Indium (EGaIn): A Liquid Metal Alloy for the Formation of Stable Structures in Microchannels at Room Temperature. *Adv. Funct. Mater.* **2008**, *18* (7), 1097–1104. https://doi.org/10.1002/adfm.200701216.

(8) Zrnic, D.; Swatik, D. S. Resistivity and Surface Tension of the Eutectic Alloy of Gallium and Indium. *Journal of the Less-Common Metals* **1969**, *18* (1), 67–68.

(9) Eaker, C. B.; Hight, D. C.; O'Regan, J. D.; Dickey, M. D.; Daniels, K. E. Oxidation-Mediated Fingering in Liquid Metals. *Phys. Rev. Lett.* **2017**, *119* (17), 174502. https://doi.org/10.1103/PhysRevLett.119.174502.

(10) Eaker, C. B.; Dickey, M. D. Liquid Metal Actuation by Electrical Control of Interfacial Tension. *Applied Physics Reviews* **2016**, *3* (3), 031103. https://doi.org/10.1063/1.4959898.

(11) Majidi, L.; Gritsenko, D.; Xu, J. Gallium-Based Room-Temperature Liquid Metals: Actuation and Manipulation of Droplets and Flows. *Front. Mech. Eng.* **2017**, *3*. https://doi.org/10.3389/fmech.2017.00009.

(12) Khan, M. R.; Trlica, C.; Dickey, M. D. Recapillarity: Electrochemically Controlled Capillary Withdrawal of a Liquid Metal Alloy from Microchannels. *Adv. Funct. Mater.* **2015**, *25* (5), 671–678. https://doi.org/10.1002/adfm.201403042.

(13) Eaker, C. B.; Hight, D. C.; O'Regan, J. D.; Dickey, M. D.; Daniels, K. E. Oxidation-Mediated Fingering in Liquid Metals. *Phys. Rev. Lett.* **2017**, *119* (17), 174502. https://doi.org/10.1103/PhysRevLett.119.174502.

(14) Sheng, L.; Zhang, J.; Liu, J. Diverse Transformations of Liquid Metals Between Different Morphologies. *Adv. Mater.* **2014**, *26* (34), 6036–6042. https://doi.org/10.1002/adma.201400843.

(15) Liao, J.; Majidi, C. Soft Actuators by Electrochemical Oxidation of Liquid Metal Surfaces. *Soft Matter* **2021**, *17* (7), 1921–1928. https://doi.org/10.1039/D0SM01851A.

(16) Perkins, R. S. Gallium Oxidation in Alkaline Solution. *J. Electrochem. Soc.* **1972**, *119* (6), 713. https://doi.org/10.1149/1.2404301.

(17) Nikitin, E. V.; Kuzovenko, S. V.; Faizullin, F. F. Special characteristics of the anodic oxidation of Ga and Te in alkali solutions. *Elektrokhimiya* **1971**, *7* (7), 1062–1064.

(18) Perkins, R. S. Anodic Oxidation of Gallium in Alkaline Solution. *Journal of Electroanalytical Chemistry and Interfacial Electrochemistry* **1979**, *101* (1), 47–57. https://doi.org/10.1016/S0022-0728(79)80078-9.

(19) Varadharaj, A.; Rao, G. P. Cyclic Voltammetric Studies on Gallium Film Electrodes in Alkaline Media. In *Proceedings of the Indian Academy of Sciences-Chemical Sciences*; Springer, 1990; Vol. 102, pp 177–187.

(20) Khan, M. R.; Trlica, C.; So, J.-H.; Valeri, M.; Dickey, M. D. Influence of Water on the Interfacial Behavior of Gallium Liquid Metal Alloys. *ACS Appl. Mater. Interfaces* **2014**, *6* (24), 22467–22473. https://doi.org/10.1021/am506496u.

(21) Lin, Y.; Liu, Y.; Genzer, J.; Dickey, M. D. Shape-Transformable Liquid Metal Nanoparticles in Aqueous Solution. *Chem. Sci.* **2017**, *8* (5), 3832–3837. https://doi.org/10.1039/C7SC00057J.

(22) Chung, Y.; Lee, C.-W. Electrochemistry of Gallium. *J. Electrochem. Sci. Technol* **2013**, *4* (1), 1–18. https://doi.org/10.33961/JECST.2013.4.1.1.

(23) Pourbaix. *Atlas of Electrochemical Equilibria in Aqueous Solutions*; National Association of Corrosion Engineers: TX, USA, 1974.

(24) Benézéth, P.; Diakonov, I. I.; Pokrovski, G. S.; Dandurand, J.-L.; Schott, J.; Khodakovsky, I. L. Gallium Speciation in Aqueous Solution. Experimental Study and Modelling: Part 2. Solubility of α-GaOOH in Acidic Solutions from 150 to 250°C and Hydrolysis Constants of Gallium (III) to 300°C. *Geochimica et Cosmochimica Acta* **1997**, *61* (7), 1345–1357. https://doi.org/10.1016/S0016-7037(97)00012-4.

(25) Diakonov, I. I.; Pokrovski, G. S.; Bénézeth, P.; Schott, J.; Dandurand, J.-L.; Escalier, J. Gallium Speciation in Aqueous Solution. Experimental Study and Modelling: Part 1. Thermodynamic Properties of Ga(OH)4− to 300°C. *Geochimica et Cosmochimica Acta* **1997**, *61* (7), 1333–1343. https://doi.org/10.1016/S0016-7037(97)00011-2.

(26) Chung, Y.; Lee, C.-W. Electrochemistry of Gallium. *Journal of Electrochemical Science and Technology* **2013**, *4* (1), 1–18. https://doi.org/10.5229/JECST.2013.4.1.1.

(27) Armstrong, R. D. The anodic behaviour of gallium in alkaline solution. 7.

(28) Allen J. Bard and Larry R. Faulkner, Electrochemical Methods: Fundamentals and Applications, New York: Wiley, 2001, 2nd Ed. *Russian Journal of Electrochemistry* **2002**, *38* (12), 1364–1365. https://doi.org/10.1023/A:1021637209564.

(29) Pokrovski, G. S.; Diakonov, I. I.; Bénézeth, P.; Gurevich, V. M.; Gavrichev, K. S.; Gorbunov, V. E.; Dandurand, J.-L.; Schott, J.; Khodakovsky, I. L. Thermodynamic Properties of Gallium Hydroxide Oxide (α-GaOOH) at Temperatures to 700 K. *ejm* **1997**, *9* (5), 941–952. https://doi.org/10.1127/ejm/9/5/0941.

(30) Zhao, J.; Luo, L.; Yang, X.; Wang, E.; Dong, S. Determination of Surface PKa of SAM Using an Electrochemical Titration Method. **1999**, No. 15, 4.

(31) Kim, K.; Kwak, J. Faradaic Impedance Titration of Pure 3-Mercaptopropionic Acid and Ethanethiol Mixed Monolayers on Gold. *Journal of Electroanalytical Chemistry* **2001**, *512* (1–2), 83–91. https://doi.org/10.1016/S0022-0728(01)00588-5.

(32) Shervedani, R. K.; Hatefi-Mehrjardi, A.; Babadi, M. K. Comparative Electrochemical Study of Self-Assembled Monolayers of 2-Mercaptobenzoxazole, 2-Mercaptobenzothiazole, and

2-Mercaptobenzimidazole Formed on Polycrystalline Gold Electrode. *Electrochimica Acta* **2007**, *52*, 7051–7060.

(33) Abacıoğlu, G.; Üstündağ, Z.; Demirci, S.; Turan, A. A. İ.; Güzel, R.; Balcı, S.; Solak, A. O. Surface PKa Determination of Benzoic Acid Modified Gold Electrode by Electrochemical and Contact Angle Measurement Methods. **2014**, 14.

Chapter 4 : Electrochemical impedance spectroscopic analysis of eutectic gallium indium in 1M NaOH

Abstract:

This chapter reports an electrochemical impedance spectroscopy (EIS) analysis of liquid metal (eGaIn) electrode in 1M NaOH at room temperature. The goal is to provide insights into the accompanying interfacial behavior of eGaIn during electrochemical oxidation. The impedance spectra have been obtained at various potential intervals from the cathodic protection regime at -0.1 V to passivation breakdown regime at -0.5 V (values are vs open circuit potential, OCP). The upcoming sections of this chapter discuss impedance results at different oxidative potentials to understand the transitions between the three oxidation regimes, namely oxidizing, passivation, and passivation breakdown, respectively. Contrary to our expectations, EIS provides evidence that the estimated thickness of the oxide decreases with increasing potential. This result is corroborated by dissolution measurements.

Introduction:

Early applications of impedance spectroscopy were used to study the dielectric properties of fluids and metal oxides[1]. Impedance spectroscopy was subsequently utilized to measure the capacitance of ideally polarizable electrode (mostly mercury) that led to the development of models for the electrified metal-electrolyte interface[2]. More recently, EIS finds extensive use for studying processes such as corrosion, deposition of films, and other electrochemical systems [1,2]. The interpretation of reaction mechanisms by steady state techniques (like cyclic voltammetry at very low scan rates) alone is difficult, as they use restrictive assumptions that make the results questionable[3], while EIS can probe the electrochemical systems at very low frequencies that help identify reaction mechanisms without unnecessary or restrictive assumptions[1,4].

The goal of this chapter is to utilize EIS to better understand what happens to the interface of eGaIn during electrochemical oxidation. The first impedance analysis of eGaIn electrodes was

done in 1 M NaOH.[5] The oxidation formation mechanism was broadly classified into 1) oxidation 2) passivation and 3) transpassive regions (now renamed as passivation breakdown) and two distinct equivalent circuit models were used to describe the three oxidation regions[5]. The oxidation and passivation breakdown regions were modeled with a Ladder circuit[5] (used to represent pit formation or corrosive behavior), while the passivation region is modeled by using a Voigt circuit (used to represent an electrode completely covered)[6], as discussed in **Figure 2.6**. Although the equivalent circuit models provide a good fit for the measured impedance data, the assumption that pit formation occurs in oxidation region is not reasonable as the pit formation has been found to only occur where there is thick oxide or adsorbed film present on the electrode[3,7,8]. Additionally, the analysis of the circuit element parameters shows that the estimated electrical double layer capacitance from EIS is an order of magnitude larger than the typical double layer capacitance (~20 $\mu F/cm^2$)[9]. Furthermore, impedance values reported in lower frequencies are scattered so the electrochemical behavior of the system at low frequency (at small time scales) has not been studied[5].

Here, we study the oxidation mechanism of an eGaIn electrode in 1M NaOH by using impedance to understand changes to the interface in the three different oxidation regimes (oxidation, passivation, and the passive film breakdown) and validate the oxidation mechanism discussed in **Chapter 3**. Toward these goals, we performed impedance measurements in the frequency range of 100 MHz to 100mHz at various potentials that span the oxidation regimes. Additionally, EIS provides a quantitative analysis of the oxide characteristics as the oxide species dissolves in NaOH when the potential is turned off [5,10]. Furthermore, we performed dissolution experiment where the surface oxide coverage and thickness are calculated to provide a comparison with the oxide thickness measured from EIS.

Results and discussion:

Description of the cyclic voltammogram:

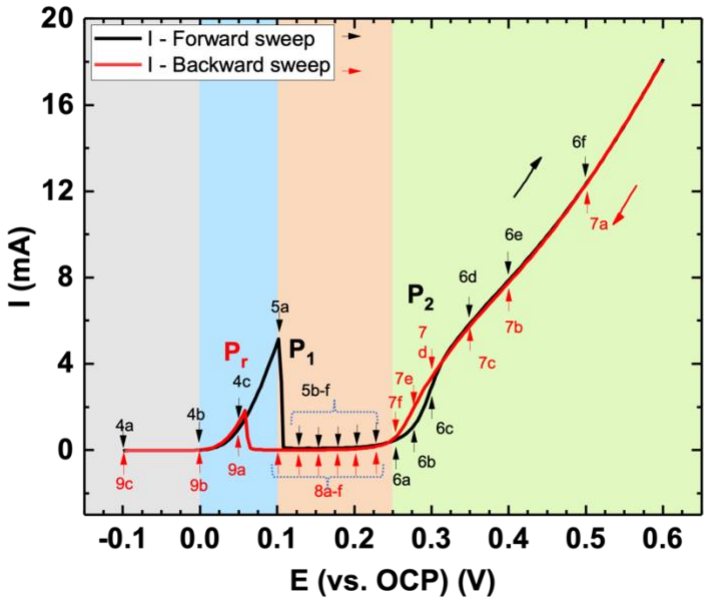

Figure 4.1. Cyclic voltammogram of a 0.1 ml eGaIn droplet in 1M NaOH with a potential scan rate of 1 mV/s, forward sweep (back line) and backward sweep (red line), respectively. Black and red arrows mark the potentials where EIS is performed. The numbers associated with the arrows indicate the figures from this chapter where the EIS spectra are plotted. The various oxidation regimes are labeled by color as cathodic protection (grey), oxidizing (blue), passivation (orange), and passivation breakdown (green), respectively.

Figure 4.1. shows the cyclic voltammogram for a 0.1 ml eGaIn droplet electrode in 1M NaOH solution. We have already discussed the oxidation mechanism in detail in **Chapter 2**. Thus, here we provide a brief review of the oxidation mechanism and the accompanying interfacial behavior. During the anodic scan (forward potential sweep), we observe the two apparent oxidation peaks (P_1 & P_2) corresponding to the different oxidation regimes and one peak in the cathodic scan (backward sweep) within the potential range -0.2 V to 0.5 V. The initial increase corresponds to the formation of a passive oxide and subsequent drop in current (P_1) to near-zero indicate the presence of a conformal oxide film that prevents additional reactions. We speculate that subsequent increase in potential draws hydroxyls to the surface and causes the surface pH to

increase, thereby changing the composition of the oxide. Applying a potential greater than 0.25 V, we observe an increase in current and peak P_2 appears. This peak is attributed to the formation of $Ga(OH)_3$ and eventually soluble gallates ($Ga(OH)_4^-$). The formation of soluble gallates causes the current to increase as higher potential is applied. During the backward sweep, we observe one peak (P_r) near open circuit potential, which is attributed to the removal of the oxide from the surface during the backward scan. As discussed in **Chapter 2**, the position and the intensity of the peaks are determined by the scan rate; however, based on the above current responses, the oxide formation can be classified into the following regimes: cathodic protection region ($-0.2\ V \leq E < Eoc$), oxidation ($Eoc < E \leq 0.05\ V$), passivation ($0.05\ V < E < 0.25\ V$) and the passive film breakdown ($0.25\ V \leq E \leq 0.50\ V$).

To further our understanding the oxide mechanism and its role in interfacial tension behavior, we perform electrochemical impedance spectroscopy at various potentials marked in **Figure 4.1**. These values were chosen to obtain a deeper insight into the transition between the oxidation regimes and its corresponding interfacial behaviors.

Description of the impedance spectra in the forward potential sweep:

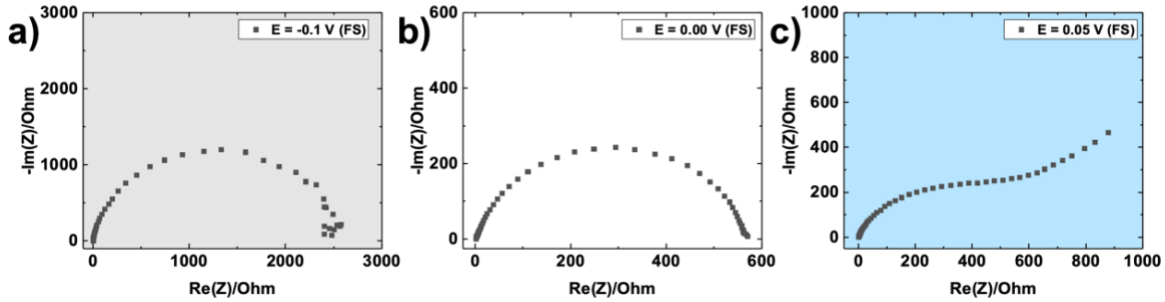

Figure 4.2. Nyquist diagrams of 0.1ml eGaIn in 1M NaOH at different potentials that correspond to a) -0.10 V (cathodic protection regime), b) 0.00 V (open circuit potential) and c) 0.05V (oxidizing regime) during the forward potential sweep. Note: the scale on the plot changes.

Figure 4.2, Figure 4.3, and Figure 4.4 show the Nyquist diagrams of impedance data for the various regions of the oxidation mechanism in the forward potential sweep. The Nyquist plots in the 'cathodic protection region' are characterized by capacitive behavior, indicated by a semicircular shape (**Figure 4.2a**). As we move from -0.1 V to 0.0 V, the magnitude of the capacitive loops decrease; this observation is consistent with the presence of an electrical double layer[1,11], and its dissipation as the applied potential nears 0.00 V (the magnitude of the impedance decreases). The oxidation mechanism discussed in chapter 4 include the three oxidation regimes namely oxidizing, passivation, and passivation breakdown. At OPC (0 V), we observe a capacitive loop due to the reaction of eGaIn with NaOH[12]. In the potential range $0.00\ \text{V} < E \leq 0.05\ V$ (i.e., oxidation regime), a semicircular trend corresponding to capacitance behavior is present in the high-frequency range, while the low-frequency range is dominated by a straight line with a slope less than 45˚, indicative of non-ideal mass transport (or diffusion behavior)[1,4,13] **Figure 4.2c**. This observation is consistent with the presence and formation of an oxide (peak P_1) **Figure 4.1**.

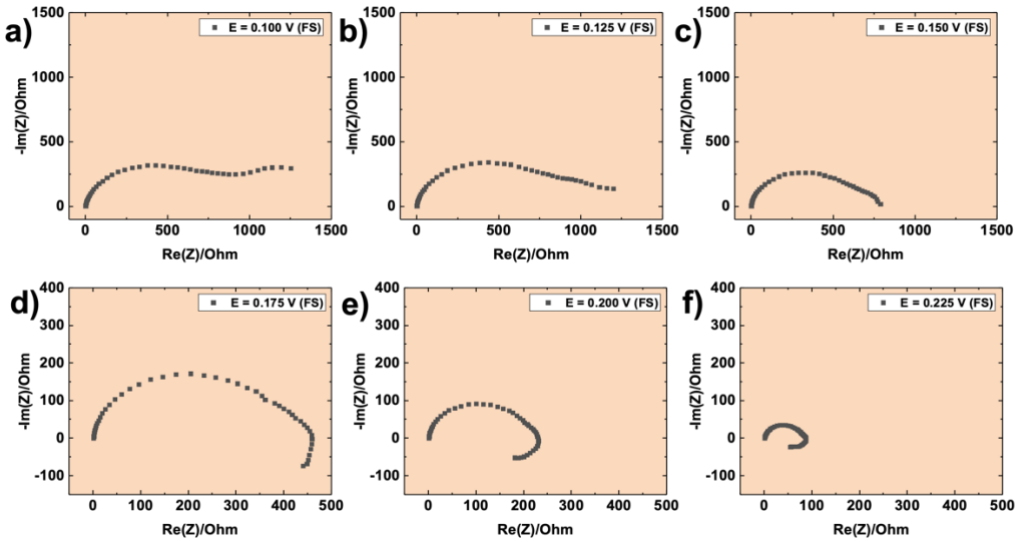

Figure 4.3. Nyquist diagrams of 0.1ml eGaIn in 1M NaOH at different oxidative potentials of 'passivation regime' during forward potential sweep. a) 0.100 V, b) 0.125 V, c) 0.150 V, d) 0.175 V, e) 0.200 and f) 0.225. Note: the first and second row of plots have different axis.

In the potential ranges $0.05\,V < E < 0.25\,V$ (passivation regime), the low-frequency behavior eventually disappears as the slope of the line decreases and as the trend transitions to a negative capacitance curve (inductive behaviour) (**Figure 4.3**). The change in low-frequency behavior in the potential range $0.05\,V < E < 0.15\,V$ is an indication of diffusive behavior accompanied with an exchange of electroactive species with electrolyte[1,3,13]. Here, as OH^- accumulates near the electrode surface, the remaining $Ga(OH)_3$ on the surface converts to $GaOOH$ and covers the entire surface of the electrode, **reaction 4.1**. Furthermore, this observation is consistent with the increase in resistance (**Figure 4.3 a-c**) and the current drop (**Figure 4.1)** due to the oxide film**.**

$$Ga(OH)_3 \rightleftharpoons GaOOH + H_2O \qquad (14)$$

The inductive loops start to appear after 0.150 V and persist until 0.225 V (**Figure 4.3d-f**). Negative capacitance loop indicates the presence of inductive behavior (i.e., the increase in current without charge transfer), and is often associated with an electrochemical/chemical reaction on the surface of the electrode, thereby exposing the metal surface while storing the charge during the reaction[1,3,14]. Additionally, the appearance of inductive behavior suggests the dependence of the reaction on surface coverage and applied potential[1]. Similar behaviors have been observed in anodic dissolution of mild steel suggesting presence of an adsorbed layer of $Fe(OH)$ and the start of passivation breakdown regime (or also called transpassivation)[3]. Hence, we speculate that the change in oxide composition from $GaOOH$ to gallates $Ga(OH)_4^-$ leads the oxide film to start breakdown; additionally at large time scales the gallium hydroxide species on the surface can convert to $GaOOH$ by chemical disproportionation reaction that exposes Ga(M) sites (**Table 3.1**). When these metal sites come in contact to the electrolyte cause inductive behavior.

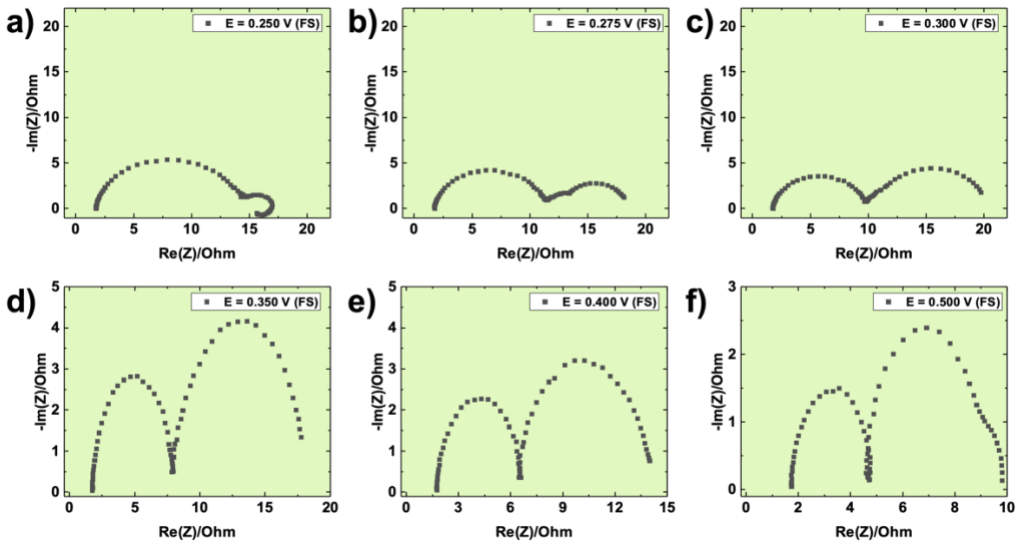

Figure 4.4. Nyquist diagrams of 0.1ml eGaIn in 1M NaOH at different oxidative potentials of 'passivation breakdown region' during the forward potential sweep. a) 0.250 V b) 0.275 c) 0.300 V, d) 0.350 V, e) 0.400 V and f) 0.500 V.

Interestingly, at the start of passivation breakdown regime at E = 0.25V, we observe one capacitance loop in the high frequency range and a small second capacitance loop with an accompanying inductive behaviour in the low frequency range, signifying the start of passivation breakdown regime, **Figure 4.4**. Additionally, this behavior has been previous reported[1,15,16] for corrosion of magnesium, where the authors suggest the reaction dependence on potential, surface coverage and concentration. Furthermore, they argue the ionic product diffuses from the surface and reacts through a backward reaction with the intermediate adsorbed species. In our reaction mechanism (proposed in **Chapter 2)** at 0.25 V a second oxidation peak (P_2) appears (**Figure 4.1**) and is attributed to the conversion of adsorbed GaOOH to soluble gallates as the surface pH increases. This impedance trend in **Figure 4.4a** is consistent with our proposed reaction mechanism.

For E > 0.25 V, we observe an increase in current due to the continued formation of gallates (**Figure 4.1**). Further, the impedance spectra between the potential range $0.25\,\mathrm{V} < E \leq 0.50\,\mathrm{V}$ shows the presence and eventual growth of a second capacitance loop in the low frequency range

suggesting the existence of another charged interface or adsorbed interface on the electrode[1]. Additionally at E ~ 0.50V, we observe a small loop at intermediate frequencies that is indicative of an anodic process that occurs at the interface. A similar behavior has also been reported[17] for the impedance analysis of pure aluminum electrode in 4M KOH at the passivation breakdown regime and has been associated with a reaction mechanism involving step wise addition of hydroxyl species to the surface of Al and chemical dissolution of adsorbed $Al(OH)_3$ to $Al(OH)_4^-$, also consistent with our impedance modeling [17]. Hence, we speculate the anodic dissolution of GaOOH and the formation of GaOOH and $Ga(OH)_4^-$ compete for bare surface sites at higher oxidative potentials.

Description of the impedance spectra in the backward sweep:

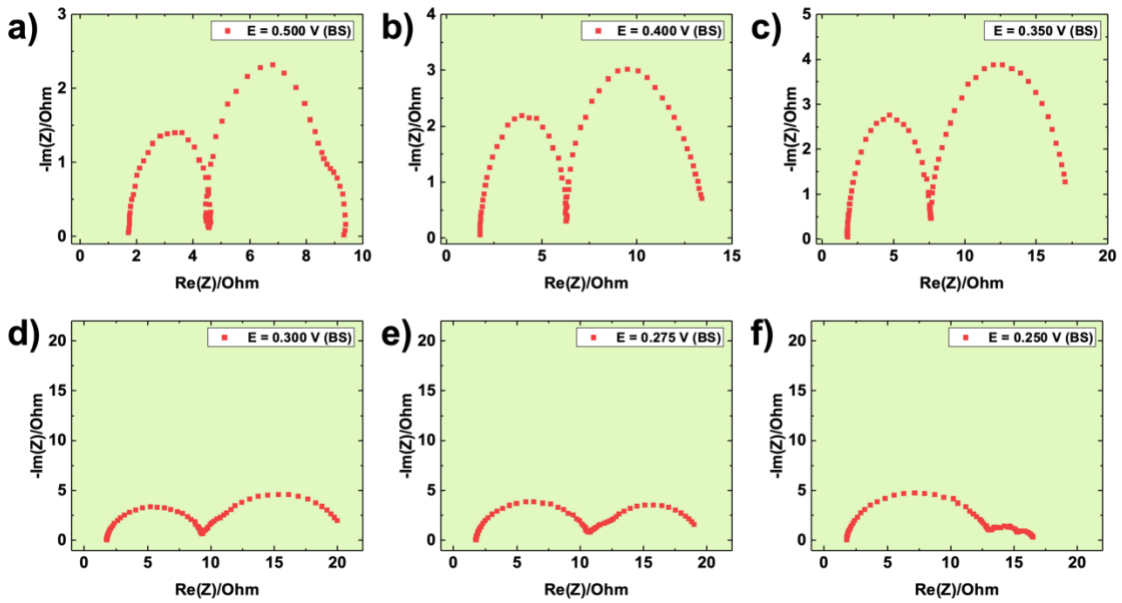

Figure 4.5. Nyquist diagrams of 0.1ml eGaIn in 1M NaOH at different oxidative potentials of 'passivation breakdown region' during the backward sweep. a) 0.500 V, b) 0.400 V, c) 0.350V, d) 0.300 V, e) 0.275 V and f) 0.250 V.

Figure 4.5, Figure 4.6 and **Figure 4.7**shows the Nyquist plots of the different regions for the backward potential sweep. EIS of the backward scan provides insight on how the presence of oxide species contributes toward the hysteresis observed in interfacial tension. The backward

potential sweep starts from 0.50 V to -0.20 V; unlike the forward potential sweep where the oxide species forms gradually, the backward sweep will have existing oxide species on the surface of the eGaIn. The Nyquist plots in the 'passivation breakdown regime' show similar behavior and trends in both forward and backward sweep. However, at E = 0.25V there is no inductive behavior at low frequency (**Figure 4.5**).

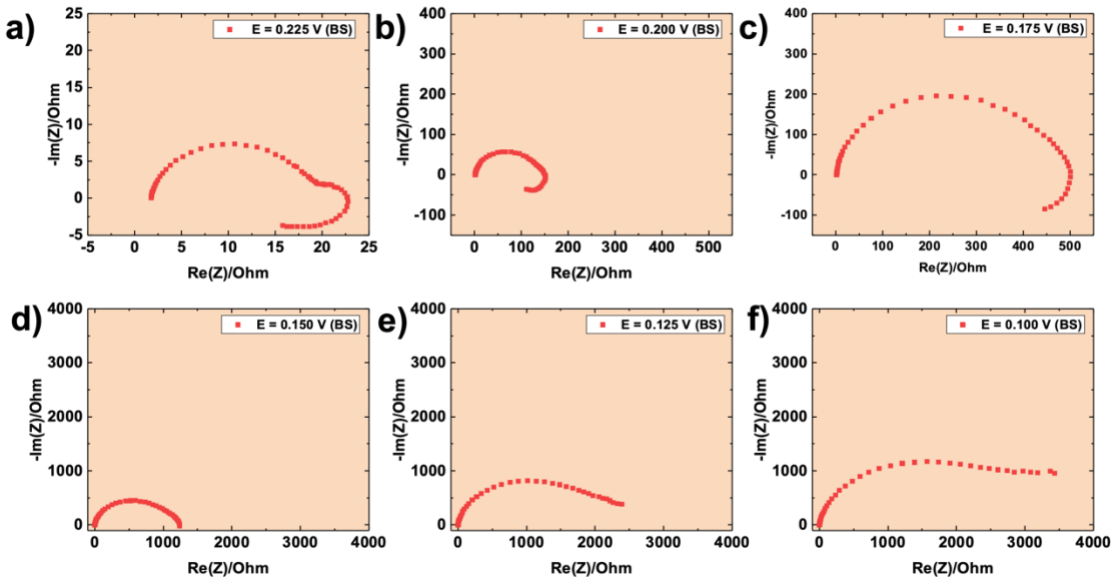

Figure 4.6. Nyquist diagrams of 0.1ml eGaIn in 1M NaOH at different oxidative potentials of 'passivation region' during the backward sweep. a) 0.225 V, b) 0.200 V, c) 0.175 V, d) 0.150 V, e) 0.125V and f) 0.100 V.

The 'passivation region' has similar tends of capacitance loops and impedance loops, but unlike the 'passivity breakdown region', the impedance values are not same as forward sweep. The magnitude of impedance between the potential range 0.225 V to 0.175 V are smaller than the forward sweep, but between potentials 0.150 V to 0.10 V the values are greater. We speculate that this behavior is due to the already existing oxide species on the surface. The inductive behavior in the lower frequency range starts to appear at 0.250 V and disappear at 0.175 V (**Figure 4.6**); when the inductive behavior in the lower frequency range end, the trends change to a horizontal line at lower frequency range. Further, the decrease in surface pH at smaller potentials promote the

conversion of $Ga(OH)_4^-$ to GaOOH that may cause the increase in impedance in the following potentials.

The trends of both the 'oxidation regime' and the' cathodic protection regime' during the backward potential sweep remain consistent with the forward potential sweep, **Figure 4.7**. However, the impedance values are larger in the backward sweep at 0.05 V (oxidizing regime) and smaller at open circuit potentials. Due to the presence of oxide species and immediate removal of oxide species at OCP the magnitude of capacitance loop is smaller than the forward sweep, while the impedance observed in the cathodic protection regime remains the same for both cases.

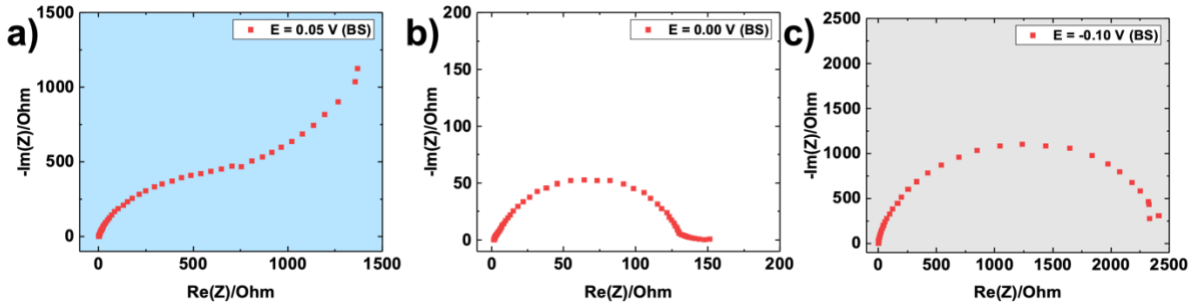

Figure 4.7. Nyquist diagrams of 0.1ml eGaIn in 1M NaOH at different oxidative potentials of 'Oxidizing region' during the backward sweep. a) 0.05 V, b) 0.00 V and c) -0.10 V

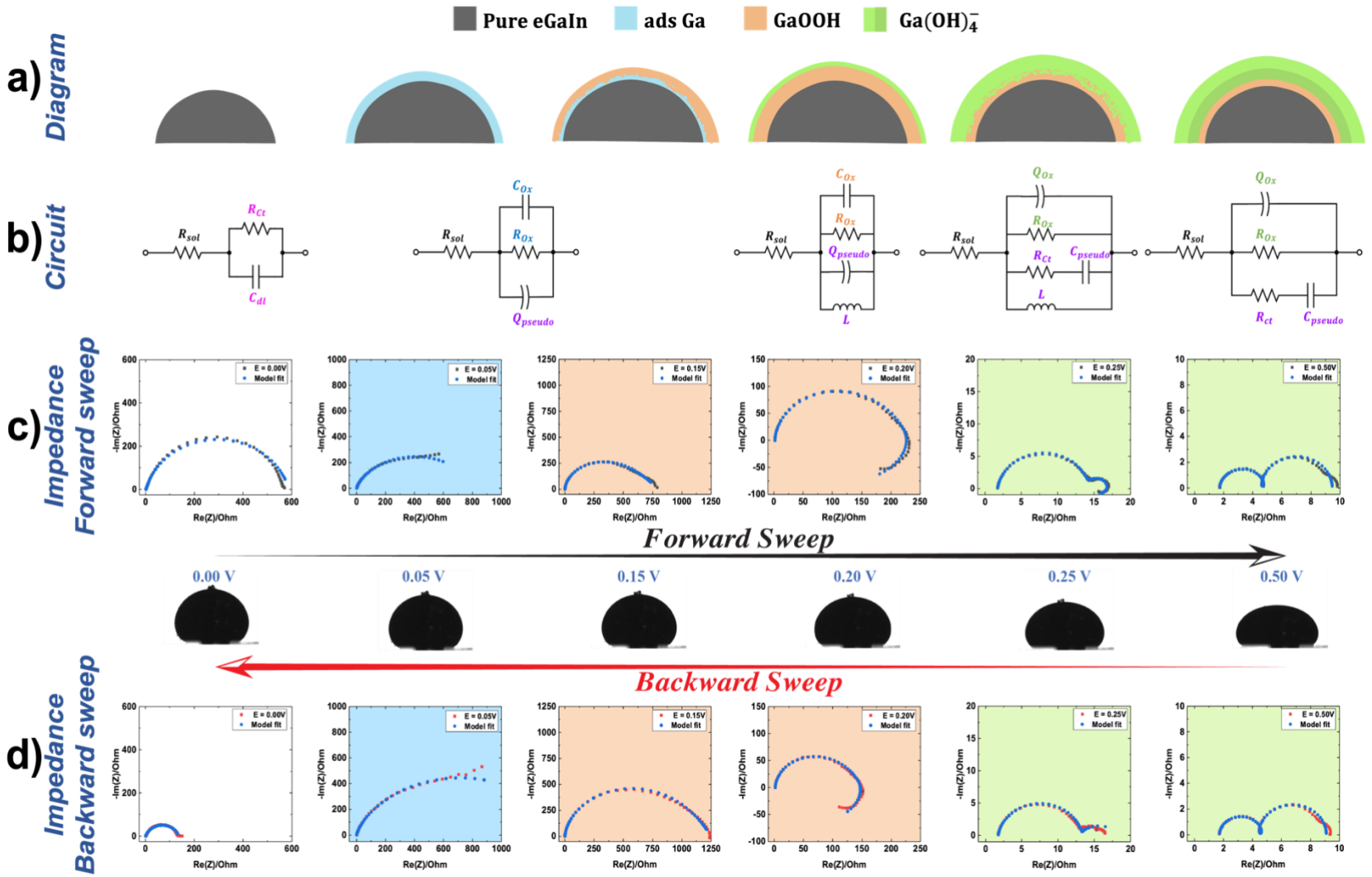

Figure 4.8. Nyquist plots and their respective equivalent circuit models for 0.1ml eGaIn electrode in 1M NaOH at different oxidative potentials for all regimes in forward and backward sweep. The black and red squares, and blue dots denote the forward and backward data points and model fit respectively for the potentials.

Relationship between reactions and impedance functions:

The impedance spectra of eGaIn in 1M NaOH between $-0.10\ \text{V} \leq E \leq 0.50\ \text{V}$, shows six unique impedance behaviors that describe three oxidation regimes (oxidizing, passivating and passivation breakdown). Based on the electro-oxidation mechanism of eGaIn discussed in chapter 2, we describe the liquid metal surface of each regime in **Figure 4.8a**. **Figure 4.8b**. shows the equivalent circuits that best represent the impedance behavior recorded. These equivalent circuit models are built based on literature precedent and physical elements used are consistent with the current-voltage behavior in **Figure 4.1**. All the impedance data points were verified with the Kramers-Kronig validity test (K-K test) and the points that did not satisfy the K-K test were removed prior to circuit modeling[11,18]. **Figure 4.8c&d** shows Nyquist plots for the unique impedance behaviors with model fit for both forward and backward sweep during oxidation.

All the oxidation regimes have an in-series contribution from the resistance of the NaOH solution R_{Sol}. R_{Ox} is used to describe the resistance through the oxide and R_{ct} is that is used to describe the resistance due to transfer of charges during an electrochemical reaction. C_{Ox} and Q_{Ox} are used to represent the capacitance of the oxide film, while C_{Pseudo} and Q_{Pseudo} are used to represent the impedance caused by the presence of reactions on the surface of the electrode. An inductor L is used to represent the negative capacitance loops (inductive behavior) in the passivation regime. Such inductive behavior has been observed for other systems in the literature and has been attributed to changes in surface of the electrode (like pit formation during corrosion or change in surface coverage of surface oxides), that may lead to the contact between electrolyte and the metal.

Equivalent circuits for forward sweep impedance spectra

At OCP ($E \approx 0V$), there is no oxide present, however a reaction between eGaIn and NaOH is present[12] and produce hydrogen bubbles, hence leading to capacitive behavior on the Nyquist plot. This behavior is common to most electrochemical systems and a Randel equivalent circuit model accurately describes the impedance observed[1,11,19]. Hence, the equivalent circuit of the electrode at this potential consist of a R_{ct} (charge transfer or polarization resistance) in parallel with C_{dl} (capacitance of the electrical double layer) (**Figure 4.8b(i)**).

In oxidation regime, the bare gallium on the surface reacts with the OH- anions near the surface to oxidize, forming an oxide film and oxidation peak P_1 (**Figure 4.1**). This oxide film causes the current to drop (passivation). The low frequency tail in the Nyquist plot has been removed since the data points do not satisfy the K-K test[18,20]. However, from **Figure 4.3(a-c)** the impedance spectra shows evidence of an unstable oxide accompanied with formation of an oxide film on the surface, this oxide film is mostly made of gallium hydroxides [1,13]. For this reason, we use a constant phase element (Q_{Pseudo}) to model the oxide formation instead of traditional Warburg element. The equivalent circuit for this regime consists of Q_{Pseudo} in parallel with R_{Ox} and C_{Ox} (**Figure 4.8b(ii)**) where R_{Ox} and C_{Ox} are used to represent the impedance caused due to the presence of oxide.

In the passivation regime, the concentration of OH- anions near the surface increases with applied potential; leading to the formation of GaOOH oxide film (**reaction 2.2).** However, when the surface pH becomes larger than 14.3, the GaOOH present on the surface starts to convert to soluble gallates $Ga(OH)_4^-$ (**reaction 2.5)** and passivation film breaks down. We observe two unique impedance trends that are consistent with our oxidation mechanism. The initial formation of GaOOH oxide at $E > 0.05V$ is attributed to a diffusive behavior (mass transport due to the oxide

formation) Figure 4.8c(iii), but eventually the impedance trends gradually transitions to an inductive loop at $E \approx 0.15\,V$. The induction loops start after $E > 0.15\,V$ and persist until $E \approx 0.25\,V$. The first equivalent circuit that describes the passivation regime is the same as the oxidation regime, **Figure 4.8b(ii),** while the second equivalent circuit is a combination of L in parallel with R_{Ox}, C_{Ox} and Q_{Pseudo} (**Figure 4.8b(iii)**)[14].

In the passivation breakdown regime, some parts of the electrode may get exposed in the passivation regime as the surface oxide continuously dissolves and reforms. Any exposed Ga metals will react with the OH- near the surface of the electrode to form $Ga(OH)_3$ and eventually to $Ga(OH)_4^-$ **reaction 2.6**. Additionally, as the surface pH increases due to the electrostatic attraction of OH-, the already present GaOOH on the surface may become soluble, forming $Ga(OH)_4^-$ gallates. These reactions cause the current response to increase, forming oxidation peak (P_2). Due to the high anodic potential, we speculated that the $Ga(OH)_4^-$ formed near the surface form a layer around eGaIn droplet (most likely an adsorbed gallate layer on the eGaIn surface). The impedance behaviors in this regime show two unique impedance behaviors. At E = 0.25 V (peak P_2), the induction loops transition into a small second impedance loop with a negative capacitance loop[1,16], and for E > 0.25, the second impedance loop fully develops into a capacitance loop with no inductive behavior[17]. The second capacitance loop indicates the presence of an additional layer of charge or oxide. Additionally, the second capacitance loop increases with applied potential while the first loop's width decreases, this suggests at higher potentials and at large time scales we the adsorbed gallates on the surface increases. The first equivalent circuit that shows inductive behavior consists of a series combination of R_{ct} and C_{Pseudo} in parallel with L, R_{Ox}, and Q_{Ox} (**Figure 4.8(iv)**) while The second equivalent circuit that describes the dual capacitance loops consists of R_{ct} and C_{Pseudo} in parallel with R_{Ox}, and Q_{Ox}(**Figure 4.8(v)**)[1].

Equivalent circuits for backward sweep impedance spectra

Due to the similarity of the impedance behaviors between the forward and backward sweep, the circuit interpretation of Nyquist plots of the forward sweep trends can be translated to the backward sweep. *In the passivation breakdown regime,* the impedance values are similar and consistent with the forward sweep data in the potential range $0.25\ \mathrm{V} < E \leq 0.50\ \mathrm{V}$. But at E = 0.25 V we do not observe any inductive behavior in the low frequency range, so we use the equivalent circuit IV (**Figure 4.8b(iv))** without an inductive element to describe the transition to passivation regime.

The impedance values for *passivation* and *oxidation regime* during the backward sweep differ from the forward sweep. In *the passivation regime,* we observed that the impedance values associated with oxide formation are *larger* in the backward sweep than the forward sweep, while the impedance values associated with inductive behavior are *smaller* in the backward sweep than the forward sweep **Figure 4.6.** This may be due to decrease in surface pH during the backward scan since the decrease in potential attracts less OH- to the surface; a lower pH can cause formation of GaOOH to be more favorable. Additionally, the impedance values during the *oxidation regime* are greater in the backward than the forward sweep as the surface of eGaIn; during backward sweep decrease in applied potential leads to decrease in surface pH, further depositing GaOOH in the surface of the electrode (as formation of GaOOH is more favorable at lower pH), This oxide remains on the surface until 0.075 V where we see the oxidation peak P_r (**Figure 4.1**), leading to larger impedance values. The impedance values observed at *OCP* ($E \approx 0V$) during the backward sweep are smaller than those of the forward sweep. This may be because of the direction of the potential sweep as decreasing the applied potential causes the OH- ions near the surface to move

away from the surface. The equivalent circuits for *passivation* and *oxidation regime* during backward sweep are the same as the forward sweep.

Oxide characterization using EIS:

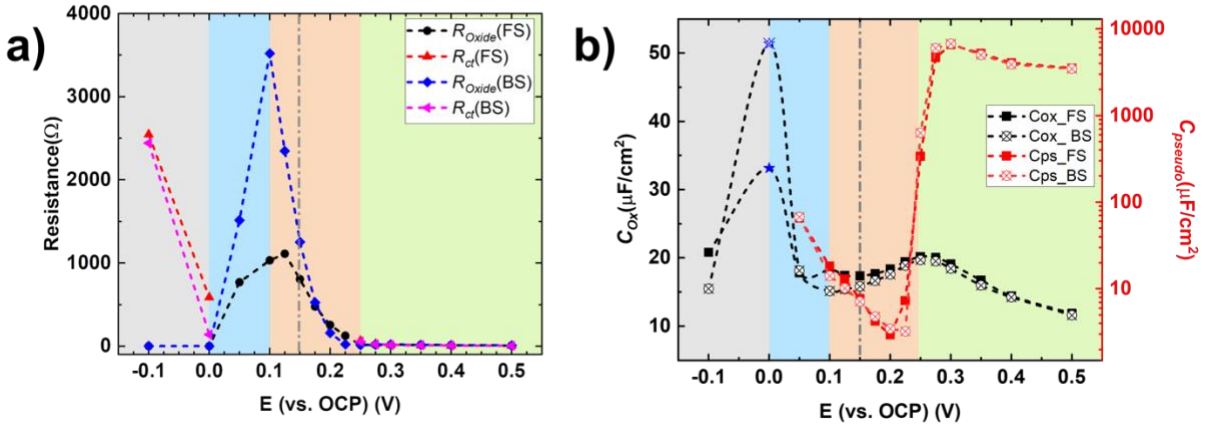

Figure 4.9. Shows the plot of impedance parameters as function of electrode potential**,** a) The resistance and b) capacitance values obtained from fitting EIS data to equivalent circuit models using non-linear least square fit. Grey (cathodic protection), blue (oxidizing), orange (passivation), and green (passivation breakdown) colors represent the different regimes. The blue stars indicate the capacitance of electrical double layer as there is no oxide present at 0V and -0.1V, and the grey line shows the potential where the inductive behavior starts to appear. The graphs are plotted with spine lines to guide the eye.

Figure 4.9 describes the four circuit elements in the equivalent circuit models that depict the different electro-oxidation regimes of eGaIn during EIS for both forward and backward sweep. **Figure 4.9a.** Shows the behavior of resistive parameters, including oxide resistance (R_{Ox}) and charge transfer resistance (R_{ct}) for both forward and backward sweep. There is no oxide resistance for E < 0.05 V as the eGaIn electrode is free of surface oxide at reductive potentials and open circuit potential. As E > 0.05 V is applied, R_{Ox} increases abruptly in the oxidation regime and gradually increases until a passive oxide film is formed completely. This observation is consistent with the low current observed in the cyclic voltammogram (**Figure 4.1)**. Beyond 0.125 V, the oxide resistance gradually decreases. Upon reaching the passivation breakdown regime (~0.25 V), the resistance drops by an order of magnitude. A further increase in potential in this regime causes the oxide resistance to drop less than 8 Ω, suggesting that any oxide species on the surface provide minimal barrier to Faradaic reactions. In addition to oxide resistance, **Figure 4.9**also plots the

charge transfer resistance (R_{ct}) in the passivation breakdown regime. Both oxidation and passivation regimes do not have R_{ct} as there is no significant increase in Faradic current in these regimes. However, R_{ct} is very high in the cathodic protection regime and at OCP since Faradaic reactions are unfavorable. The decrease in R_{Ox} in the *passivation regime* is consistent with the reconstruction of the oxide film. Additionally, the inductive behavior observed after E > 0.125 suggests that the surface oxide species changes from GaOOH to $Ga(OH)_4^-$, thus leading to a decrease in resistance **Figure 4.3.** R_{ct} in both forward and backward sweeps are consistent; however, R_{Ox} spikes at 0.175 V during the backward sweep suggesting the reformation of a passivating oxide film of GaOOH on the surface and only disappears after 0.05 V as R_{Ox} drops.

The constant phase elements (CPE), Q_{Pseudo} and Q_{Ox} are converted to effective capacitance C_{Pseudo} and C_{Ox} using the equation[21]:

$$C_i = \frac{(Q_i * R_{Ox})^{\frac{1}{n}}}{R_{Ox} * A} \qquad (4.1)^{21}$$

where R_{Ox} is in parallel with the CPE, A is the area of the electrode, and n is the non-ideality factor of the CPE. **Figure 4.9b.** Shows the changes in effective oxide capacitance (C_{Ox}) and pseudo-capacitance (C_{Pseudo}) in the three oxidation regimes for forward and backward potential sweeps. Pseudo-capacitance (C_{Pseudo}) is attributed to reactions[22] while C_{Ox} represents oxide capacitance. C_{Ox} at E < 0.05 V indicates the electrical double layer capacitance (EDL), as there is no oxide present on the electrode surface; therefore, it is marked by blue stars (solid color for forward sweep and hollow color with a cross for backward sweep). The observed EDL capacitance values are consistent with the typical literature values for EDL (~20 μF/cm^2) on bare metal in electrolyte.[9] When an anodic potential is applied, the Ga ions on the electrode surface oxidize, causing C_{Ox} to decrease. In the *passivation regime*, C_{Ox} does not change significantly until

0.25 V where it increases slightly. For E > 0.25 V, the decreasing C_{Ox} suggests the formation of defects or dissolution of surface oxides.

C_{Pseudo} is associated with the reaction that occurs on the surface of the electrode and oxide film and appears in the oxidation regime. C_{Pseudo} is larger than C_{Ox} at 0.05 V and is consistent with the formation of an oxide film. C_{Pseudo} initially decreases in the passivation regime until 0.20 V as the passivation oxide film completely forms. However, increasing the applied potential causes the C_{Pseudo} to increase and cause it to reach a maximum at 0.275V in the passivation breakdown regime. This observation is consistent with the formation of $Ga(OH)_4^-$ and $Ga(OH)_3$ as the passive oxide film breaks down. The C_{Pseudo} and C_{Ox} values in the backward sweep are consistent with the forward sweep during the passivation breakdown regime. But C_{Ox} deviates from the capacitance trends for E < 0.15 V during the backward sweep. We speculate that this behavior is due to pre-existing oxide on the surface of the electrode.

Oxide thickness analysis using EIS and dissolution experiments:

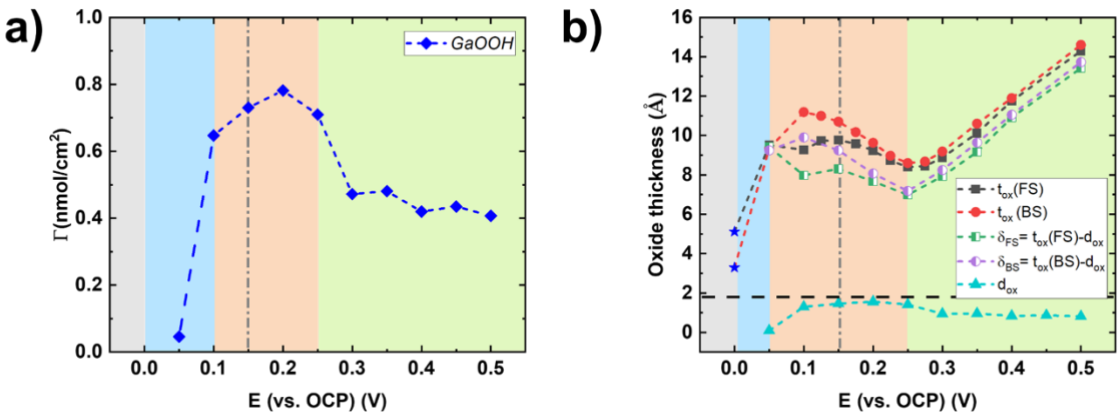

Figure 4.10. a) The estimated oxide coverage density (assuming the surface oxide as GaOOH) as a function of potential was calculated using the charges retrieved from the voltammetric stripping of the oxide shell (i.e., removing oxide using a reductive current). b) Effective oxide thickness (assuming the oxide covered is GaOOH) derived from dissolution and EIS analysis as a function of applied potential. The blue stars show the thickness of the electrical double layer as at E ~ 0 V due to the absence of surface oxide, and the grey vertical line indicates the potential where the inductive behavior starts to appear, and the black horizontal line indicates the GaO bond length of the oxide. The graphs are plotted with spine lines to guide the eye.

We use the EIS circuit parameters to estimate the thickness of oxide. Assuming an ideal parallel plate capacitor approximation, we can estimate the oxide thickness (t_{Ox}) using the formula $t_{Ox} = \varepsilon_o \varepsilon_r A / C_{Ox}$, where ε_r is the permittivity of the GaOOH (~19.13 at 25˚C)[23] , ε_o is the permittivity of vacuum (8.85x10^{-8} μF/cm), A is the area of the electrode and C_{OX} is the previously determined oxide capacitance.

Additionally, to estimate the effective oxide thickness, we designed dissolution experiments that work on the principle of stripping voltammetry[24]. The surface of the electrode is deposited with oxide by applying a linear potential sweep to a target potential. A reduction current (I_{red}) is immediately applied to strip the oxide species from the surface while recording the time taken for the oxide species to reduce and reach open circuit potential (t_{red}). We repeated the dissolution experiments for multiple target potentials steps with different reduction currents ($I_{red} = 1\ mA, 100\mu$A and 0 A). The experiments were performed thrice to confirm the reproducibility and consistency of the data.

The amount of Faradic charge needed to reduce the oxide on the surface helps determine the number of reducible oxidized Ga species on the surface. The total faradic charge (Q) can be extracted using the formula $Q = I_{red}.t_{red}$. However, oxide reduction can follow both an electrochemical and a chemical pathway; for example, Ga oxide species can dissolve into the electrolyte without being reduced. Thus, the total moles of oxide on the surface (n_{surf}) can be written as sum of moles of oxide reduced by an electrochemical pathway (n_{echem}) and moles of oxide removed from the surface by a chemical pathway (n_{chem}), given by

$$n_{surf} = n_{echem} + n_{chem} \quad (1)$$

$$n_{echem} = \frac{Q}{nF} \quad (2)$$

$$n_{chem} = v_{diss}.t_{diss} \quad (3)$$

We assume that the charges recorded are only associated with the conversion of Ga^{3+}, so we find the n_{echem} and n_{chem} values using equations (2) and (3), respectively. Where Q is the faradic charge (C), n is the number of electrons (3 for Ga^{3+}), F is the faradic constant (96485 C/mol), v_{diss} is the dissolution rate of oxide (chemical) and t_{diss} is the time taken to dissolve the oxide chemically.

To measure t_{diss}, we perform the experiment without reductive current ($I_{red} = 0A$) to eliminate electrochemical reactions. By solving equations 1 and 3 by the linear combination method, we can find the dissolution rate (i.e., $v_{diss} = n_{echem}/(t_{diss} - t_{red})$). Using the following, we estimated the oxide coverage density (Γ_{GaOOH}) with the formula $\Gamma_{GaOOH} = n_{surf}/A$, where A is the electrode area. **Figure 4.10a** plots oxide coverage density (Γ_{GaOOH}) as a function of potential. We then converted the surface oxide concentration to effective oxide thickness (d_{ox}) using the formula: $d_{ox} = \Gamma_{GaOOH}.m/\rho$, by assuming GaOOH as the surface oxide species, where m is the molar mass of GaOOH = 102.73 g/mol and ρ is the density of GaOOH = 5.23g/cm^3 [25]. According to **Figure 4.10a**, the surface oxide coverage density increases as GaOOH forms in the oxidation and passivation regime. Upon increasing the potential, the GaOOH species decrease on the surface at 0.20V and plateaus at ~0.4 nmol/cm^2 in the passivation breakdown regime. This decrease is consistent with the proposed oxidation mechanism as GaOOH gets converted to soluble $Ga(OH)_4^-$ and therefore does not get thicker with increased potential. It is also consistent with the impedance spectra, where we observe the onset of inductive behaviour.

Figure 4.10b plots effective oxide thickness as a function of applied potential for dissolution (d_{ox}) and EIS (t_{ox}) methods. d_{ox} increases initially in the passivation regime and reaches a plateau in the passivation regime. On the other hand, t_{ox} estimated using EIS is at least one order of magnitude larger than d_{ox}, as t_{ox} includes the electrical double layer ($\delta = t_{ox} - d_{ox}$).

The electrical double layer initially decreases in the passivation regime due to the deposition of GaOOH. However, as the surface pH increases (due to the electrostatic attraction of OH- or gallate anions), there is linear increase in the electrical double layer with potential. Further, δ increases linearly with applied potential. The forward and backward sweep have similar oxide thickness trends in the passivation breakdown regime. However, the δ is larger in the backward sweep than forward sweep because sweeping the potential backward causes the surface pH to decrease, hence the precipitating GaOOH oxide on the surface of the electrode

Conclusion:

An electrochemical impedance (EIS) study of liquid metal (eGaIn) electrodes in 1M NaOH is reported here. The impedance spectra were obtained at multiple DC potentials in the different oxidation regimes (oxidation, passivation, and the passive film breakdown) for both forward and backward potential scans. The generation, accumulation, dissolution, and adsorption of the oxide species are accounted for in the reaction model. At $E \leq OCP$ $(0\ V)$ a capacitive loop is consistent with presence of an electrical double layer since the bare metal contacts the electrolyte without oxidation. During the transition from the *oxidation* to the *passivation regime* ($E \approx 0.05\ V$), a tail is observed in the low frequency range corresponding to diffusive behavior coupled with the formation of oxide film (most likely $Ga(OH_3$ or GaOOH, at slow time scales). In the *passivation regime*, $0.05\ V < E < 0.25\ V$ the oxide appears to be relatively stable in the low frequency range until 0.15V, where it transitions into an inductive loop until 0.25 V; this observation is consistent with the formation of GaOOH film and the eventual conversion to soluble gallates $Ga(OH)_4^-$. When the electrode is at the transition potential between *passivation* and *passivation breakdown regime* ($E \approx 0.25\ V$), the Nyquist plot shows the start of a second capacitance loop but with an inductive behavior in the lower frequencies. This trend suggests the presence of an adsorbed film

that depends on the surface coverage density of GaOOH and applied potential. Upon reaching *passivation breakdown*, $0.25\,V < E \leq 0.50\,V$ we observe a fully formed secondary capacitive loop that suggests the presence of a second adsorbed layer that depends on applied potential. Furthermore, at E = 0.50 V we observe an additional small loop in the intermediate frequencies. These observations suggest a stepwise addition of surface hydroxy species in the oxidation mechanism with applied potential. Thus, we infer that due to the anodic dissolution of GaOOH and the formation of GaOOH and $\mathrm{Ga(OH)_4^-}$ may compete for the formed bare surface sites.

Additionally, we indirectly characterize the oxide species on the surface of the electrode by using the impedance parameters and oxide dissolution method. The estimated thickness of the adsorbed $\mathrm{Ga(OH)_4^-}$ layer increases with potential. Meanwhile, reducible species (GaOOH oxide) form during passivation and then decrease to a plateau value in the passivation breakdown regime. Although the absolute values are rough estimates, they suggest a film that is approximately a monolayer in thickness.

Taken in sum, these observations provide validation for the reaction mechanism reported in **chapter 3**. The next chapter will discuss how the oxidation and impedance analysis is used to cause the drop in surface tension.

References

(1) Orazem, M. E.; Tribollet, B. Electrochemical Impedance Spectroscopy; The ECS Series of Texts and Monographs; Wiley, 2017.

(2) Macdonald, D. D. Reflections on the History of Electrochemical Impedance Spectroscopy. Electrochimica Acta 2006, 51 (8), 1376–1388. https://doi.org/10.1016/j.electacta.2005.02.107.

(3) Li, P.; Tan, T. C.; Lee, J. Y. Impedance Spectra of the Anodic Dissolution of Mild Steel in Sulfuric Acid. Corrosion Science 1996, 38 (11), 1935–1955. https://doi.org/10.1016/S0010-938X(96)00079-0.

(4) Pletcher, D.; Greff, R.; Peat, R.; Peter, L. M.; Robinson, J. Instrumental Methods in Electrochemistry; Chemical Science; Elsevier Science, 2001.

(5) Song, M.; Daniels, K.; Kiani, A.; Rashidnadimi, S.; Dickey, M. Interfacial Tension Modulation of Liquid Metal via Electrochemical Oxidation; 2021.

(6) Boukamp, B. A. A Linear Kronig-Kramers Transform Test for Immittance Data Validation. Journal of The Electrochemical Society 1995, 142 (6), 1885–1894. https://doi.org/10.1149/1.2044210.

(7) Deslouis, C.; Frateur, I.; Kiene, L.; Levi, Y.; Tribollet, B. Corrosion Study of Cast Iron Pipes in Water Distribution Systems by Impedance. Application to Chlorine Consumption. MSF 1998, 289–292, 135–146. https://doi.org/10.4028/www.scientific.net/MSF.289-292.135.

(8) Macdonald, D. D. The Point Defect Model for the Passive State. J. Electrochem. Soc. 1992, 139 (12), 3434–3449. https://doi.org/10.1149/1.2069096.

(9) Garche, J.; Karden, E.; Moseley, P. T.; Rand, D. Lead-Acid Batteries for Future Automobiles; 2017; p 674.

(10) Dickey, M. D. Stretchable and Soft Electronics Using Liquid Metals. Adv. Mater. 2017, 29 (27), 1606425. https://doi.org/10.1002/adma.201606425.

(11) Basics-of-EIS, Application Note Rev. 1.0 9/3/2010 @ Copyright 1990-2009 Gamry Instruments, Inc..Pdf.

(12) Bagotska.Ia; Morozov, A. M.; Grigorye.Nb. On Zero-Charge Potential of Gallium in Aqueous Solutions and Origin of High Capacitance at Gallium/Solution Interface. Electrochim. Acta 1968, 13 (4), 873–876.

(13) Warburg, E. Ueber Das Verhalten Sogenannter Unpolarisirbarer Elektroden Gegen Wechselstrom. Annalen der Physik 303, 493–499.

(14) Klotz, D. Negative Capacitance or Inductive Loop? – A General Assessment of a Common Low Frequency Impedance Feature. Electrochemistry Communications 2019, 98, 58–62. https://doi.org/10.1016/j.elecom.2018.11.017.

(15) Baril, G.; Blanc, C.; Pébère, N. AC Impedance Spectroscopy in Characterizing Time-Dependent Corrosion of AZ91 and AM50 Magnesium Alloys Characterization with Respect to Their Microstructures. Journal of The Electrochemical Society 2001, 148 (12), B489. https://doi.org/10.1149/1.1415722.

(16) Baril, G.; Galicia, G.; Deslouis, C.; Pébère, N.; Tribollet, B.; Vivier, V. An Impedance Investigation of the Mechanism of Pure Magnesium Corrosion in Sodium Sulfate Solutions. J. Electrochem. Soc. 2007, 154 (2), C108. https://doi.org/10.1149/1.2401056.

(17) Macdonald, D. D.; Real, S.; Smedley, S. I.; Urquidi-Macdonald, M. Evaluation of Alloy Anodes for Aluminum-Air Batteries. 135 (10), 6.

(18) Boukamp, B.; Bouwmeester, H. Interpretation of the Gerischer Impedance in Solid State Ionics. Solid State Ionics 2003, 157, 29–33. https://doi.org/10.1016/S0167-2738(02)00185-6.

(19) Chang, B.-Y.; Park, S.-M. Electrochemical Impedance Spectroscopy. Annual Rev. Anal. Chem. 2010, 3 (1), 207–229. https://doi.org/10.1146/annurev.anchem.012809.102211.

(20) BioLogic (2017). Potentiostat: BT-Lab & EC-Lab software Analysis and Data Process manual, France. MA: Author.

(21) Orazem, M. E.; Shukla, P.; Membrino, M. A. Extension of the Measurement Model Approach for Deconvolution of Underlying Distributions for Impedance Measurements. Electrochimica Acta 2002, 47 (13), 2027–2034. https://doi.org/10.1016/S0013-4686(02)00065-8.

(22) Nguyen, T.; Montemor, M. de F. Metal Oxide and Hydroxide–Based Aqueous Supercapacitors: From Charge Storage Mechanisms and Functional Electrode Engineering to Need-Tailored Devices. Adv. Sci. 2019, 6 (9), 1801797. https://doi.org/10.1002/advs.201801797.

(23) Yuwen, C.; Liu, B.; Zhang, L. Dielectric Properties, Structure and Morphology during Synthesis of β-Ga2O3 by Microwave Calcination of GaOOH. Ceramics International 2020, 46 (16, Part A), 24923–24929. https://doi.org/10.1016/j.ceramint.2020.06.278.

(24) Allen J. Bard and Larry R. Faulkner, Electrochemical Methods: Fundamentals and Applications, New York: Wiley, 2001, 2nd Ed. Russian Journal of Electrochemistry 2002, 38 (12), 1364–1365. https://doi.org/10.1023/A:1021637209564.

(25) CRC Handbook of Chemistry and Physics, 101st edition.; Rumble, J., Ed.; CRC Press: Boca Raton, FL, USA, 2020.

Chapter 5 : Conclusion - Effect of electrochemical oxidation on interfacial tension.

Abstract:

Based on the electrochemical oxidation mechanism presented in **Chapter 3** and the impedance results presented in **Chapter 4**, here we discuss the effect of electrochemical oxidation on interfacial tension change in this chapter. This chapter will serve as the conclusion for the thesis.

Introduction:

The thermodynamic theory established by Gibbs[1] and Lippman[2] describe the interfacial tension changes of liquid metal electrodes in contact with an electrolyte as a function of electrode potential[3]. Gouy performed initial interfacial measurements on mercury electrodes in electrolyte to validate this theory[3]. Thereby, characterizing the metal-electrolyte interface using interfacial tension measurement[3]. This theory was later extended to solid electrodes, to describe the surface stress on electrodes as a function of surface charges or potential[3,4]. Some examples include, studies that use potential to induce bending of thin polycrystalline gold and platinum cantilever electrodes due to the surface stress[5,6], while others have measured surface stress of well-defined gold single crystal surfaces due to potential modulation[7,8]. However, the description of surface stress as a function potential using thermodynamic theory has proved to be controversial[3]. Some authors report a parabolic dependence of stress (similar to electrocapillary behavior of liquid mercury electrodes)[9], while others report a monotonically linear decrease in surface stress with increasing electrode potential[7,8]. Even though both authors agree that adsorbed interface is the reason for surface stress the differences in their conclusion stem from their approaches; [9] measured the surface stress of the sputtered Au film in the potential range where no oxidation or reduction peaks were observed (i.e., the passivation film has already formed), whereas [7,10] measured surface stress of the Au (111) film during electrodeposition of Cu on the Au(111) layer. For example, **Figure 5.1** Shows the cyclic voltammogram and the accompanying surface stress change of a Au(111)

electrode[3,10]. Furthermore, [11,12] also report a linear increase in surface stress with increase in surface coverage.

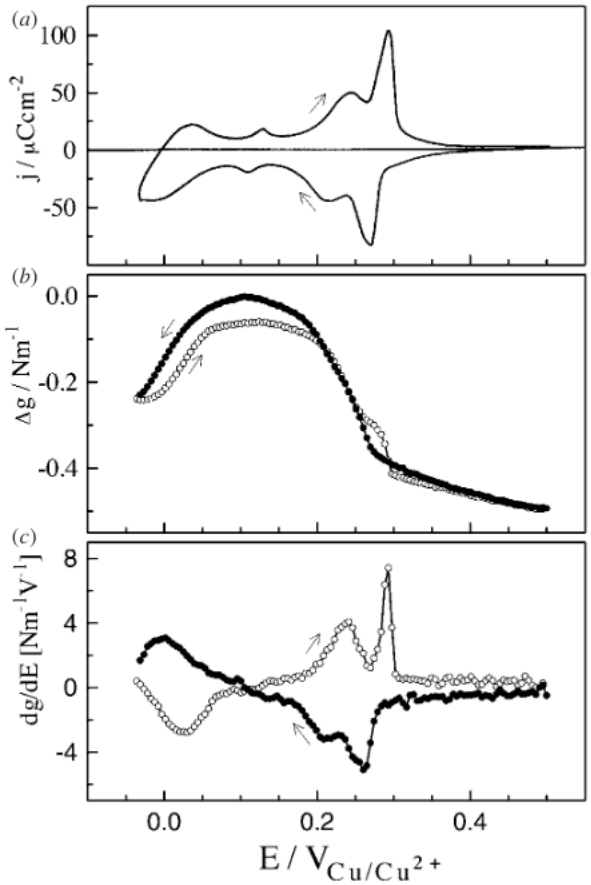

Figure 5.1 Copper under-potential deposition (UPD) on Au (111) in the presence of bromide (from [10]). Shows the a) cyclic voltammogram, b) its accompanying surface stress change and c) derivative of the surface stress with respect to the electrode potential, for a Au(111) electrode in 0.1MH_2SO_4 + 1 mM $CuSO_4$ + 1 mM CsBr during a potential scan rate of 20 mV s−1 [3,10]

For liquid mercury, the parabolic dependence of interfacial tension with respect to electrode potential is a well-established relationship that can be explained using the electrocapillarity **Equation 1.1**. This equation, derived by Lippmann,[2] describes the interfacial tension change by including the effect of surface charges in the electrical double layer at the electrode surface. Essentially, this layer resembles a capacitor and thereby lowers the interfacial energy by the energy of a capacitor (½ CV^2, in which C is capacitance and V is potential) and the interfacial tension change is therefore parabolic. Yet, previous work from our group [13] shows that the interfacial tension behavior of gallium based liquid metal (eGaIn) does not follow the regular

electrocapillarity trend[14,15]. The interfacial tension of eGaIn was found to follow the electrocapillarity curve until E~0.10 V after which the measured interfacial tension drops and deviates from electrocapillarity behavior (later, we show that portions of the plot of tension versus potential are linear)[13,14]. Initially, it was proposed that the unique interfacial tension behavior was caused due to the surfactant like behavior of surface oxides on the eGaIn electrode[15]. Additional studies suggested there may be compressive forces generated by the electrochemical deposition of the oxide[14]. The exact mechanism remains poorly understood.

There are three challenges with elucidating the mechanism. First, the interfacial tension is an 'effective' value that represents effects arising from the metal/oxide and oxide/ambient interfaces, plus any mechanical effects arising from the coating. Prior studies suggest that the surface is likely visco-elastic during electrochemical oxidation and therefore not purely fluid[13]. While interfacial tension and surface stress are the same for liquids, they are not the same for solids (such as the oxide 'coating' that forms during electrochemical oxidation)[9]. This significantly complicates the interfacial behavior. Second, it is challenging (if not impossible) to directly probe what is on the surface during electrochemical oxidation since any oxide species dissolve in the absence of potential. This motivates the use of indirect methods (electrochemistry, EIS) described in this chapter to elucidate what forms on the surface as a function of potential. Third, we observe a hysteresis in interfacial tension between the forward and reverse potential scan[13].

Here we describe the interfacial tension behavior of eGaIn electrode and how the electro-oxidation of liquid metals contributes to it.

Results and discussions:

Interpretation of interfacial tension:

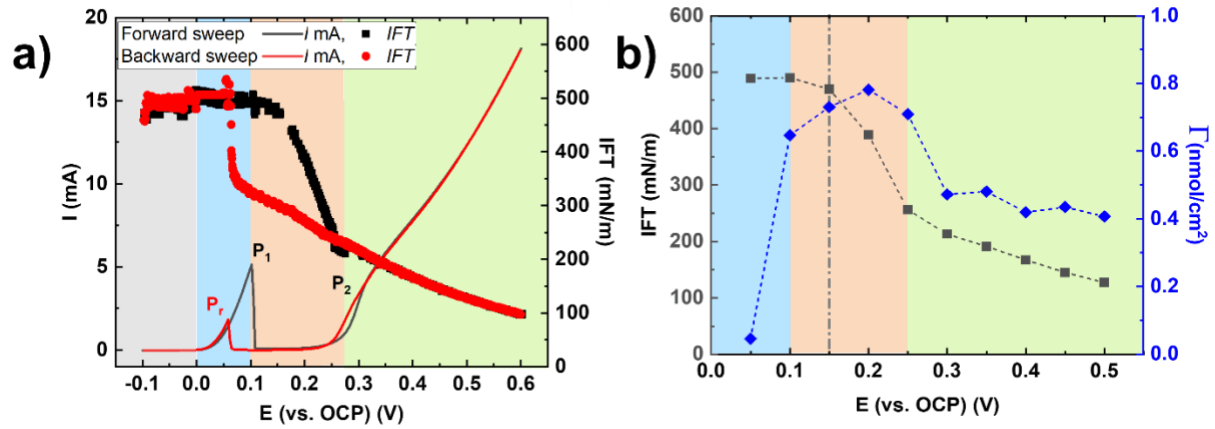

Figure 5.2. The interfacial tension of liquid metal (eGaIn) in 1M NaOH analyzed using sessile drop shape analysis. A cyclic voltammogram co-plotted with interfacial tension of liquid metal vs. electrical potential. b) Interfacial tension, co-plotted with surface oxide coverage density (assuming GaOOH oxide on surface) as a function of potential, reused from **Figure 4.10**. The volume of eGaIn droplet and the potential scan rate is 0.1 ml and 1 mV/s, respectively. Red and black colors are used to represent forward sweep (FS) and backward sweep (BS) respectively, lines correspond to cyclic voltammetry data and dots correspond to interfacial tension data (IFT, γ). The various oxidation regimes are labeled by color as cathodic protection (grey), oxidizing (blue), passivation (orange), and passivation breakdown (green), respectively. (Contributions: Keith Hillarie helped to measure the interfacial tension values for Figure 5)

Figure 5.2a shows the effective interfacial tension (IFT, γ) of a 0.1ml eGaln droplet in 1M NaOH during electro-oxidation. The interfacial tension of the eGaIn droplet is ~ 500 mN/m in the absence of potential as NaOH dissolves the surface oxide. Previous work from our group speculated that the oxide acts as a surfactant (possibly in conjunction with electrocapillarity) to lower interfacial tension; contrary to our expectations, interfacial tension analysis shows no change in *IFT* in the *'oxidizing regime'* and starts to show signs of change only in the *'passivation regime'* at $E \sim 0.15\ V$. As $E > 0.15\ V$ is applied, the interfacial tension suddenly drops from 500 mN/m to 200 mN/m in a narrow potential window between 0.15 V to 0.25 V in the *'passivation regime'*.

As discussed in **Chapter 3**, We speculate that this change occurs due to the accumulation of OH^- ions (i.e., charges) near the electrolyte/oxide interface leads to change in the composition of the already existing oxide film, resulting in the formation of either GaOOH or $Ga(OH)_4^-$ as the

new passive oxide film. The presence of the passivating oxide creates a barrier to electrochemical reactions on the metal, thereby lowering the current readings. The OH^- anions are not consumed in the oxidation reaction; hence increase in potential causes the OH^- ions in bulk to accumulate at the electrode surface, thereby increasing the surface pH. Then the passive oxide film (most likely GaOOH) covers the surface, the interfacial tension does not change for reasons we do not fully understand, but one possibility is that the oxide is sufficiently rigid to prevent the droplet from changing shape. However, once the surface composition starts to change (at E~0.15V) the interfacial tension drops. Additionally, the analysis of impedance spectroscopy in the *passivation regime (*$0.05 > E > 0.25\ V$*)* (discussed in **chapter 4)** shows two unique impedance trends; The first tend in the potential range $0.05 > E \geq\ 0.15\ V$ (**Figure 4.3** and **Figure 4.6)**, we observe a tail in the low frequency range corresponding to formation of GaOOH from the adsorbed gallium hydroxide species on the oxide film, while in the later potentials ranges ($0.15 > E > 0.25\ V$), a negative impedance loops (inductive behavior) appears in the low frequency regime. Inductive behavior is often associated with electrochemical or chemical reactions[16–18]. We suspect that the change in oxide composition from GaOOH to soluble gallates $Ga(OH)_4^-$ leads to changes to the composition of the interface, allowing the bare metal to encounter the electrolyte causing inductive behavior. The drop in tension across this range ($0.05 > E \geq\ 0.15\ V$) may be from multiple factors; we direct the reader to the thesis of Keith Hillaire (2022) for more information. Note that the drop in tension in this range is not reproduced during the reverse voltage sweep (i.e., hysteresis). This hysteresis is apparent by comparing the red and black data in **Figure 5.2a**.

At higher oxidative potentials ($E >\ 0.25\ V$)**,** the interfacial tension decreases linearly with applied potential in the *'passivation breakdown'* regime. A decrease in interfacial tension suggests changes to the surface of the electrode, while the presence of an oxidation peak P_2 occurs due to

the continued formation of soluble gallates. Next, we explore the possible mechanisms for lowering the tension and use process of elimination to identify the most likely explanation.

Electrocapillarity: Initially, we suspected that the tension lowers by electrocapillarity; however, if it was simply surface charge, the interfacial tension change should be parabolic with respect to potential (i.e., electrocapillarity) rather than linear. Furthermore, the change in tension with respect to potential is much larger than what is possible by conventional electrocapillarity assuming a capacitance of an electrical double layer (approximately 20 of $\mu F/cm^2$). Thus, if it is electrocapillarity, it would be anomalous relative to conventional theory. The electrocapillarity curve is shown in **Figure 1.2.**

Current: Driving electrochemical oxidation of the surface could create stress by, for example, driving ions through any surface film. While the current increases as the tension drops (cf. Figure 5.1a), the drop in tension is not proportional to current. This is most apparent in the reverse sweep (red data) in Figure 5.1a; the tension changes linearly with potential, but the current changes non-linearly. Thus, current alone cannot explain the linear decrease in tension.

Surfactant: The prior chapters suggest that the surface changes from GaOOH to gallate salts or $Ga(OH)_3$. Changes to the chemistry of the surface could result in a decrease in tension of the species like 'surfactants'. However, if this is the case, they would be the best surfactants ever reported. Furthermore, it does not explain why tension drops with respect to potential as opposed to a sudden decrease in tension once certain species form on the surface. In **Chapter 4**, we showed two unique measurements (dissolution and EIS) that suggest that surface layer is of approximately constant thickness **Figure 4.10**.

Surface stress: Given the linear decrease in tension (Figure 5.1a), it seems most likely that the decrease in tension is due to surface stress in the thin layer of adsorbed oxidation species, as

reported on other solid metal films[6]. The impedance spectra for the *'passivation breakdown regime'* shows the appearance of a second capacitance loop. We also see the first loop becoming smaller and the second one becoming wider with potential (suggesting an increase in oxide thickness), while the cyclic voltammogram shows the increase in current and the formation of peak P_2 at $E = 0.25\ V$ (**Figure 5.2a**.). This increase in oxide thickness may impart surface stress on the electrode, that is reflected on the surface tension curve**.** Additionally, at E = 0.50 V we observe an additional small loop in the intermediate frequencies **Figure 4.4f-Figure 4.5a**. These observations suggest a stepwise addition of surface hydroxyl species that could create the stress necessary to lower the effective tension of the metal.

Prior work has shown a linear dependence of surface stress on metals based on coverage of monolayers. This linear dependence has been reported for most adsorbate systems at the gas-solid (electrode) interface[3]. For example oxygen adsorbed on Ni (100) substrates cause compressive stress for low coverages[12]. The previously calculated oxide coverage (assuming only GaOOH oxide is present on the surface) (in **Chapter 4**, **Figure 4.10**) is co-plotted with interfacial tension as a function of potential during forward sweep, (**Figure 5.2b)**. We observe that the surfaces coverage of GaOOH peaks and drops at E = 0.20V (in the passivation regime), when the inductive loops appear. This suggests conversion of GaOOH to $Ga(OH)_4^-$. Furthermore, after E > 0.25 V the interfacial tension drops along with the drop in surface coverage of GaOOH in the passivation breakdown regime, contrary to our increase in oxide thickness. Thus, we speculate that either $Ga(OH)_3$ or $Ga(OH)_4^-$ contribute to the surface stress. Similar study on uracil adsorbed on Au (111) have shown a linear relationship between surface stress and surface charges on the surface of the electrode, consistent with our observations[3,19,20].

An interesting observation is the interfacial behavior during the backward sweep shows hysteresis **Figure 5.2a**. During the backward sweep, the interfacial tension increases with applied potential linearly in all the oxidation regimes and returns to 500 mN/m in the oxidation regime. This hysteresis indicates that the interface is different in the passivation regime during the forward and backward scans. Given the linear increase in tension during the reverse scan (through the passivation regime), we reason that the surface of the eGaIn electrode is covered with gallates and GaOOH until ~0.15 V. This happens because during the reverse potential scan the surface pH decreases as we move toward smaller potentials, and the conversion of some gallates to GaOOH as is more favorable. We suspect these oxide species helps maintain the shape of the droplet until all the surface oxide completely dissolves, as the interfacial tension increases suddenly with the appearance of a peak P_r (at E~0.05 V). Additionally,[3] prior measurements on gold show hysteresis in surface stress when the reconstruction of chemisorbed Uracil in the cathodic scan and its subsequent removal in the anodic scan occurs. This observation is analogous to our observations, during the anodic scan; the impedance spectra in the *passivation regime* shows the presence of an inductive behaviour that suggests the appearance of bare metals (removal of GaOOH) while during the cathodic scan the decrease in surface pH causes deposition of GaOOH on the surface (reformation of the oxide layer). This is the most likely the reason for the hysteresis to appear in the interfacial tension behavior.

Conclusion:

Based on the oxidation mechanism presented in **Chapter 3** and the impedance results presented in **Chapter 4**, we propose that the change in the interfacial behavior occurs as follows.

The interfacial tension of the eGaIn droplet is ~ 500 mN/m in the absence of potential as NaOH dissolves the surface oxide. Contrary to our expectations the interfacial tension does not

change upon formation of oxide in the *oxidation regime*; instead, it drops rapidly from 500 mN/m to 200 mN/m in a narrow potential window between 0.15 V to 0.25 V in the *passivation regime.* This decrease is most likely due to the increase in the surface pH from electrostatically attracted OH- from the bulk. The change in pH can convert $GaOOH$ to $Ga(OH)_4^-$. The latter is soluble, so at smaller time scales it is possible to have some metal sites exposed (indicative of inductive behaviour in EIS spectra). At E > 0.25 V, the interfacial tension decreases linearly with potential, along with continuous and dynamic formation of soluble gallates. The anodic dissolution of GaOOH and the formation of GaOOH and $Ga(OH)_4^-$ compete for bare metal surface sites, this maintains the thickness of oxide film on surface (assuming only GaOOH) while the thickness of adsorbed $Ga(OH)_4^-$ increases, the surface coverage of GaOOH is shown to decrease very slowly in the *passivation breakdown regime.* The oxides species deposited electrochemically cause the interfacial tension to decrease linearly with applied potential presumably due to surface stress.

Additionally, during the backward scan the interfacial tension increases linearly with the applied the electrode potential demonstrating a hysteresis behavior. we speculate that the oxide film on the surface of the electrode does not disappear until E~0.05 V, this oxide film is most likely gallates and GaOOH on the surface of the electrode (due to decrease in surface pH) causing the hysteresis in interfacial tension behavior.

For future work, modeling the EIS results with reaction kinetics will provide a better understanding of the surface coverage of the oxide species and will validate our speculations about the mechanism for interfacial tension change.

References

(1) Gibbs, J. W. *The Collected Works of J. Willard Gibbs.*; Yale Univ. Press: New Haven, 1948.

(2) Stock, J. T. Gabriel Lippmann, and the capillary electrometer. *Bull. Hist. Chem.* **2004**, *29* (1), 5.

(3) Haiss, W. Surface Stress of Clean and Adsorbate-Covered Solids. *Rep. Prog. Phys.* **2001**, *64* (5), 591–648. https://doi.org/10.1088/0034-4885/64/5/201.

(4) Lipkowski, J.; Stolberg, L.; Yang, D.-F.; Pettinger, B.; Mirwald, S.; Henglein, F.; Kolb, D. M. Molecular Adsorption at Metal Electrodes. *Electrochimica Acta* **1994**, *39* (8), 1045–1056. https://doi.org/10.1016/0013-4686(94)E0019-V.

(5) Fredlein, R. A.; Damjanovic, A.; Bockris, J. O. Differential Surface Tension Measurements at Thin Solid Metal Electrodes. *Surface Science* **1971**, *25* (2), 261–264. https://doi.org/10.1016/0039-6028(71)90246-9.

(6) Fredlein, R. A.; Bockris, J. O. An "Electrocapillary" Study of the Gold-Perchloric Acid Solution Interface. *Surface Science* **1974**, *46* (2), 641–652. https://doi.org/10.1016/0039-6028(74)90330-6.

(7) Haiss, W.; Nichols, R. J.; Sass, J. K.; Charle, K. P. Linear Correlation between Surface Stress and Surface Charge in Anion Adsorption on Au(111). *Journal of Electroanalytical Chemistry* **1998**, *452* (2), 199–202. https://doi.org/10.1016/S0022-0728(98)00137-5.

(8) Haiss, W.; Sass, J.-K. Quantitative Surface Stress Measurements on Au(111) Electrodes by Scanning Tunneling Microscopy. *Langmuir* **1996**, *12* (18), 4311–4313. https://doi.org/10.1021/la9602224.

(9) Láng, G.; Heusler, K. E. Changes of the Specific Surface Energy of Gold Due to the Chemisorption of Sulphate. *Journal of Electroanalytical Chemistry* **1995**, *391* (1), 169–179. https://doi.org/10.1016/0022-0728(94)03832-N.

(10) Haiss, W.; Sass, J.-K. Quantitative Surface Stress Measurements on Au(111) Electrodes by Scanning Tunneling Microscopy. *Langmuir* **1996**, *12* (18), 4311–4313. https://doi.org/10.1021/la9602224.

(11) Ibach, H. The Role of Surface Stress in Reconstruction, Epitaxial Growth and Stabilization of Mesoscopic Structures. *Surface Science Reports* **1997**, *29* (5), 195–263. https://doi.org/10.1016/S0167-5729(97)00010-1.

(12) Grossmann, A.; Erley, W.; Ibach, H. Adsorbate-Induced Surface Stress and Surface Reconstruction: Oxygen, Sulfur and Carbon on Ni(111). *Surface Science* **1995**, *337* (3), 183–189. https://doi.org/10.1016/0039-6028(95)00615-X.

(13) Song, M.; Daniels, K.; Kiani, A.; Rashidnadimi, S.; Dickey, M. *Interfacial Tension Modulation of Liquid Metal via Electrochemical Oxidation*; 2021.

(14) Eaker, C. B.; Hight, D. C.; O'Regan, J. D.; Dickey, M. D.; Daniels, K. E. Oxidation-Mediated Fingering in Liquid Metals. *Phys. Rev. Lett.* **2017**, *119* (17), 174502. https://doi.org/10.1103/PhysRevLett.119.174502.

(15) Khan, M. R.; Eaker, C. B.; Bowden, E. F.; Dickey, M. D. Giant and Switchable Surface Activity of Liquid Metal via Surface Oxidation. *Proc Natl Acad Sci USA* **2014**, *111* (39), 14047–14051. https://doi.org/10.1073/pnas.1412227111.

(16) Orazem, M. E.; Tribollet, B. *Electrochemical Impedance Spectroscopy*; The ECS Series of Texts and Monographs; Wiley, 2017.

(17) Klotz, D. Negative Capacitance or Inductive Loop? – A General Assessment of a Common Low Frequency Impedance Feature. *Electrochemistry Communications* **2019**, *98*, 58–62. https://doi.org/10.1016/j.elecom.2018.11.017.

(18) Li, P.; Tan, T. C.; Lee, J. Y. Impedance Spectra of the Anodic Dissolution of Mild Steel in Sulfuric Acid. *Corrosion Science* **1996**, *38* (11), 1935–1955. https://doi.org/10.1016/S0010-938X(96)00079-0.

(19) Dretschkow, Th.; Dakkouri, A. S.; Wandlowski, Th. In-Situ Scanning Tunneling Microscopy Study of Uracil on Au(111) and Au(100). *Langmuir* **1997**, *13* (10), 2843–2856. https://doi.org/10.1021/la970026c.

(20) Li, W.-H.; Haiss, W.; Floate, S.; Nichols, R. J. In-Situ Infrared Spectroscopic and Scanning Tunneling Microscopy Investigations of the Chemisorption Phases of Uracil, Thymine, and 3-Methyl Uracil on Au(111) Electrodes. *Langmuir* **1999**, *15* (14), 4875–4883. https://doi.org/10.1021/la9815594.